UNIVERSITY OF CALIFORNIA,
IRVINE

Elucidating the mechanism through which loss-of-function in *RB1* mediates poor prognosis in osteosarcoma

DISSERTATION

submitted in partial satisfaction of the requirements
for the degree of

DOCTOR OF PHILOSOPHY

in Biological Sciences

by

Stephanie Cherie Wu

Dissertation Committee:
Assistant Professor Claudia A. Benavente, Chair
Assistant Professor Scott Atwood
Associate professor Robert Spitale
Professor Marian L. Waterman
Assistant Professor Zeba Wunderlich

2019

DEDICATION

To

my momma

sender of the best care packages

"Nothing in life is to be feared, it is only to be understood. Now is the time to understand more, so that we may fear less." –*Marie Curie*

TABLE OF CONTENTS

LIST OF FIGURES

LIST OF TABLES

ACKNOWLEDGMENTS

I would like to thank my advisor Dr. Claudia Benavente for her excellent mentorship. Her relentless encouragement and selfless support throughout my graduate career made my journey as smooth sailing as could be. She allowed creative freedom in shaping my project and at the same time guided me to be as efficient as possible. I was extremely lucky to have the opportunity to learn from and grow with someone with such immeasurable intelligence and compassion. I'm proud to say that Claudia was the one who molded me into the scientist that I am today. The bond we share will be one that I forever cherish and be grateful for.

I would like to express my gratitude towards my committee members, for constantly challenging me to become a better-rounded scientist and having my best interest at heart. Specifically, Dr. Marian Waterman, for her invaluable inputs on various ways to broaden the impact of my research. Dr. Zeba Wunderlich, for her patience, attentions to details, and kind words of encouragement. Dr. Robert Spitale, for his thought-provoking questions and challenges. Dr. Scott Atwood, for his playful wisdom, and for introducing me to Claudia. I would also like to thank Dr. David Fruman for extending the invitation for me to travel internationally for an interview at UCI, which kick-started an incredible chapter of my life. I would also like to thank Dr. Michael Mulligan and Dr. Christine Suetterlin, for their help and their faith in me during a hard transition period in my career.

I would not be ending this journey with a big smile on my face if it weren't for the support of the friends I've made at UCI. I'd like to thank Dr. Riann Egusquiza, who came to be the sister I never had, and has been my rock through all the ups and downs. I would also like to thank Dr. Honyin Chiu, Dr. Aditi Mehta, Dr. Julius Edson, future doctors Albert Ta, Melissa Thone, Saad Mohammad for their friendship. I'm blessed to have met Cameron Pavelic, who managed to always make me laugh even in the toughest times and has provided immense love and reassurance that made every day a celebration. The love and support from my fellow lab members did not go without notice. Dr. Loredana Zocchi, who has been both a great mentor and a friend, her companionship and support has made every day more enjoyable. I'd like to also acknowledge my hard working undergraduate students, Erin Yamanaka, Josselyn Peña, Sara Akhlaghi, and Annie Jeon. I appreciate their support and friendship tremendously.

Finally, I would like to thank Dr. Meilan Tsao, for being the best parent, teacher, friend, and role model. I came to realize that the reason I remained curious about the world as an adult and what ultimately guided me to pursue a career in science was through her teaching. Growing up, every question I asked she took seriously, and answered in the most memorable ways. I asked her why the moon changes shapes, she answered by showing me how the Sun, Earth and Moon move in relation to each other using a flashlight and two miniature toy basketballs. She delivers discipline and life lessons through fun, love, encouragement and support. I had the most amazing upbringing that paved way for an easier future because of her. I'd like her to know that my effort in making her proud does not stop at receiving a PhD. No matter where life takes me, I'll always be the curious little girl who thinks her momma has all the answers in the world.

CURRICULUM VITAE

Stephanie Cherie Wu
PhD candidate, Department of Developmental and Cell Biology,
University of California, Irvine
Email: scwu1@uci.edu

EDUCATION

2013-2019 Ph.D., University of California, Irvine
Department of Developmental and Cell Biology
Cellular and Molecular Biosciences Gateway Ph.D. Program

2009-2013 B.S., National Chung Cheng University, Taiwan
Department of Life Sciences

RESEARCH EXPERIENCE

2015-2019 Ph.D. candidate (2017)/ Graduate Student Researcher (2015-2016)
Benavente Laboratory, Department of Developmental and Cell Biology
University of California, Irvine
Project title: Elucidating the mechanism through which loss-of-function in *RB1* mediates poor prognosis in osteosarcoma.

2013-2015 Graduate Student Researcher
Blumberg Laboratory, Department of Developmental and Cell Biology
University of California, Irvine
Project title: Regulation of proliferation-differentiation switch- Opposing signaling effects of FGF and RA.

2010-2013 Undergraduate Student Researcher
Chiang Laboratory, Department of Life Sciences
National Chung Cheng University, Taiwan
Project title: Investigation of the machinery by which Neurogenin3 inhibits the expression of Ptf1a via Sirtuin1.

PUBLICATIONS

2019 **Wu S.C.**, Lopez J., Zocchi L., Benavente C.A. (in preparation) UHRF1 is critical for the RB1-mediated poor prognosis in osteosarcoma.

Zocchi L., **Wu S.C.**, Gu Y., Cruz S., Benavente C.A. (in preparation) UHRF1 is dispensable for retinal development but critical for retinoblastoma tumor formation.

Zocchi L., Mehta A., **Wu S.C.**, Wu J., Gu Y., Wang J., Suh S., Spitale R.C., Benavente C.A. (in revision) Chromatin remodeling protein HELLS is critical for retinoblastoma tumor initiation and progression, Oncogenesis.

Wang S., Drummond M.L., Guerrero-Juarez C.F., Tarapore E., MacLean A.L., Stabell A.R., **Wu S.**, Gutierrez G., Benavente C., Nie Q., Atwood S. (submitted) Single-cell transcriptomics of human epidermis reveals basal stem cell transition states.

2018 **Wu S.C.**, Benavente CA. Chromatin remodeling protein HELLS is upregulated by inactivation of the RB-E2F pathway and is nonessential for osteosarcoma tumorigenesis. Oncotarget. 2018; 9 (66):32580-32592

Zocchi L, **Wu S.C.**, Wu J, Hayama KL, Benavente CA. The cyclin-dependent kinase inhibitor flavopiridol (alvocidib) inhibits metastasis of human osteosarcoma cells. Oncotarget. 2018; 9 (34):23505-23518

2015 Janesick, A., **Wu, S. C.**, Blumberg, B. Retinoic acid signaling and neuronal differentiation. Cell Mol Life Sci 2015; 72 (8):1559-76

AWARDS AND GRANTS

2018 Annual Ewha-UCI Symposium - 1st place poster presentation

2014-2015 California Institute for Regenerative Medicine (CIRM) Training Grant Award# TG2-01152

2012-2013 National Science Council Undergraduate Research Project NSC 101-2815-C-194-030-B

2012 Student Micro-symposia competition - 1st place

2009 Graduated with Outstanding Academic Achievement Award

ABSTRACT PUBLISHED

2019 Benavente, C.A., **Wu, S.C.**, Zocchi L, (2019). UHRF1 overexpression is a significant driver of tumor progression in RB-mediated cancers. Cancer Research, 79 (13 Supplement), 2148.

2018 **Wu, S.C.**, Benavente, C.A. (2018). Role of UHRF1 in tumorigenesis and metastasis of osteosarcoma. Cancer Research, 78 (19 Supplement), A41.

PRESENTATIONS

2019 "Role of UHRF1 in tumorigenesis and metastasis of osteosarcoma", **Wu, S.C.**, Benavente, C.A., –St. Jude National Graduate Student Symposium

2018 "Role of UHRF1 in tumorigenesis and metastasis of osteosarcoma", **Wu, S.C.**, Benavente, C.A., –AACR Special Conference on Pediatric Cancer Research (poster presentation)

2015 Chao Family Cancer Center Retreat (poster presentation)

TEACHING EXPERIENCE

2014-2019 Research mentor for Bio199 and PharmSci 199 students

2017 Teaching assistant for undergraduate level Cell Biology (D103)
Department of Developmental and Cell Biology
University of California, Irvine
Duties: Develop Problem based learning worksheets, hold weekly discussion sessions and pre-test review sessions.

2016 Teaching assistant for undergraduate level Molecular Pharmacology (PharmSci170B)
Department of Pharmaceutical Sciences
University of California, Irvine
Duties: Develop worksheets, lecture in weekly discussion sessions, and hold pre-test review sessions.

2015 Teaching assistant for undergraduate level Scientific Writing (Bio100)
School of Biological Sciences
University of California, Irvine
Duties: Hold weekly office hours, develop quiz questions, and grade written assays.

TECHNICAL EXPERIENCE

Cell Biology	Mammalian tissue culture Plasmid DNA transfection Recombinant virus production Viral transduction Stem cell reprogramming Bacterial and yeast culture Cloning Hypoxic treatment
Molecular Biology	Isolation of DNA, RNA and proteins Chromatin immunoprecipitation PCR, RT-QPCR Western blot analysis Whole-mount in situ hybridization
Histology	Mouse embryo sectioning Immunohistochemistry
Animal models	Xenopus laevis Housekeeping In Vitro fertilization Micro-injection of embryos Mus musculus Housekeeping Husbandry Genotyping Tumor grafting Subcutaneous, intraperitoneal, intravenous injections

ABSTRACT OF THE DISSERTATION

Elucidating the mechanism through which loss-of-function in *RB1* mediates poor prognosis in osteosarcoma

By

Stephanie Cherie Wu

Doctor of Philosophy in Biological Sciences

University of California, Irvine, 2019

Assistant Professor Claudia A. Benavente, Chair

Osteosarcoma is the most common primary bone malignancy in children and adolescents. Among the various molecular mechanisms implicated in osteosarcomagenesis reviewed in **Chapter 1**, the RB/E2F pathway is of particular importance as virtually all cases of osteosarcoma display alterations in the this signaling pathway. Loss of function mutations at the retinoblastoma (*RB1*) gene are associated with increased mortality, metastasis and poor therapeutic outlook in osteosarcoma. However, the mechanism(s) through which loss of RB worsens clinical outcome remain to be elucidated. We examined the transcription factor E2F family members that are associated with increased malignancy in RB-null osteosarcoma tumors and found that loss of activator E2Fs, E2F1 and E2F3, significantly delays tumor progression and increases the overall survival of the *Tp53*/*Rb1*-deficient osteosarcoma mouse model (**Chapter 2**). We then studied the role of two critical downstream effectors of the RB/E2F pathway, HELLS and UHRF1. While both are upregulated and overexpressed in osteosarcoma, we observed that HELLS has limited effect on tumor proliferation and migration. Loss of *Hells* in osteosarcoma has no effect in tumor initiation and overall survival

of osteosarcoma mice. This suggests that while HELLS may serve as a biomarker for tumorigenesis and for RB/E2F pathway status, it is unlikely to serve as a relevant target for therapeutics in osteosarcoma (**Chapter 3**). On the contrary, we showed that UHRF1 upregulation is critical in rendering osteosarcoma cells more aggressive. Using gain/loss-of-function assays to study the role of UHRF1 in osteosarcoma, we observed that UHRF1 is involved in promoting cell proliferation, migration, and invasion. Loss of *Uhrf1* in genetically engineered osteosarcoma model lengthens the life span of mice bearing osteosarcoma and decreases pulmonary metastases. These are described in **chapter 4**, where we discuss how UHRF1 mediates its tumor-promoting functions in osteosarcoma, and provide evidence supporting UHRF1 targeting as a novel therapeutic option. Taken together, this study illuminates new mechanistic insights of RB-mediated poor prognosis that could improve current therapeutic strategies of osteosarcoma, as well as other malignancies harboring RB/E2F pathway inactivation. Following our discovery, **chapter 5** documents our proposed methods in attempting to provide a more comprehensive mechanistic understanding of the RB-UHRF1 network.

CHAPTER 1

Introduction

Overview

Sarcomas are defined as malignancies that arise in tissues derived from the embryonic mesoderm such as bone, cartilage, fat, muscle and the vascular system [1]. Among various kinds of sarcomas, osteosarcoma (OS) is one of the many types of malignant neoplasms of bone origin. It is a mesenchymal tumor that is histologically characterized by the presence of malignant mesenchymal cells and the production of a bone stroma. Although OS can arise in all bones, the most common sites of occurrence include femur (42%), tibia (19%), and humerus (10%) [2]. More specifically, OS often occurs near the metaphyseal growth plates of these long bones. Other rare sites of occurrence include skull, jaw, pelvis, and ribs [3]. Patients with primary OS in the extremities generally display a better prognosis than those with primary tumor located at other sites [4]. The 5-year survival rate of localized OS is between 60-80%; however, 15-20% of OS patients present metastasis upon initial diagnosis, which significantly decreases 5-year survival rate to as low as 15-30% [2, 5, 6]. Pulmonary metastases are observed in approximately 50% of OS patients [4]. Unfortunately, survival rate of OS has plateaued ever since the introduction of adjuvant and neoadjuvant multiagent chemotherapy in the early 1980s [7]. The current treatment paradigm includes generic chemotherapeutic agents such as methotrexate, cisplatin, and doxorubicin.

Systematic review of the OS genomic landscape uncovers extensive inter- and intra-tumoral heterogeneity, harboring various chromosomal rearrangements, hypermutations, copy number alterations, etc. [8-10]. Some common genetic abnormalities in OS, including the most found genetic mutations in OS, tumor suppressor genes, *TP53* and *RB1* [8, 11] are reviewed later in this chapter.

OS cell of origin

The cell of origin and its relation to the observed heterogeneity in OS continues to be a heated topic in OS related research. Two conceptual models have been proposed to explain the intertumoral heterogeneity [12]. One model predicts that a single type of cell gives rise to various subtypes of OS (e.g. chondroblastic, fibroblastic and osteoblastic) depending on the genetic/epigenetic background the cell inherits and acquires. Another model suggests that different subtypes arise from cells in the differentiation lineage hierarchy from mesenchymal stem cells (MSCs) to matured osteoblasts [13]. As a malignancy that arises from the bone, it is generally agreed upon that transformation occurs somewhere along the osteogenic differentiation pathway, as MSCs commit to becoming pre-osteoblasts, mature into osteoblasts, and terminally differentiate into osteocytes.

The finding that mice bearing *Tp53* germline mutations are highly predisposed to different malignancies, including OS [14], marks the beginning of various efforts aiming to pinpoint the stage at which OS arises utilizing *in vivo* models. Clinical studies have indicated that in addition to *TP53*, genetic lesions in the *RB1* gene are the most significant recurrent genetic lesions observed in OS patients. Thus, the study of *Rb1* mutations along with *Tp53* is common in OS genetically engineered mouse models [8, 15-17].

Evidence suggesting that uncommitted MSCs are unlikely to be the cell of origin comes from the observation that subcutaneous injection of MSCs with homozygous deletion of *Tp53* or deletion of both *Tp53* and *Rb1* into mice results in mice developing leiomyosarcoma at higher rates than OS [18]. This observation has held true regardless of the source of MSC being bone

marrow-derived or adipose-derived. Subcutaneous injections of *Tp53*$^{-/-}$ and *Tp53*$^{-/-}$; *Rb1*$^{-/-}$ bone marrow-derived MSCs give rise to OS only when subjected to osteogenic differentiation prior to injection. This suggests that a committed progenitor such as pre-osteoblast or osteoblast is more likely to be the tumor-initiating cell [19]. Further support of the notion that a cell type committed to the osteogenic lineage is likely to be the OS cell of origin comes from studies using genetically engineered mouse models bearing conditional alleles to knockout of *Tp53* or a combination of *Tp53* and *Rb1* expressing Cre-recombinase downstream of various promoters driving allelic recombination at specific stages of osteogenic differentiation. The recombination of *Tp53* conditional alleles in uncommitted MSC using *Prx1-Cre* develops OS with a 61% penetrance, while homozygous deletion of *Tp53* in pre-osteoblasts, using *Col1a1-Cre* transgenic mice, have a 85% chance of developing OS instead of other sarcomas [20]. A better model, which utilizes preosteoblast-specific marker *Osterix* as a driver for Cre-recombinase (*Osx-Cre)* facilitates preosteoblast-specific loss of *Tp53*, resulting in osteosarcoma development with complete penetrance. Gene expression profiles, histology and metastatic potential of these *Osx-Cre* transgenic mice are also comparable to that of human OS [21]. Conditional double knockout of *Tp53* and *Rb1* in MSCs using *Prx1-Cre* transgenic mice, in preosteoblasts using *Col1a1-Cre* transgenic mice, and in osteocytes using *Oc-Cre* transgenic mice, give rise to osteosarcoma with ~100%, ~90%, and 44% penetrance, respectively [22]. Together, these studies suggest that transformation is likely to occur at the preosteoblastic stage of osteogenic differentiation.

In addition to the low penetrance of OS tumors in osteocyte-driven tumorigenesis, little evidence supports the notion of osteocytes being the tumor initiating cells of OS. As

terminally differentiated cells, osteocytes are less likely to give rise to heterogeneous tumors. The ability of osteocytes to give rise to tumor may be explained by the potential of osteocytes dedifferentiating into osteoblasts, thus regaining differentiation potency [23]. Injection of immortalized osteocyte cell lines give rise to OS that do not metastasize to lung, liver, nor spleen [24]. The development of tumors without metastatic potential suggests that the differentiation state from which the tumor arises does affect OS subtypes. This would be a direct contradiction from the finding that the differentiation state of the lineage from which tumors originate does not correlate with the differentiation state of tumors [22]. Given the complexity of evidences, it is likely that the two models of heterogeneity work together to affect tumor pathology and behavior.

Developmental models of osteosarcoma

As a disease of mesenchymal origin that arises within the bone and characterized by the unique production of osteoid, an unmineralized bone matrix, the osteogenic lineage stemming from the multipotent mesenchymal stem cells (MSCs) is heavily implicated in the origination of OS. It comes as no surprise that cell types along the osteogenic differentiation pathway are popular targets in which malignant transformations are induced for the establishment of developmental model of OS. The first genetically engineered mouse model (GEMM) to display OS was the H2K-cfos transgenic mouse model, where c-fos, a member of the activator protein 1 (AP-1) transcription factor, is overexpressed. Despite similar histopathology with human OS, the lack of metastatic potential in this model rendered it less suitable in studying the disease [25]. However, analyses done in OS arising from these

transgenic mice were the first piece of evidence suggesting that transformation of committed progenitors such as osteoblasts are more likely to be the cell of origin of OS [26]. The utilization of *Osterix*-driven cre recombinase (*Osx-cre*), a transgene that is actively expressed in preosteoblasts, leads to OS with high penetrance [21]. This model recapitulates many of the defining features of human OS including cytogenetic complexity, comparable expression signatures, histology and metastatic behavior. This model also exhibits the negative impact brought about by *RB1* mutations that potentiates OS. In our study, we used this *Osx-cre* transgenic mouse model to investigate the mechanisms behind loss of proliferative and epigenetic control.

Genetic abnormalities in the TP53 pathway

TP53 is the most frequently altered gene in cancer. Ever since the tumor suppressor function of *TP53* was described [27], it was established throughout the years that p53 function is abnormal in most human cancers. Most p53 inactivation is a result of genetic lesion in the *TP53* gene, which may lead to complete loss of p53, or p53 loss-/gain-of-function. In other cases, the p53 pathway is inactivated through the deregulation of proteins that are directly or indirectly involved in the pathway [28]. In OS, whole genome analyses have demonstrated a near-universal inactivation of the p53 pathway through different mechanisms. Mutation at the *TP53* gene results in genome instability, predisposing cells in the osteogenic lineage to aberrant transformation. Silencing of *TP53* is sufficient to drive OS tumorigenesis [21, 29]. A study conducted by Chen et al. analyzing whole-genome of 19 OS tumors acquire from patients revealed that while most of the genetic alterations in the *TP53* gene observed in OS

tumors are structural variations, other genetic events at the *TP53* gene including single-nucleotide variations, somatic splice-site mutations, insertions and deletions were also observed. Loss of heterozygosity at the *TP53* locus was evident in approximately half of the osteosarcoma tumors [8]. Interestingly, the mechanism through which the *TP53* gene is altered has no correlation with patient survival.

The activity of p53 is tightly regulated by oncoproteins MDM2 and MDMX (MDM4). Heterodimerization of these MDM homologs initiates MDM2-mediated ubiquitination of p53, which results in the degradation of p53 [30, 31]. In turn, *MDM2* is transcriptionally regulated by p53, thus creating a negative feedback loop [32-34]. Specifically, low MDM2 activity results in monoubiquitination and nuclear export of p53, whereas high MDM2 activity leads to polyubiquitination and nuclear degradation of p53 [35]. It comes as no surprise that mutations which lead to MDM2 and/or MDMX amplification would result in functional inactivation of p53. MDM2 gene amplification were observed more frequently in metastatic and recurrent OS compared to primary OS [36]. Immunohistological analysis of OS tumors correlates high MDM2 expression with high-grade OS or areas of dedifferentiation in low-grade OS [37], supporting the correlation between MDM2 gene amplification and tumor malignancy. Counterintuitively, down-regulation of MDMX has been associated with aggressive/advanced OS [38]. In fact, a tumor-suppressing role of this oncoprotein has been reported. The RING domain of MDMX was shown to suppress proliferation independent of p53 [39]. In addition, cancer cells, including OS cell line SJSA-1, that exhibit low endogenous level of MDMX was observed to have higher basal level of MDM2 [40]. It is unclear whether

the low MDMX expression in some cases is merely a result of excessive MDM2-mediated ubiquitination of MDMX [41], and that malignancy is still related to MDM amplification.

Following DNA damage or other stressors, p53 is activated, leading to transient expression of many proteins crucial for facilitating cell cycle arrest. Genetic or epigenetic alterations in these pathway members phenocopy *Tp53* loss, many of such events are reported in OS. Encoded by the CDKN2a gene, $p14^{ARF}$ act as a tumor suppressor by initiating p53-dependent cell cycle arrest and apoptosis through the inhibition of MDM2 [42]. Promoter hypermethylation of the CDKN2a gene has been reported in multiple OS cases. In a study that examined 32 osteosarcoma tissues, hypermethylation is correlated with decreased $p14^{ARF}$ protein expression and poor survival [43]. The cyclin-dependent kinase inhibitor, $p21^{Cip1}$ aids cell cycle arrest by blocking S-phase entry [44-46]. Low levels of $p21^{Cip1}$ was observed in OS cell lines, possibly a result of CUL4B overexpression in OS, a major component of an E3 ligase complex known to target for degradation $p21^{Cip1}$ [47]. Exogenous expression of $p21^{Cip1}$ is reported to sensitize OS cells to cisplatin [48]. Growth arrest and DNA damage (*GADD45*) is another gene activated by p53 in response to stress signals [49]. GADD45 facilitates cell cycle arrest by inhibiting the Cdc2/CyclinB1 complex [50, 51]. Hypermethylation on the CpG islands of GADD45A promoter that translates into reduced protein expression is observed in osteosarcoma cell line and xenografts [52]. Treatment with DNA demethylating agents relieved the epigenetic silencing of GADD45A in osteosarcoma cell lines but not in their drug-resistant counterparts [53].

Although a significant number of OS tumorigenesis is driven by loss-of-function mutation in the *TP53* gene, proteins directly or indirectly involved in the p53 pathway contributes a

significant amount to OS promotion, progression and metastasis. Alteration in expression of any member reviewed above either leads to functional inactivation of the p53 pathway, or contribute to increased malignancy of the disease.

RB/E2F pathway inactivation in osteosarcoma

In most human neoplasms, the RB pathway is functionally inactivated either by loss-of-function (null) mutation, deletion at the *RB1* gene or by alterations in expression and/or activity of upstream regulators such as *CDKN2A, CCND,* and *CDK4/6* [54]. Genetic or functional inactivation of the RB/E2F pathway seems to be indispensable for deregulated proliferation in most cancer settings [55]. In OS, the rate of loss of heterozygosity in *RB1* ranges from 29%-72% [56-59]. Multiple studies have shown that loss-of-function mutation in the *RB1* gene is correlated with a poor prognosis for patients with osteosarcoma [60-64]. Most often in OS, the RB pathway is inactivated by means other than *RB1* null mutation or deletion, in these cases, having an intact *RB1* translates to better clinical outlook in terms of the risk of developing metastatic disease, or sensitivity to chemotherapy, etc. [61, 65, 66]. Suggesting that loss of function due to genetic ablation of the *RB1* gene is not completely synonymous to theloss of E2F binding activity due to hyperphosphorylation of RB. However, the mechanism(s) through which *RB1* loss leads to poor prognosis in OS remain to be elucidated.

The *RB1* gene encodes for the tumor suppressor protein retinoblastoma (RB), whose most defined role is the modulator of cell cycle. RB represses transcriptional activation of genes required for S-phase entry by forming a transcriptional repression complex with the E2F

family of transcription factors [67]. In response to growth stimuli, the Cyclin D–CDK4/6 complex phosphorylates RB, releasing E2F and thereby allowing G1-S transition [68]. Since the association of RB with E2F family of transcription factors is pivotal for the negative control of cell cycle progression, we sought to determine which E2F family member(s) is RB acting through to mediate poor prognosis in OS. **Chapter 2** describes our effort in pinpointing activator E2Fs, specifically E2F1, as our research interest, and thereafter aimed to identify downstream effectors targeted by the RB-E2F1 complex.

In addition to E2F, RB associates with a large number of nuclear proteins, including a variety of chromatin-associated proteins that have diverse activities [69-71]. Research in the last decade highlight the complexity of the RB regulatory networks that ensure proper cell proliferation and identified multiple cellular functions beyond cell cycle regulation. Increasing evidence points to a role of RB as a molecular adaptor at the crossroads of multiple pathways, ensuring cellular homeostasis in different contexts including cell cycle, cellular differentiation, mitochondrial biogenesis, cell death and cancer progression [72].

RB has been implicated in regulating most major epigenetic processes, including DNA methylation, histone modifications, and microRNA regulation [73-77]. Helicase, Lymphoid specific (HELLS) and Ubiquitin Like with PHD and Ring Finger Domains 1 (UHRF1) came about as two candidates of particular interest, as both are presented not only as transcriptional targets of the RB-E2F1 complex deregulated upon RB loss, but also as chromatin remodeling proteins capable of exerting epigenetic functions globally. These

characteristics extends the function of RB regulatory network beyond the canonical role of cell cycle regulation.

HELLS

HELLS (helicase, lymphoid specific; also known as LSH) is a SWI/SNF-related matrix-associated regulator of chromatin [78, 79]. HELLS is a multidomain protein containing 7 putative helicase domains. Domain I contains the ATP-binding site and domain II contains the DExH box [80]. HELLS is critical for normal development of mammals by establishing DNA methylation patterns across the genome [81]. HELLS remodels chromatin to render DNA accessible to DNA methyltransferase enzymes Dnmt3a or Dnmt3b, but not Dnmt1, and therefore supports *de novo* DNA methylation and stable gene silencing during cellular differentiation [82, 83].

In retinoblastoma, HELLS was identified as a critical contributor of RB-mediated tumorigenesis [84]. Upregulation of HELLS following *RB1* inactivation is linked to the epigenetic deregulation of spleen tyrosine kinase (*SYK*), a key protein for human retinoblastoma survival [77, 84]. HELLS has an interesting connection to the RB/E2F pathway: the *HELLS* gene is a direct target of E2F1 [85] and HELLS protein interacts with E2F3 at several E2F target genes that control cell cycle entry [86]. Similar to the observation in retinoblastoma, depletion of HELLS in prostate cancer and breast cancer cell lines impairs growth, suggesting that HELLS may contribute to the malignant progression of other tumors [86, 87]. Indeed, several reports have shown that HELLS overexpression contributes to

malignant progression including renal cell carcinoma, gliomas, prostate cancer, melanoma, and nasopharyngeal carcinoma [88-92]. In astrocytomas and glioblastomas, upregulation of E2F1 correlated with increased HELLS expression and increased along with tumor grades [92]. However, the role of HELLS in tumor initiation, particularly in osteosarcoma, has never been examined prior to our effort. **Chapter 3** of this dissertation discusses the role of HELLS as a driver for tumorigenesis in a context-specific manner.

UHRF1

UHRF1 (a.k.a. Np95 and ICBP90) is an essential epigenetic "reader" and "writer" overexpressed in multiple human cancers including breast, lung, colorectal, prostate and bladder cancer [93-96]. This suggests that UHRF1 may play a role in carcinogenesis and is a putative anticancer therapeutic target. UHRF1 has several functional domains: NIRF_N (N-terminal ubiquitin-like) domain, TTD (Tandem Tudor Domain), PHD (Plant Homeo Domain), SRA (Set and Ring Associated) and RING (Really Interesting New Gene) finger domains. Through these domains, UHRF1 interacts with various proteins to facilitate various functions. UHRF1 is most known for its role in maintaining DNA methylation throughout replication by recruiting DNA methyltransferase 1 (DNMT1) to hemi-methylated DNA at the replication fork. This process is facilitated by its SRA domain [97, 98], which is also involved in the recruitment of histone deacetylase 1 (HDAC1) to methylated CpG islands [99]. UHRF1 can also interact with DNMT1 through the PHD domain. The TTD and PHD domains are involved in the readout of histone methylation such as H3K9me2/3 that are catalyzed by histone methyltransferases G9a and Suv39H1 [100, 101], and sometimes unmodified

histone such as H3R2 [102]. The RING domain has an E3 ligase activity involved in histone and protein ubiquitination [103-105]. The role of NIRF_N domain remains unclear, but may be required for protein-protein interactions and transport to aggresomes [106]. Further, two consensus RB-binding sequences (LXCXE) are found in the PHD domain and RING finger [107]. UHRF1 can also bind directly to DNA through a CCAAT motif under the regulation of protein kinase A [108, 109]. Acting concomitantly with its binding partners, it has been proposed that UHRF1 inhibits key tumor suppressors that are frequently mutated in lung, breast cancer, and retinoblastoma, including CDKN2A, BRCA1, and RB1 [77, 110, 111], through epigenetic silencing [112-115]. **Chapter 4** of this dissertation examined the consequences of endogenous UHRF1 overexpression and defined the mechanisms by which it modulates tumor progression in osteosarcoma.

CHAPTER 2

RB mediates poor prognosis in osteosarcoma through its association with activator E2F family of transcription factors, E2F1 and E2F3

Summary

OS is the most common primary bone malignancy presented in children and adolescents. Among the various molecular mechanisms implicated in osteosarcomagenesis, the RB/E2F pathway is of particular interest as virtually all cases of OS display alterations in the RB/E2F pathway, either directly through the mutation of *RB1* gene or indirectly through altered activity of other pathway components. As RB negatively regulates transcription activation of its downstream targets by means of associating with members of the E2F family of transcription factors, we sought to determine which E2F family member(s) are associated with increased malignancy in OS following RB loss. Through loss-of-function assays *in vitro*, we demonstrated that the ablation of a single E2F family member is insufficient to inhibit transcriptional activity of its downstream targets. Rather, functional inactivation of downstream targets requires the combinatorial knockdown of E2F1 and E2F3, suggesting compensatory mechanisms between the two aE2Fs. Using genetically engineered mouse models of osteosarcoma, we found that loss of activator E2Fs, specifically E2F1 and E2F3, significantly delays tumor progression and increases the overall survival of the *p53/Rb1*-deficient OS mouse model. These results put into focus the potential of E2F1 and/or E2F3 direct targets being the downstream effector of RB-mediated poor prognosis, as opposed to targets preferentially regulated by other E2F members.

Introduction

OS is a tumor of mesenchymal origin that is histologically characterized by the presence of malignant mesenchymal cells and the production of osteoids. Osteosarcomas are commonly characterized by an appendicular primary tumor with a high rate of metastasizing to the lungs [116]. The most common genetic findings in OS are the deregulation of the *TP53* and *RB1* tumor suppressor genes [8, 11]. Loss-of-function mutations of the *RB1* gene in osteosarcoma are associated with poor therapeutic outcome, as defined by increased mortality, metastasis, and poor response to chemotherapy [60-64]. Unfortunately, clinical outcomes for osteosarcoma patients have not substantially improved in over 30 years. As a result, the 5-year overall survival rate has remained stable at ~65% in case of local disease and ~20% for patients with metastatic disease [2, 5, 6, 117].

The *RB1* gene encodes the tumor suppressor protein RB. RB forms a transcriptional repression complex with the E2F family of transcription factors and thereby negatively regulates G_1-S transition during the cell cycle through the suppression of E2F target genes. There are six E2F family members that bind to the RB family and are classified as activator E2Fs (aE2Fs: E2F1, E2F2 and E2F3a) and repressor E2Fs (rE2Fs: E2F3b, E2F4, and E2F5) [118]. Of these, aE2Fs show preferential binding to RB protein. In response to growth stimuli, the cyclinD–CDK4/6 complex phosphorylates RB, relieving aE2Fs to facilitate the transcription activation of genes required to progress through G_1-S transition. A previous study performed in retinoblastoma, a childhood cancer caused by bi-allelic loss of *RB1*, indicated that retinal tumorigenesis was driven by E2F1- and E2F3-transcribed genes,

following the lack of transcriptional repression due to RB loss [84]. The same study also reported the participation in tumorigenesis of two chromatin remodeling proteins, Helicase, lymphoid specific (HELLS) and Ubiquitin-like, containing PHD and RING finger domains 1 (UHRF1). Both RB/E2F transcriptional targets, the roles of HELLS and UHRF1 in the context of OS are discussed in detail in later chapters (chapters 3 and 4). In this portion of our study, the expression of HELLS and UHRF1 were examined as a readout of the status of RB/E2F control.

We showed through loss-of-function assay that knocking down of a single activator E2F family member by itself has minimal to no effect on the transcriptional activity of downstream targets *HELLS* and *UHRF1*. The specific combination of E2F1 and E2F3 knockdown, however, was sufficient in reversing the otherwise upregulated and overexpressed targets. These data points to the presence of compensatory mechanisms between activator E2Fs, E2F1 and E2F3.

To study the role of E2Fs in OS tumor development, we proceeded to generate a series of genetically engineered mouse models of OS. As we validated previous reports describing E2F1 and E2F3 as the two aE2F members more heavily implicated in RB-mediated tumorigenesis, we focused on E2F1 and E2F3, while utilizing E2F5 as a rE2F control. We found that E2F1 and E2F3, more so E2F1 than E2F3, contribute to increased malignancy associated with loss of RB. These results stood as our rationale in investigating downstream effectors of the RB/E2F pathway that's preferentially regulated by the RB-E2F1 axis.

Results

Loss of E2F1 is functionally compensated by E2F3

To determine whether E2F1 is the member that RB mediates poor prognosis through, we performed loss-of-function assay by transducing human OS cell lines with lentiviral vectors encoding shRNAs targeting E2F1 (shE2F1). Interestingly, we found that E2F1 knockdown was not effective at reducing expression levels of its downstream targets, HELLS and UHRF1, in any of the OS cell lines examined (Figure 2.1A). To determine if other aE2F family members could compensate for the loss of E2F1, we acquired lentiviral vectors encoding shRNAs targeting E2F2 (shE2F2) and E2F3 (shE2F3). Knockdown of E2F2 or E2F3 using shE2F2 or shE2F3 alone did not affect expression of downstream targets. (Data not shown, Figure 2.1D); neither did the combination of shE2F1 and shE2F2 (Figure 2.1B). However, combinatorial knockdown of E2F1 and E2F3 using shE2F1 and shE2F3 together achieved a significant reduction in expression of downstream targets (Figure 2.1C).

To determine, functionally, if E2F1 loss can revert the increased malignancy in OS associated with loss of RB by means of reducing phenotypic characteristics commonly associated with malignancies, such as proliferation and migratory capacity, we generated growth curves using the CellTiter-Glo viability assay and compared E2F1 knockdown OS cells to their scrambled control. We found no difference in proliferation upon E2F1 knockdown (Figure 2.2A-D), consistent with our report that E2F1 knockdown alone being insufficient to repress transcriptional activation of downstream targets. E2F1 knockdown in OS cells has very minimal effect on OS cell migratory capacity, as revealed by scratch-wound assay. SJSA-1 remains the only OS cell line examined that exhibit statistically significant reduction of

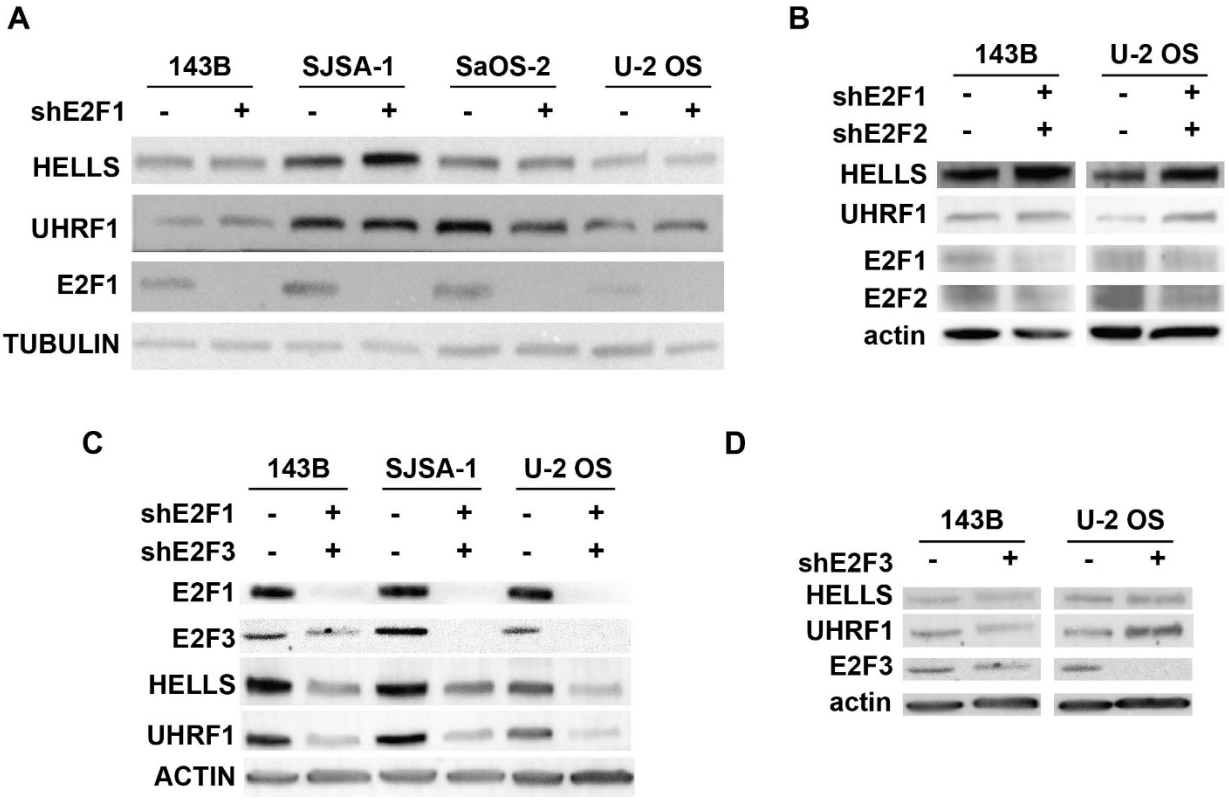

Figure 2.1. Combinatorial knockdown of E2F1 and E2F3, but not E2F1 or E2F3 alone is sufficient in repressing transcriptional activation of downstream targets.

(A-D) Western blot detection of HELLS and UHRF1 expression in OS cell lines upon (co-)transduction of shRNA targeting (A) E2F1, (B) E2F1 and E2F2 , (C) E2F1 and E2F3, (D) E2F3 through lentiviral vectors. Expressions of E2Fs were probed to verify sucessful knockdowns. Tubulin or actin as loading control.

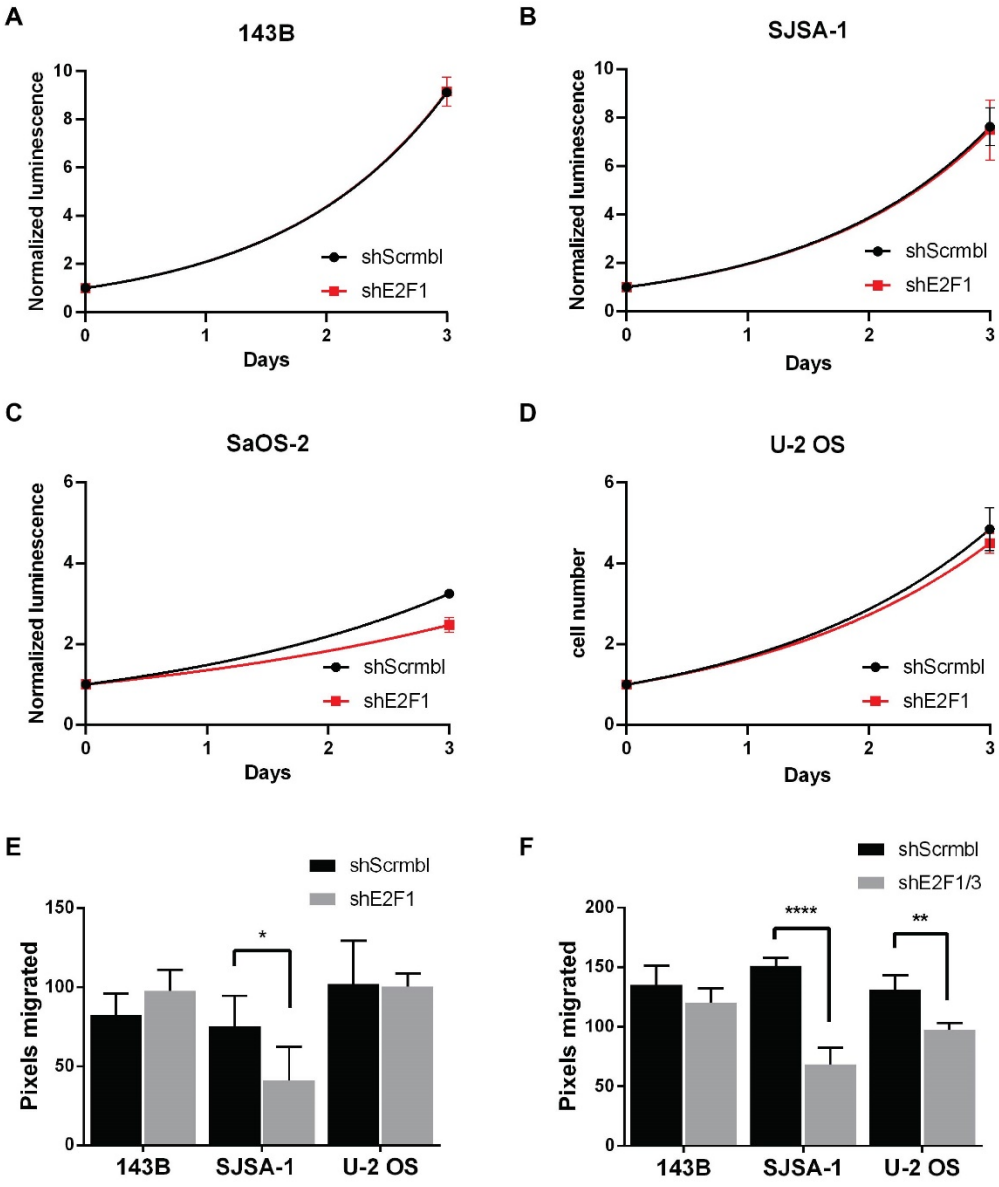

Figure 2.2. E2F1 knockdown alone is insufficent in repressing tumor phenotype.

(A-D) Growth curves of OS cells transduced with shRNA targeting E2F1(shE2F1) and scrambled control (shScrmbl) were generated through Cell TiterGlo viability assay. Luminescence measured correlates with cell viability. Fold change in luminescence normalized to day 0 of study were plotted. Each point is mean ± s.d. of triplicate samples. (E, F) Quantitative measurement of pixels migrated in scratch-wound assay in OS cells (co-) transduced with shRNA targeting (E) E2F1 (shE2F1) or (F) E2F1 and E2F3 (shE2F1/3) compared to scrabled control (shScrmbl). Each data point is mean ± s.d. of ten measurements in triplicate samples. *p < 0.0332, ** p < 0.0021, ****p < 0.0001 by two-tailed t test.

migratory capacity upon E2F1 loss (Figure 2.2E). In contrast, migratory potential all OS cell lines examined significantly decreased when E2F3 is knocked down along with E2F1 (Figure 2.2F), further validating functional compensation between these two aE2Fs. RT-QPCR analysis of E2F1 knocked-down OS cells reveals no difference in the transcriptional expression of other E2F members, suggesting that compensation upon E2F1 knockdown does not occur at the transcriptional level (Figure 2.3).

RB regulates tumor progression through E2F1 and E2F3

Recombination of *Tp53* in conditional knockout mice driven by *osterix-cre* recombinase (*Osx-cre*), a transgene that is actively expressed in more differentiated pre-osteoblasts, results in osteosarcoma with high penetrance (*p53* cKO: *Osx-cre; p53*$^{lox/lox}$). This disease model is potentiated by the loss of *Rb1* (*p53/Rb1* DKO: *Osx-cre; p53*$^{lox/lox}$*; Rb1*$^{lox/lox}$), recapitulating the negative impact of *RB1* mutations in human osteosarcoma [21]. Previous studies have shown that loss of *E2f1* and *E2f3*, but not *E2f5*, prevents retinoblastoma formation in *Rb1*-deficient mice [84, 119]. We hypothesized that in *Rb1*-deficient mice, aE2Fs (E2F1 and E2F3) constitutively facilitate transcriptional activation of downstream targets that associate with poor outcome.

To determine if loss of these E2F family members can revert the increased malignancy associated with loss of *Rb1*, we developed *Osx-cre; p53*$^{lox/lox}$*; Rb1*$^{lox/lox}$*; E2f1*$^{-/-}$ (*p53/Rb1/E2f1* TKO), *Osx-cre; p53*$^{lox/lox}$*; Rb1*$^{lox/lox}$*; E2f3*$^{lox/lox}$ (*p53/Rb1/E2f3* TKO), and *Osx-cre; p53*$^{lox/lox}$*; Rb1*$^{lox/lox}$*; E2f5*$^{lox/lox}$ (*p53/Rb1/E2f5* TKO) triple-knockout mice. To characterize the tumor incidence in these mouse models, we monitored mice weekly until

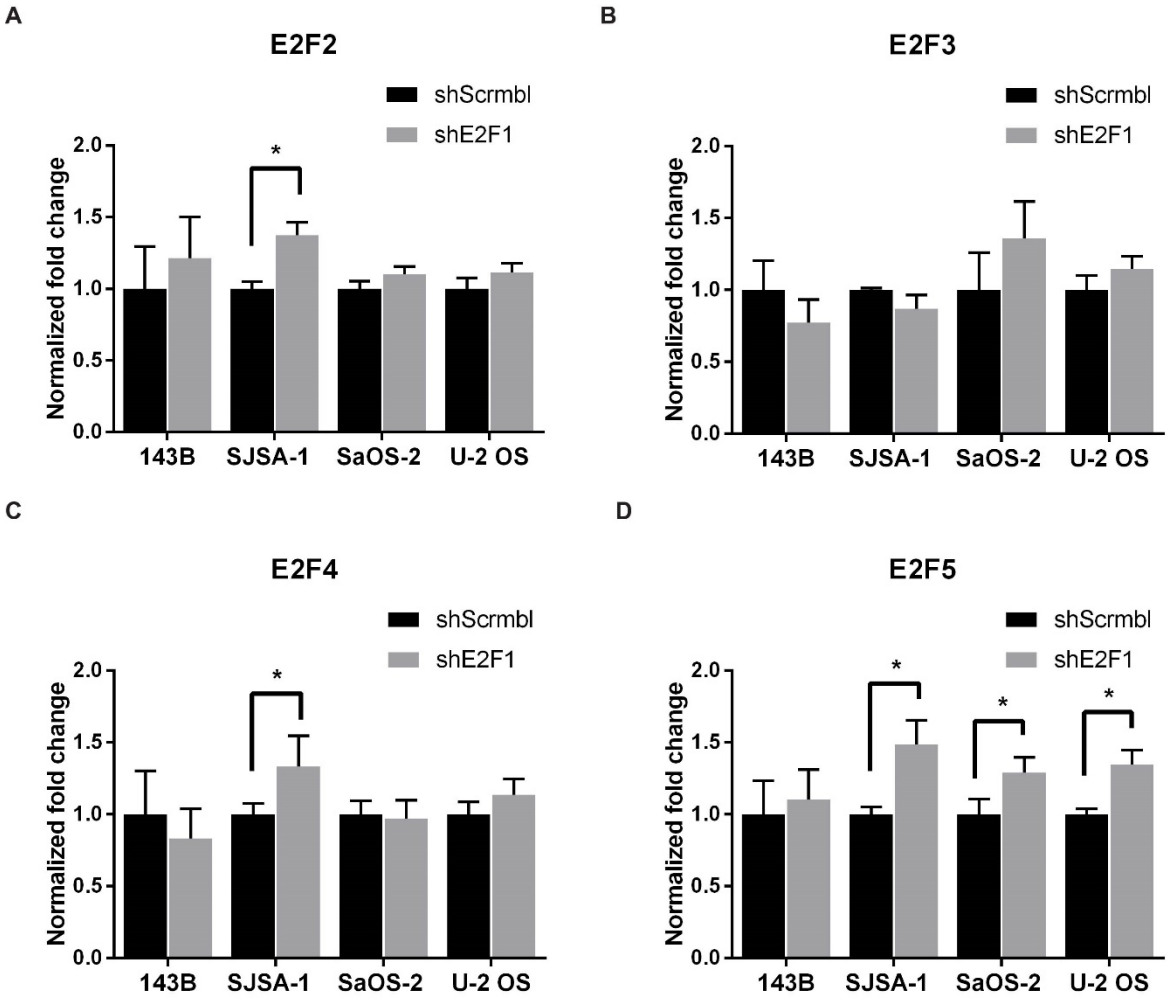

Figure 2.3. Compensation from other E2F family members upon E2F1 knockdown does not occur at the transcriptional level.

(A-D) RT-qPCR analysis of (A) *E2F2*, (B) *E2F3*, (C) *E2F4*, and (D) *E2F5* expression in OS cell lines transduced with shRNA targeting E2F1 (shE2F1), normalized to scrambled control (shScrmbl). Each point is mean ± s.d. of triplicate samples. *$p < 0.0332$, by two-tailed t test.

advanced tumor burden required euthanasia. 100% (n = 35) of the *p53* cKO mice developed tumors by 65 weeks with a median survival of 58.45 weeks (Figure 2.4A). 100% (n = 29) of the *p53/Rb1* DKO mice developed tumors by 40.4 weeks with a median survival of 26.9 weeks (Figure 2.4A). 100% (n = 25) of the *p53/Rb1/E2f1* TKO mice developed tumors by 48.6 weeks with a median survival of 37 weeks, significantly higher than *p53/Rb1* DKO mice (p = 0.0001; Figure 2.4B). 100% (n = 34) of the *p53/Rb1/E2f3* TKO mice developed tumors by 42.4 weeks with a median survival of 32.75 weeks, also significantly higher than p53/Rb1 DKO mice (p = 0.0104; Figure 2.4C). In contrast, 100% (n = 22) of the *p53/Rb1/E2f5* TKO mice developed tumors by 41.7 weeks with a median survival of 29.2 weeks, which was not significantly different from *p53/Rb1* DKO mice (p = 0.3783) (Figure 2.4D). Further, we found no significant gender differences in any of these mouse models (Figure 2.5).

Discussion

Preosteoblast-specific loss of *Tp53* is sufficient in driving OS tumorigenesis in mouse [21]. Disease presentation in this model is potentiated by the additional loss of *Rb1*, which we were able to recapitulate. Here, we tried to elucidate the mechanism through which RB inactivation contributes to poor clinical outcome in OS. We found that loss of either *E2f1* or *E2f3* significantly increased the median survival age of *p53/Rb1* DKO mice, loss of *E2f1* more so than *E2f3*; whereas loss of *E2f5* did not affect overall survival. These results are consistent with other studies reporting that loss of transcriptional control by

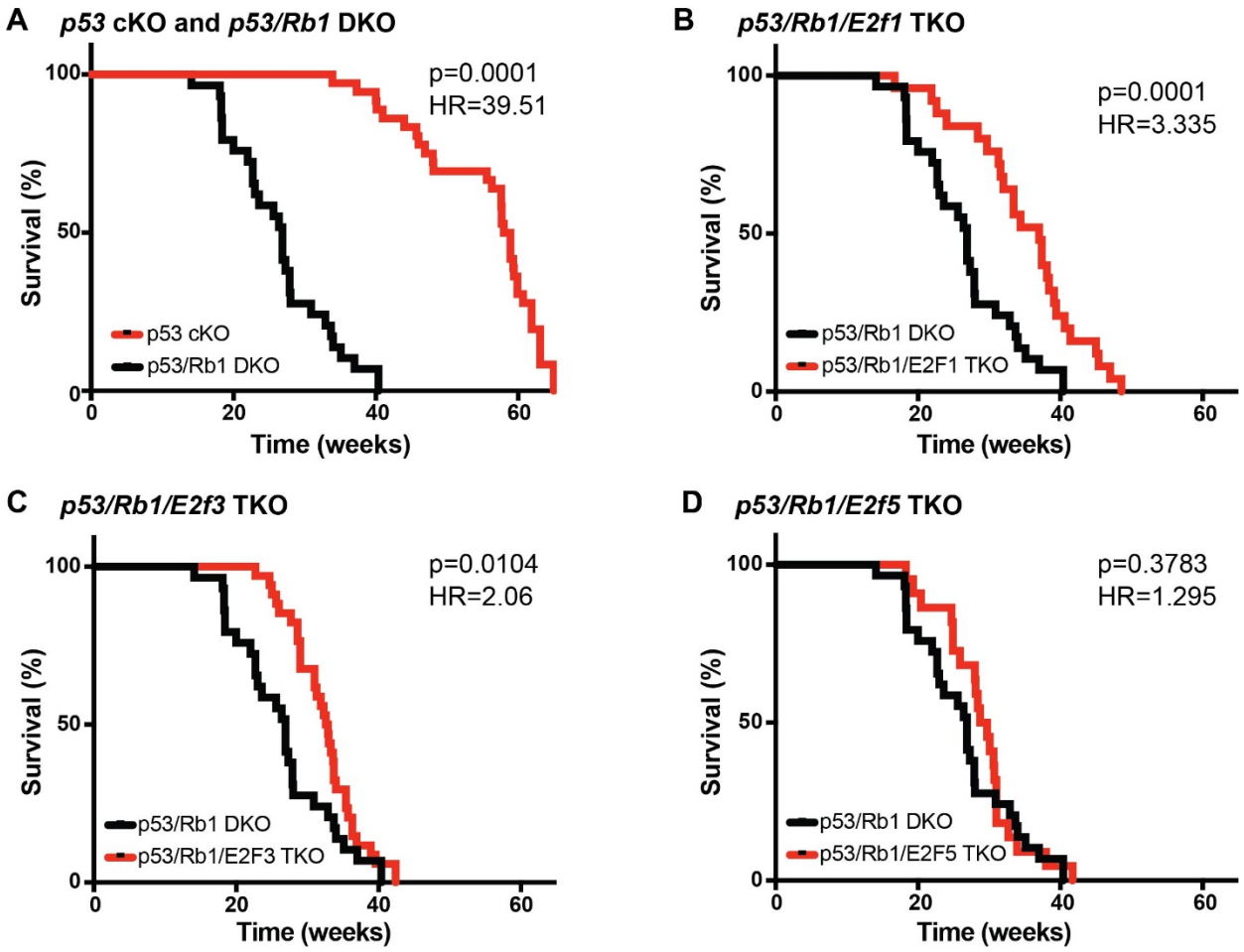

Figure 2.4. Loss of *E2f1* or *E2f3* increases survival in osteosarcomas bearing *Rb1* mutations

(A–D) Kaplan–Meier curves showing the survival of osteosarcoma-prone mouse models. (A) Mice bearing *Rb1* mutations *p53/Rb1* DKO: *Osx-cre*; $p53^{lox/lox}$; $Rb1^{lox/lox}$ (black, n = 29) have significantly shorter lifespan compared to *p53* cKO: *Osx-cre*; $Tp53^{lox/lox}$ (red, n = 35). This survival time was significantly increased in (B) *p53/Rb1/E2f1* TKO: *Osx-cre*; $p53^{lox/lox}$; $Rb1^{lox/lox}$; $E2f1^{-/-}$(red, n = 25) and (C) *p53/Rb1/E2f3* TKO: *Osx-cre*; $p53^{lox/lox}$;$Rb1^{lox/lox}$; $E2f3^{lox/lox}$ (red, n = 34); but not in (D) *p53/Rb1/E2f5* TKO: *Osx-cre*; $p53^{lox/lox}$;$Rb1^{lox/lox}$; $E2f5^{lox/lox}$ (red, n = 22). Mantel-Cox test and Mantel-Haenszel hazard ratio (HR) were used for curve comparisons.

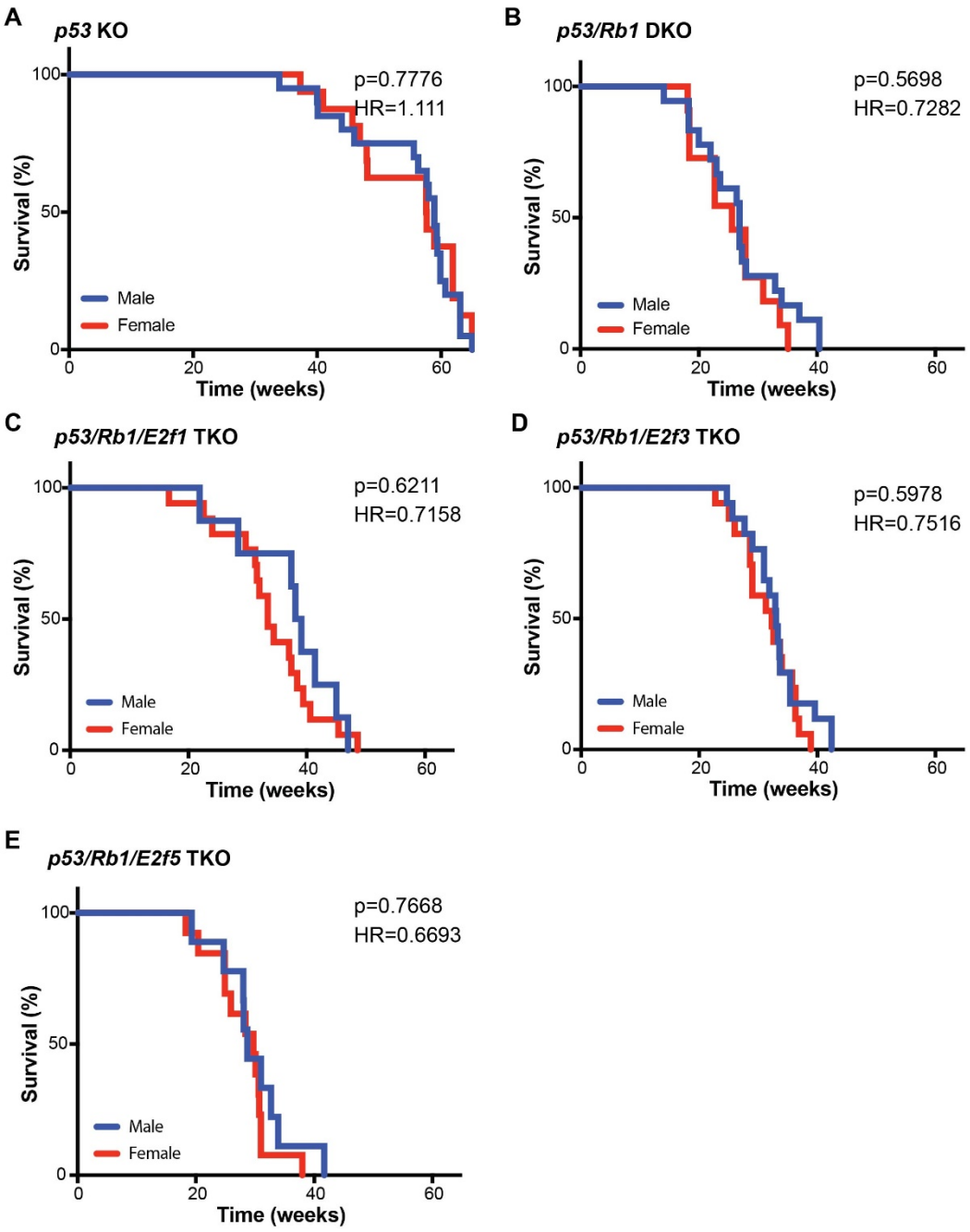

Figure 2.5. Osteosarcoma mouse models display no gender variation.

Kaplan–Meier curves showing the survival of osteosarcoma-prone mouse models divided by gender. (A) p53 cKO: *Osx-cre*; *p53lox/lox* (male: *n* = 19; female: *n* = 16). (B) p53/Rb1 DKO: *Osx-cre*; *Tp53*$^{lox/lox}$; *Rb1*$^{lox/lox}$ (male: *n* = 18; female: *n* = 11). Mantel-Cox test and Mantel-Haenszel hazard ratio (HR) were used for curve comparisons. (C) *p53/Rb1/E2f1* TKO: *Osx-cre*; *p53*$^{lox/lox}$; *Rb1*$^{lox/lox}$; *E2f1*$^{-/-}$ (male: *n* = 8; female: *n* = 17). (D) *p53/Rb1/E2f3* TKO: *Osx-cre*; *p53*$^{lox/lox}$;*Rb1*$^{lox/lox}$;*E2f3*$^{lox/lox}$ (male: *n* = 17; female: *n* = 17). (E) *p53/Rb1/E2f5* TKO: *Osx-cre*; *p53*$^{lox/lox}$;*Rb1*$^{lox/lox}$;*E2f5*$^{lox/lox}$ (male: *n* = 9; female: *n* = 13). Mantel-Cox test and Mantel-Haenszel hazard ratio (HR) were used for curve comparisons.

aE2Fs, particularly E2F1 and E2F3, is responsible for tumorigenesis following *Rb1* inactivation [84, 119-122]. However, in OS, loss of neither aE2F was sufficient to completely reverse the potentiation of the disease caused by *Rb1* loss. This could be due, at least in part, to compensation by other E2F family members. The observation that inactivation of either E2F1 or E2F3 could significantly increase the overall survival of OS-bearing mice hints that the increased malignancy upon *Rb1* loss might be reversible, and that direct downstream targets of aE2Fs are valuable potential therapeutic targets.

Interestingly, significant reduction of protein expression in downstream targets HELLS and UHRF1 was only achieved through combinatorial knockdown of E2F1 and E2F3, and not by E2F1 or E2F3 knockdown alone or the combination of E2F1 and E2F2. This suggests that E2F1 and E2F3 functionally compensate for the loss of each other to regulate the expression of their downstream targets. This observation could begin to explain why losses of neither *E2f1* (*p53/Rb1/E2f1* TKO) nor *E2f3* (*p53/Rb1/E3f3 TKO*) were sufficient to reverse the increased malignancy observed upon *Rb1* loss (*p53/Rb1* DKO) in OS but rather provided only partial improvements. The observation that the rescue of altered expression of RB/E2F transcriptional gene targets is orchestrated by more than one E2F family member is an important consideration for therapeutic approaches being developed that aim to inhibit E2Fs directly. Taken together, our observations underscore both the practicality and the value of targeting proteins transcriptionally regulated by the RB/E2F pathway, as opposed to directly alter E2Fs, which could be complicated by compensatory mechanisms between aE2Fs. Our data also suggests that targeting downstream effectors that are preferentially regulated by E2F1 and E2F3 are more likely to be efficacious.

Materials and methods

Mouse models of osteosarcoma and cell lines

The *p53*$^{lox/lox}$ and *Rb1*$^{lox/lox}$ conditional-knockout mice were obtained from the Mouse Models of Human Cancer Consortium at the National Cancer Institute; the *Osx-cre* mice were obtained from The Jackson Laboratory *E2f1*-knockout and *E2f3*$^{lox/lox}$ conditional knockout mice were obtained from Dr. Gustavo Leone (The Ohio State University); *E2f5*$^{lox/lox}$ mice were obtained from Dr. Joseph Nevins (Duke University). Mice were monitored weekly for signs of osteosarcoma. Moribund status was defined as the point when tumors had reached 10% body weight or induced paralysis in the mouse. The University of California Irvine Institutional Animal Care and Use Committee approved all animal procedures. Survival curves were generated using GraphPad Prism. Mantel-Cox test was used for statistical analyzes of the curves.

Osteosarcoma cell lines 143B, SJSA-1, SaOS-2 and U-2 OS, as well as MSCs and HEK293T cells were acquired from the American Type Culture Collection (ATCC). Cells were cultured in a humidified atmosphere at 37° C and 5% CO2. 143B were cultured in MEM (Gibco), with 10% BCS, penicillin/streptomycin, and 0.015 mg/ml BrdU. SJSA-1 were cultured in RPMI (Gibco), with 10% BCS and penicillin/streptomycin. SaOS-2 were cultured in McCoy's 5A (Gibco), with 15% BCS and penicillin/streptomycin. U-2 OS were cultured in McCoy's 5A (Gibco), with 10% BCS and penicillin/streptomycin. MSCs were cultured in Alpha-MEM (Gibco), with 10% FBS and penicillin/streptomycin. HEK293T cells were culture in high-glucose DMEM (Gibco), with 10% BCS, penicillin/streptomycin and sodium pyruvate. Cells were passaged

every 3 to 4 days or when they reached 70–80% confluency. At the time of passage, cells were split to 20% confluence.

Real-time RT-PCR

Total RNA was isolated from cells or tumor tissues by homogenizing samples with TRIzol Reagent. RNA was isolated through chloroform extraction. 1 μg of total RNA was used for cDNA synthesis with the SuperScript™III First-strand synthesis system (Invitrogen) according to manufacturer's protocol at a reaction volume of 20 μl. Quantitative PCR amplification was performed using 1 μl of reverse-transcribed product in Power SYBR Green PCR Master Mix (4367659, Life Technologies). Primers were designed using IDT Real-Time PCR tool (Integrated DNA Technologies). Reaction was carried out using 7500 Real-Time PCR system (Applied Biosciences). Data were normalized to those obtained with endogenous control 18S mRNA, and analyzed using ΔΔCt method. Primer sequence for PCR amplification are as follows: E2F2 (Forward 5′-CATGCTCCTAACTCCTTTCCC-3′; Reverse 5′-TCAGAACCATCCTAAAGCCAG-3′), E2F3 (Forward 5′-AAGACAGATGACACCAGCAC-3′; Reverse 5′-AGGAAGATAGTCTGCACCTTT-3′), E2F4 (Forward 5′-GTGTTTGCTTCTCCCTTTCTG-3′; Reverse 5′-TGGCAGGAACAAGACACTG-3′), E2F5 (Forward: 5′-ACTGCCACTAAACTGCCTG-3′; Reverse: 5′-TCCTCGTTTACATCCTTCACTTTA-3′), 18S (Forward 5′-GTAACCCGTTGAACCCCATT-3′; Reverse 5′-CCATCCAATCGGTAGTAGCG-3′).

Western blotting

Cell pellets or tumor tissues were homogenized by pipetting or pellet pestle in RIPA buffer (50 mM Tris-HCl, pH = 8, 150 mM NaCl, 1% NP-40, 0.5% Sodium deoxycholate, 0.1% SDS, 1

mM EDTA) supplemented with protease inhibitor (cOmplete™, Mini, EDTA-free Protease Inhibitor Cocktail, Roche). Samples were allowed to lyse for 30 min on ice before centrifugation at 14000 RPM at 4° C for 30 min. Protein concentration was measured using BCA protein assay (Pierce™ BCA Protein Assay Kit). 40 µg of total protein were resolved in 4–15% SDS-PAGE gel (Mini-PROTEAN TGX Gels (4–15%), Bio-rad), and transferred onto PVDF membrane (Immobilon-P Membrane, PVDF, EMD Millipore) using semi-dry transfer apparatus (Bio-rad). Ponceau S stain was used to validate successful transfer. Non-specific binding was prevented by incubating the membrane in 3% non-fat dry milk in TBS-0.25% Tween (TBS-T) for 1 hour at room temperature, shaking. Primary antibodies were diluted in 0.5% non-fat dry milk in TBS-T as follows: 1:1000 anti-HELLS (sc-28202, Santa Cruz Biotechnology), 1: 5000 anti-actin (A1978, Sigma), 1:1000 anti-Rb (9313T, Cell Signaling), 1:1000 anti-E2F1 (3742, Cell Signaling), 1:200 anti-E2F2 (sc-9967, Santa Cruz), and 2 µg/ml anti-E2F3 (PG37, Thermo Scientific). Membranes were incubated in primary antibody overnight, shaking, at 4° C. Membranes were then rinsed 3 times with TBS-T on shaker and incubated with secondary antibody for 40min at room temperature, shaking. Secondary antibodies were diluted in 0.5% non-fat dry milk in TBS-T as follows: 1:1000 peroxidase labeled anti-mouse IgG (PI-2000, Vector Laboratories), 1:1000 peroxidase labeled anti-rabbit IgG (PI-1000, Vector Laboratories). Membranes were again rinsed 3 times with TBS-T on shaker. Chemiluminescence was detected using SuperSignal™ West Pico Chemiluminescent Substrate (34077, Thermo Scientific). Relative band intensity was analyzed using ImageJ software.

Lentivirus production and transduction

Lentiviral particles were produced by co-transfecting the envelope plasmid pCMV-VSV-G (Addgene), packaging plasmid pCMV-dR8.2 dvpr (Addgene), and GIPZ shRNA vectors (GE Dharmacon): E2F1 shRNA (V3LHS_393591), E2F2 shRNA (V3LHS_324068), E2F3 shRNA (V3LHS_325936), or GIPZ lentiviral empty vector shRNA control into HEK293T cells using calcium phosphate transfection method. Supernatants containing lentiviral particles were harvested at 24 and 48 hours post-transfection. Cell debris were cleared by centrifugation at 1600 × g for 10 min at 4° C. Supernatants were then filtered through 0.45μm PES filter (25–223, Genesee Scientific), and concentrated by ultracentrifugation at 23000 RPM for 2 hours at 4° C. Lentiviral particles were resuspended in ice-cold PBS and stored at −80° C. Transduction of target cells were achieved by exposing cells to viral particles in serum-free condition for 6 hours. Puromycin selection was carried out at a concentration of 2 μg/ml.

Cell viability assay

All cells were seeded into 96-well black assay plates (Costar) at a density of 3,000 cells per well. Cell viability was determined at 24, and 96 hours after seeding using CellTiter-Glo (Promega) according to manufacturer's instructions. Luminescence readings were normalized to the 24 h post-seeding reading. Survival curves were generated using GraphPad Prism.

Scratch-wound healing assay

Scratch-wound assay was performed as previously described [123] Cells (1×10^6/well) were plated on 6-well plates. The day after, once cells were grown to a confluence of about 80%,

the monolayer was scratched using a 10 µl sterile pipette tip. Images were captured immediately and 8 h after the wound. The exact location of the image was marked to identify the same gap. The distances between the boundaries of the wound at 0 and 8 h at 10 different locations were measured in pixels using Zen software (Zeiss).

CHAPTER 3

Chromatin remodeling protein HELLS is upregulated by inactivation of the RB-E2F pathway and is nonessential for osteosarcoma tumorigenesis

Summary

Loss of function mutations at the retinoblastoma (*RB1*) gene are associated with increased mortality, metastasis and poor therapeutic outcome in several cancers, including OS. However, the mechanism(s) through which RB1 worsens clinical outcome remain to be elucidated. In this study, we investigated the role of helicase, lymphoid specific (HELLS), a chromatin remodeling protein identified as a critical downstream effector of the RB/E2F signaling pathway with high level expression in various cancers. Here, we confirmed that the RB/E2F pathway directly regulates transcriptional activation of *HELLS* gene. We showed that *HELLS* mRNA is upregulated, and its protein overexpressed in OS. Using loss-of-function assays to study the role of HELLS in human OS, we observed that HELLS has minimal to no effect on tumor proliferation and migration. Further, we pioneered the study of *Hells* in developmental tumor models by generating *Hells* conditional knockout OS mouse models to examine the role of HELLS in osteosarcoma tumor development. We found that loss of *Hells* in OS has no effect in tumor initiation and overall survival of mice. This suggests that while HELLS may serve as a biomarker for tumorigenesis that reflects RB/E2F pathway status, it is unlikely to serve as a relevant target for therapeutics in the context of OS.

Introduction

HELLS (helicase, lymphoid specific; also known as LSH) is a protein that belongs to the SNF2 family of chromatin-remodeling ATPases that contributes to global genome methylation [78, 79]. HELLS is critical for normal development of mammals by establishing DNA methylation patterns across the genome [81]. More specifically, HELLS facilitates *de novo* DNA methylation through its association with DNMT3A and DNMT3B, an event critical for stable gene silencing during cellular differentiation [124, 125]. In retinoblastoma, HELLS was identified as a critical contributor of Rb-mediated tumorigenesis [84]. In addition to retinoblastoma, several reports have shown that HELLS overexpression contributes to malignant progression including renal cell carcinoma, gliomas, prostate cancer, melanoma, and nasopharyngeal carcinoma [88-92]. In astrocytomas and glioblastomas, upregulation of E2F1 correlated with increased HELLS expression and increased along with tumor grades [92]. However, the role of HELLS in tumor initiation, particularly in osteosarcoma, has never been examined.

Since HELLS was identified as an activator E2F (aE2F) target gene and characterized as a critical contributor of tumorigenesis in retinoblastoma, we evaluated the role of HELLS in OS tumorigenesis. We demonstrated that activator E2Fs, E2F1 and E2F3, directly regulate *HELLS* expression. We proceeded to show that RB/E2F pathway inactivation, present in almost all OS cases, results in increased HELLS expression. Further, we evaluated the role of HELLS in OS cell survival, proliferation, migration, and tumorigenesis both *in vitro* and *in vivo*. We demonstrated that, unlike what has been observed in other malignancies, targeting

HELLS in human osteosarcoma has a modest effect in osteosarcoma survival and no effect on migration. Further, using a *Hells* conditional knockout mouse model, we found that loss of *Hells* has no effect on osteosarcoma tumor incidence and overall survival. This suggests that HELLS is not critical for tumor initiation and progression in OS.

Results

HELLS is overexpressed in both human and mouse osteosarcoma

A previous study in retinoblastoma identified HELLS as a key target gene downstream of the RB-E2F signaling pathway that is overexpressed following the loss of RB, and contributes to tumorigenesis [84]. Given that *RB1* loss in OS patients is associated with poor prognosis, we hypothesized that loss of RB potentiates OS through transcriptional deregulation of chromatin remodeling genes including *HELLS*. Initial analysis of The Cancer Genome Atlas (TCGA) data set of 263 sarcoma tumor samples indicated that *HELLS* is upregulated by 4.27-fold compared to normal controls, making HELLS an attractive target to study in OS (Figure 3.1A). Further analyses of *HELLS* gene expression using real-time qPCR in human OS cell lines (143B, SJSA-1, SaOS-2, and U-2 OS) and patient derived xenografts (PDX1-5) showed a significant upregulation of *HELLS* mRNA level in most OS samples when compared to human mesenchymal stem cells (MSCs) (Figure 3.1B, C). At the protein level, HELLS was also highly overexpressed across all analyzed osteosarcoma subjects compared to MSCs and human osteoblasts (hOB) controls (Figure 3.1D). Increased HELLS protein expression was observed even in U-2 OS and PDX2, which showed no upregulation at the mRNA level. Further, HELLS

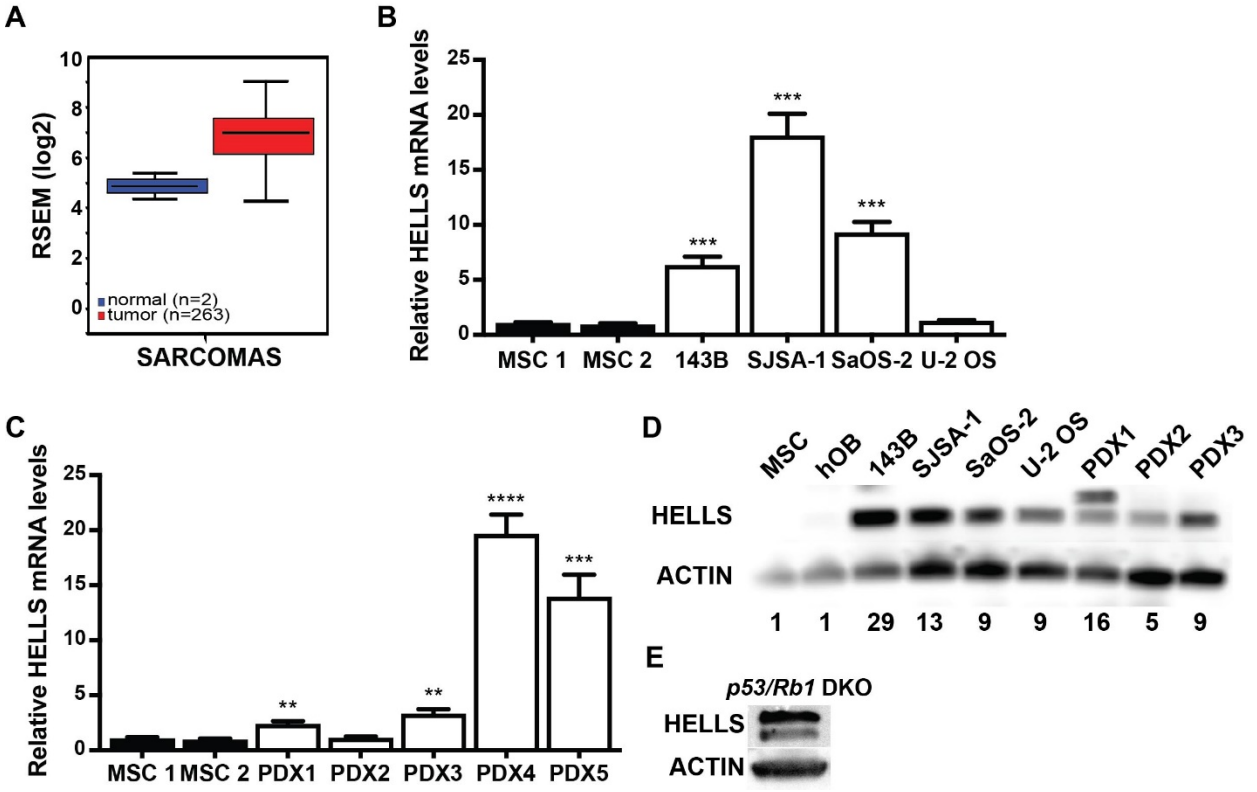

Figure 3.1. HELLS is overexpressed in human and mouse osteosarcoma

(A) The Cancer Genome Atlas data of RNA-Seq by Expectation-Maximation (RSEM) values from 263 human sarcoma samples (red) compared to normal control (blue) show a 4.27-fold increase in *HELLS* mRNA expression. (B–C) RT-qPCR analysis of *HELLS* mRNA expression in (B) 143B, SJSA-1, SaOS-2 and U-2 OS osteosarcoma cell lines and (C) patient-derived xenografts (PDX1-5), normalized to mesenchymal stem cells (MSC1 and MSC2). Each point is mean ± s.d. of triplicate samples. (D) Western blot detection of HELLS in osteosarcoma cell lines and PDXs show increased protein levels compared to two lineage progenitor controls, MSCs and human osteoblasts (hOB). Actin used as loading control. Band intensities were quantified by densitometry and normalized to MSC. (E) Western blot detection of HELLS in a mouse *p53*/*Rb1* DKO tumor. ** $p < 0.0021$, *** $p < 0.0002$, **** $p < 0.0001$ by two-tailed t test.

protein overexpression was also observed in the *p53/Rb1* DKO OS mouse model (Figure 3.1E). We also noted that some primary tumors, both in human and mouse, express a larger HELLS protein. Whether this is representative of post-translational modifications (HELLS can be phosphorylated, acetylated, ubiquitinated, methylated and sumoylated) or a HELLS isoform was not investigated.

HELLS is a direct target of the RB-E2F signaling pathway in the osteogenic lineage

Evidence of direct regulation of *HELLS* by the RB/E2F signaling pathway is limited to a single *in vitro* study in gliomas [92]. To confirm that the RB/E2F pathway transcriptionally represses HELLS, we performed chromatin immunoprecipitation analysis (ChIP) in the OS lineage of origin using MSCs. Motif mapping using MotifMap revealed a putative E2F1 binding motif within the promoter region of *HELLS*, 97 bp upstream of the start codon [126]. PCR primers were designed to flank this area of putative E2F1 binding motif. We observed enrichment of E2F1 at the consensus binding site within the *HELLS* promoter (Figure 3.2A).

Of the four OS cell lines used in this study, SaOS-2 is the only one bearing an *RB1* mutation that leads to loss of RB; however, HELLS overexpression were observed in all OS cell lines examined, suggesting pathway inactivation that in RB wildtype OS cells through indirect means. To assess the mechanism through which the RB/E2F pathway is being deregulated in the OS cell lines without *RB1* mutations, we analyzed *CDK4* and *CDK6* gene expression. *CDK4* and *CDK6* amplification and overexpression has been reported in some OS, resulting in RB hyperphosphorylation [127]. Real time qPCR analysis of *CDK4* showed a significant increase in its transcription in all osteosarcoma cell lines (Figure 3.2B). A

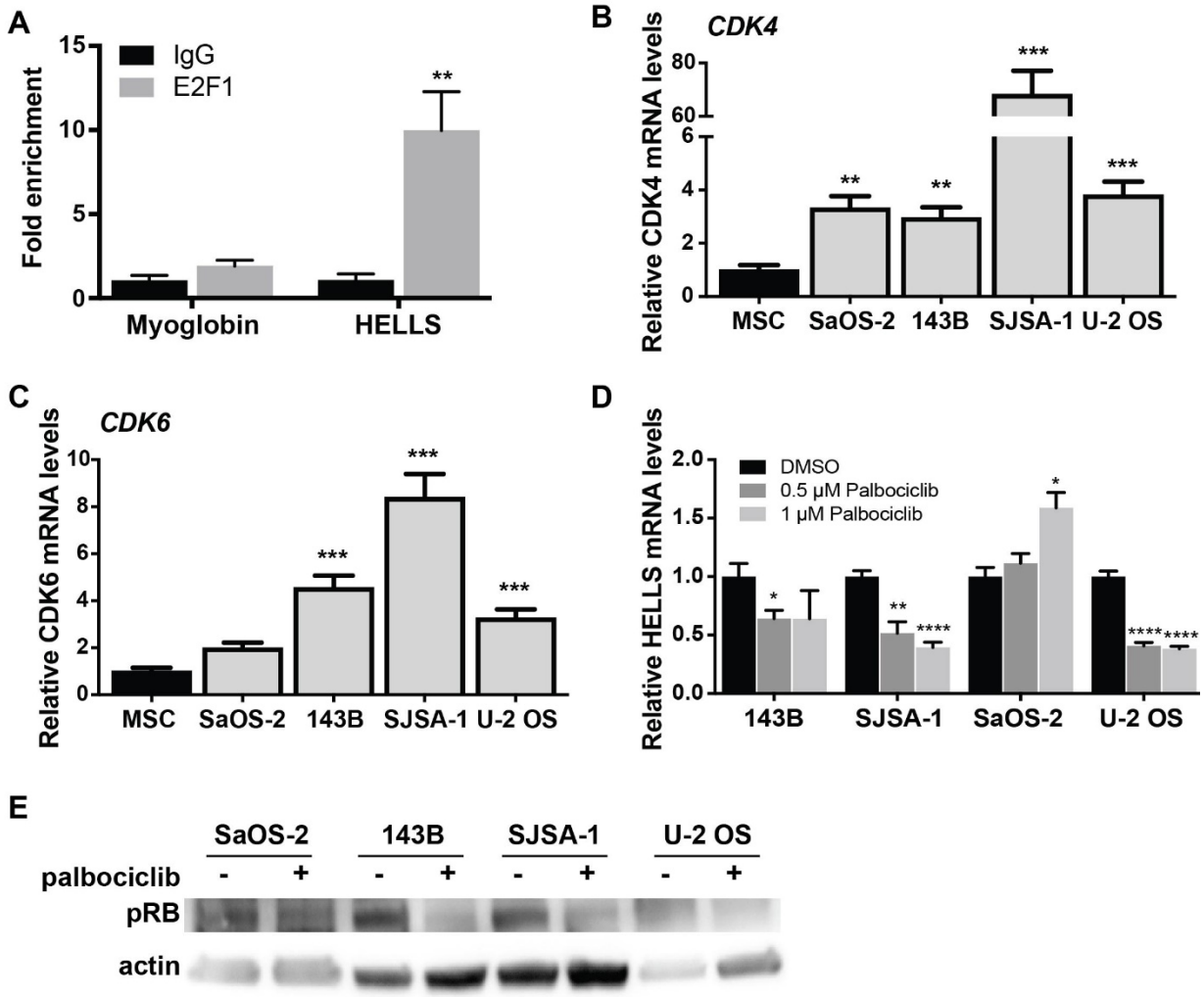

Figure 3.2. HELLS is a direct transcriptional target of the RB-E2F pathway

(A) Chromatin immunoprecipitation (ChIP) assay reveals enrichment of E2F1 within *HELLS* promoter. Primers flanking the myoglobin promoter were used as negative control. Each point is mean ± s.d. of triplicate samples. (B, C) RT-qPCR analysis of basal expression of (B) *CDK4* and (C) *CDK6* mRNA in different osteosarcoma cell lines normalized to mesenchymal stem cells (MSC). (D) RT-qPCR analysis of *HELLS* mRNA expression in osteosarcoma cell lines after Palbociclib-treated for 24 h, normalized to DMSO control cells. Each point is mean ± s.d. of triplicate samples. *p < 0.0332, ** p < 0.0021, ***p < 0.0002, ****p < 0.0001 by two-tailed t test. (E) Western blot detection of phosphorlyated RB level in osteosarcoma cells lines after 24 h Palbociclib treatment, compared to DMSO control cells.

particular high expression of *CDK4* was observed in SJSA-1, a cell line with known *CDK4* amplification [128]. *CDK6* was also upregulated in the 3 osteosarcoma cell lines without *RB1* mutations: 143B, SJSA-1 and U-2 OS (Figure 3.2C). In order to confirm that increased CDK4 and CDK6 activity results in RB hyperphosphorylation and result in overexpression of HELLS, we treated all four human OS cell lines with CDK4/6 inhibitor, palbociclib [129]. Real-time qPCR analysis of *HELLS* mRNA levels revealed significant decreases in *HELLS* expression upon palbociclib treatment, with the exception of the *RB1*-null cell line, SaOS-2, which served as a negative control (Figure 3.2D). Western blot analysis confirmed reduction in RB phosphorylation following palbociclib treatment (Figure 3.2E).

HELLS has limited effect on human osteosarcoma cell proliferation and no effect on migration

Emerging reports have linked HELLS overexpression in cancers with its ability to promote proliferation [84, 91]. To study the role of HELLS overexpression in osteosarcoma, we acquired a lentivirus encoding an shRNA sequence complimentary to *HELLS* (shHELLS) to facilitate HELLS gene knockdown in OS cell lines, as well as vector-only control. Western blot analysis was used to validate successful HELLS knockdown in each OS cell line (Figure 3.3A). We performed colony-forming assay on transduced osteosarcoma cell lines to assess their ability to give rise to colonies at a single-cell level. HELLS knockdown in OS cell lines results in modest reduction (31.6–40.5%) in the ability to form colonies when compared to controls but reached statistical significance in 143B and U-2 OS cell lines (Figure 3.3B, C). Further evaluation of cellular proliferation and survival upon HELLS knockdown using CellTiter-Glo cell viability assay revealed a significant increase in cell survival and proliferation in 143B

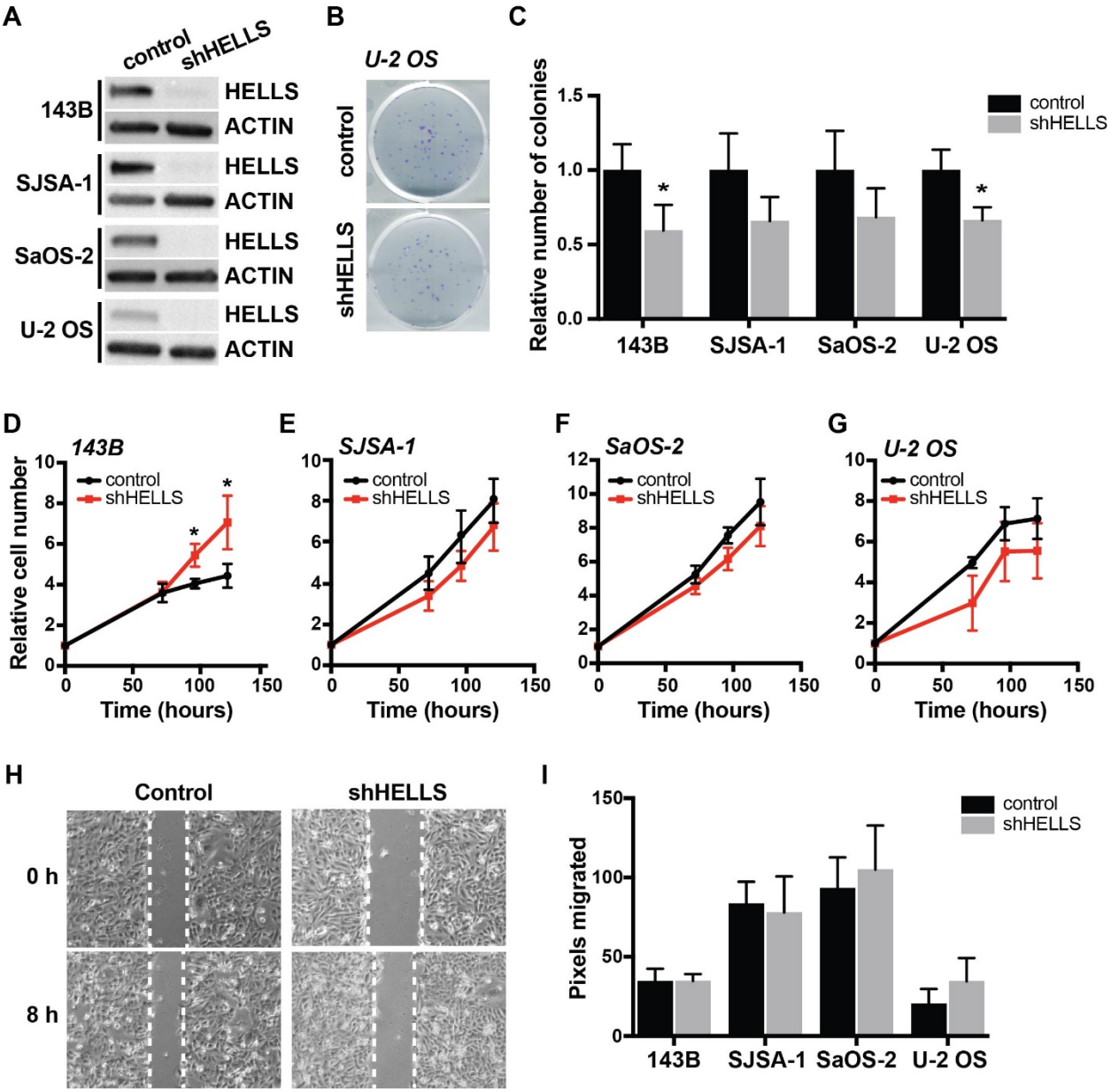

Figure 3.3. HELLS knockdown does not affect in osteosarcoma cell proliferation and migration

(A) Western blot detection of HELLS protein level in osteosarcoma cells after transduction with shRNA against HELLS (shHELLS) compared to non-silencing controls (control) show effective decrease in HELLS protein. (B) Representative images from colony-forming wells with U-2OS cells transduced with shHELLS or non-silencing control. (C) Histogram of the proportion of number of colonies formed in osteosarcoma cells transduced with shHELLS or non-silencing control. Each bar is the mean ± s.d. of triplicate experiments. (D–G) Relative number of shHELLS and control cells over time measured by CellTiter-Glo Luminescence cell viability assay. Each data point is mean ± s.d. of four experiments. (H) Representative image for control (non-silencing control) and shHELLS in 143B cells. (I) Quantification of the distance (pixels) migrated for each of the osteosarcoma cell lines. Each data point is mean ± s.d. of ten measurements in triplicate samples. *$p < 0.0332$ by two-tailed t test.

cells, but no significant change in the relative number of cells in SJSA-1, SaOS-2 and U-2 OS cells (Figure 3.3D-G). This confirms the modest decreases or absence of changes observed in the colony-forming assay.

HELLS expression is reported to be positively correlated with metastatic potential, shown by increased migratory capacity of cells [81, 89]. Using scratch-wound healing assay, we assessed changes in migration potential in HELLS knockdown and control OS cell lines. We detected no significant changes in the ability to heal the wounds within 8 h in any of the four cell lines analyzed (Figure 3.3H-J).

HELLS is dispensable for tumor initiation and progression in mouse OS

In order to study the role of HELLS in osteosarcomagenesis, we generated genetically engineered mice to facilitate preosteoblast-specific knockout of *Hells* in two distinct genetic engineered mouse models of osteosarcoma: *p53* cKO and *p53/Rb1* DKO [21]. The resulting *p53*/*Hells* DKO (*Osx-cre p53*$^{lox/lox}$; *Hells*$^{lox/lox}$) and *p53*/*Rb1*/*Hells* triple knockout (TKO; *Osx-cre p53*$^{lox/lox}$; *Rb1*$^{lox/lox}$; *Hells*$^{lox/lox}$) were compared to their corresponding littermate controls (*p53* cKO and *p53/Rb1* DKO, respectively) for the assessment of the role of HELLS in tumor initiation and promotion during osteosarcoma development. All genotypes lead to the development of osteosarcoma in mice with 100% penetrance. As seen in Figure 3.4A, no differences were detected between the mice bearing *Hells* conditional knockout alleles compared to their littermate controls. The median survival in *p53/Rb1/Hells* TKO mice was 27.7 weeks (n = 23) compared to 26.9 weeks (n = 29; p = 0.8805) in *p53/Rb1* DKO mice (Figure 3.4A). The median survival in *p53/Hells* DKO mice was

52.7 weeks (n = 22), compared to 58.45 weeks in *p53* cKO (n = 35; p = 0.9739) (Figure 3.4B). Intriguingly, analysis of gender differences between the *Hells*-null mice indicated a significantly lower survival in *p53/Hells* DKO females compared to males (p = 0.0057; Figure 3.5). Despite this difference, both males and females show no significant difference when compared to *p53* cKO mice (p = 0.2076 and p = 0.0851, respectively). Western blot analysis of *Hells* wildtype (*p53/Rb1* DKO and *p53* cKO) and *Hells*-null (*p53/Rb1/Hells* TKO and *p53/Hells* DKO) tumors confirmed that HELLS was efficiently knocked-out in these osteosarcomas (Figure 3.4C).

Discussion

Others and we have identified HELLS as a transcriptional downstream target gene of aE2Fs that is overexpressed in cancer and often times contributes to tumor progression [84, 89, 92]. To determine if *HELLS* is overexpressed in OS, we blasted The Cancer Genome Atlas (TCGA) data set and found that *HELLS* is upregulated in sarcoma tumor samples compared to normal controls. We confirmed *HELLS* gene upregulation in the human OS cell lines 143B, SJSA-1, and SaOS-2, as well as in four of the five independent patient-derived orthotopic xenografts used in this study. Despite the lack of mRNA upregulation in some cell lines and tumors, HELLS protein overexpression was observed in all the human OS cell lines and xenografts analyzed in this study. The discordance between mRNA and protein levels in some of the samples suggests that while HELLS protein levels are predominantly transcriptionally regulating, there are also translational and post-transcriptional regulatory

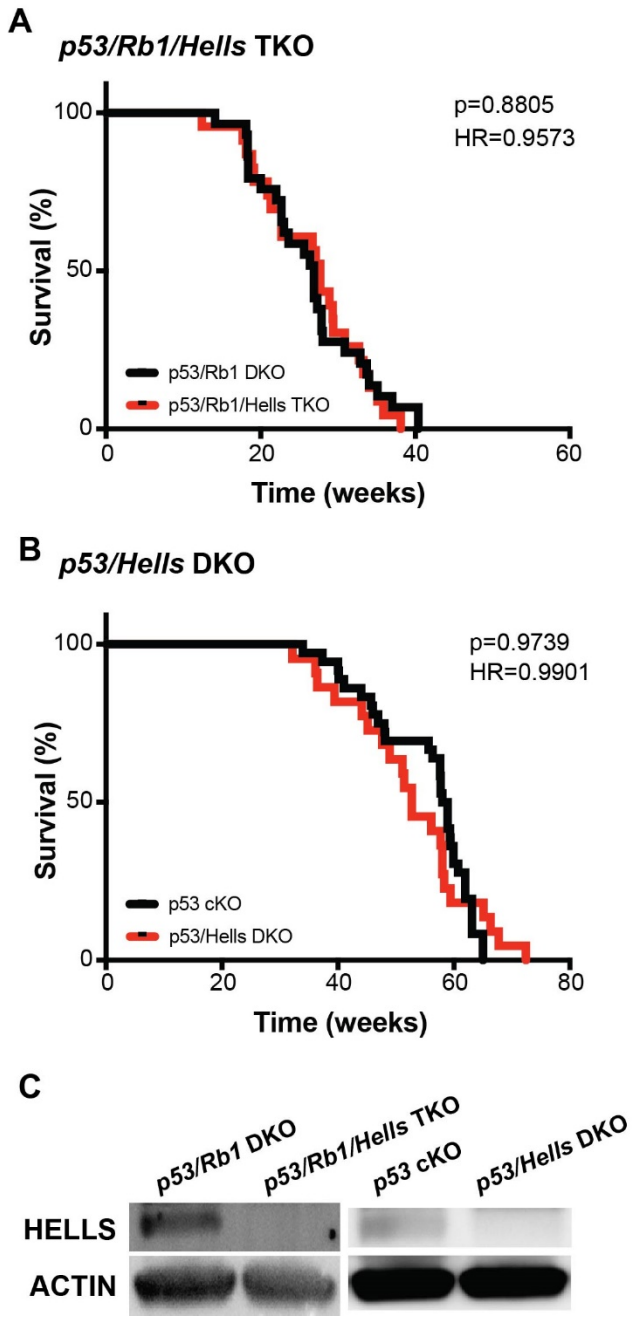

Figure 3.4. *Hells* has no effect on osteosarcoma tumorigenesis

(A–B) Kaplan–Meier curves showing the survival of osteosarcoma-prone mouse models. Loss of *Hells* in osteosarcoma-prone mice show no changes in overall survival in (A) *Tp53/Rb1/Hells* TKO: *Osx-cre; Tp53*$^{lox/lox}$*; Rb1*$^{lox/lox}$*; Hells* $^{lox/lox}$ (red; n = 23) compared to *p53/Rb1* DKO: *Osx-cre; Tp53*$^{lox/lox}$*; Rb1*$^{lox/lox}$ (black; n = 24) nor (B) *p53/Hells* DKO: *Osx-cre; p53*$^{lox/lox}$*; Hells* $^{lox/lox}$ (red; n = 22) compared to *p53* cKO: *Osx-cre; p53*$^{lox/lox}$ (black; n = 35). Mantel-Cox test and Mantel-Haenszel hazard ratio (HR) were used for curve comparisons. (C) Western blot detection of HELLS confirms loss of HELLS protein in *p53/Rb1/Hells* TKO mice and *p53/Hells* DKO mice and HELLS expression in *p53/Rb1* DKO and *p53* cKO osteosarcoma tumors.

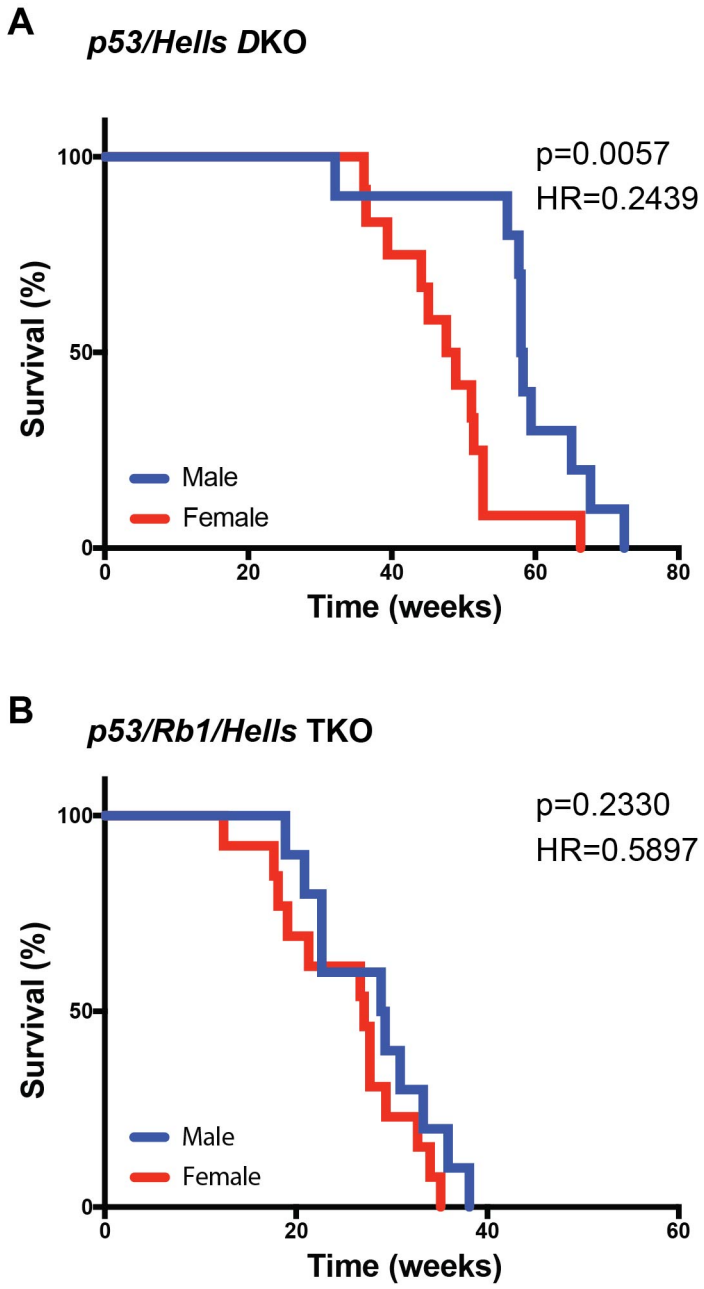

Figure 3.5: Males present a better prognosis in p53/Hells DKO mice.

Kaplan–Meier curves showing the survival of *Hells*-null osteosarcoma mouse models divided by gender. (A) p53/Hells DKO: *Osx-cre*; *Tp53*$^{lox/lox}$; *Hells*$^{lox/lox}$ (male: n = 10; female: n = 13). (B) *Tp53/Rb1/Hells* TKO: *Osx-cre*; *Tp53*$^{lox/lox}$; *Rb1*$^{lox/lox}$; *Hells* $^{lox/lox}$ (male: n = 10; female: n = 12). Mantel-Cox test and Mantel-Haenszel hazard ratio (HR) were used for curve comparisons

mechanisms of protein expression. Further, the HELLS protein overexpression observed in human OS is recapitulated in the *p53/Rb1* DKO osteosarcoma mouse model, strengthening its validity as a study model for this disease.

Little evidence supports the direct regulation of *HELLS* by the RB/E2F signaling pathway [92]. In this study, we confirmed that the RB/E2F signaling pathway directly regulates transcriptional activation of *HELLS* in the osteogenic lineage. ChIP analysis revealed enrichment of E2F1 on the promoter region of *HELLS* where putative E2F1 binding motifs reside. The RB/E2F signaling pathway is often inactivated in cancer due to reasons beyond *RB1* loss-of-function mutations or deletion, RB hyperphosphorylation through increased activity of CDK4/CDK6 being one example of the prevention of repression of E2Fs from binding to downstream targets. This could begin to explain why HELLS upregulation and overexpression in OS is not strictly limited to *RB1*-null cases, but rather a generalized event observed across samples that bear RB/E2F pathway inactivation. Of the OS cell lines examined in this study, SaOS-2 harbors a deletion in the *RB1* gene that leads to a non-functional truncated protein [130], SJSA-1 has *CDK4* amplification [128] (Figure 3.2B), and U-2 OS is *p16* null [131]. Here, we detected upregulation of *CDK4* and/or *CDK6* mRNA levels in all OS cell lines (Figure 3.2B, C), which suggests a predominant mechanism of RB/E2F pathway inactivation through RB hyperphosphorylation in OS. This was further confirmed by our observation of HELLS down-regulation upon treatment with CDK4/6 inhibitor, palbociclib.

The expression of HELLS has been positively associated with proliferation in both normal and malignant cells [78, 84, 89, 132]. Multiple studies have shown that HELLS knockdown *in vitro* results in decreased proliferation of various human neoplasms [81, 84, 89, 92], and that engraftment of cells carrying ectopically expressed HELLS gives rise to heavier tumor burden. In some cases, HELLS expression is positively correlated with metastatic potential, shown by increased migratory capacity of cells and promotion of epithelial to mesenchymal transition [81, 89]. In this study, we demonstrated that HELLS knockdown in OS cell lines modestly decreased colonizing capacity and had no effect on proliferation, except in 143B cells where we found increased proliferative capacity, contrary to what was expected. Further, we found no effect of HELLS on migratory potential in OS.

Beyond *in vitro* loss-of-function studies in human osteosarcoma models, we generated novel genetic engineered mouse models to study the role of *Hells* in OS tumor formation. We observed that *p53/Hells* DKO and *p53/Rb1/Hells* TKO mice showed no improvement in tumor incidence or overall survival compared to their respective littermate controls, *p53* cKO and *p53/Rb1* DKO. This result suggests that HELLS is not a critical driver of RB-mediated malignancy in murine OS tumors.

Taken together, our studies and others indicate that HELLS may be a reliable biomarker for RB/E2F pathway inactivation. However, HELLS upregulation may not always be synonymous to a critical role in tumorigenesis or tumor progression across various malignancies, nor a warranted target for therapeutics in all neoplasms where HELLS overexpression is observed.

Materials and methods

Xenografts, mouse models of osteosarcoma and cell lines

The five orthotopic xenografts used in this study: SJOS001105 (PDX1), SJOS001112 (PDX2), SJOS001107 (PDX3), SJSO010930 (PDX4), and SJOS001121 (PDX5) were obtained from the Childhood Solid Tumor Network [133]. Athymic nude (NU/J) mice were obtained from The Jackson Laboratories.

The $p53^{lox/lox}$ and $Rb1^{lox/lox}$ conditional-knockout mice were obtained from the Mouse Models of Human Cancer Consortium at the National Cancer Institute; the *Osx-cre* mice were obtained from The Jackson Laboratory. The Hells-conditional knockout mouse was generated from mice obtained from the European Mouse Mutant Archive, backcrossed to Flp mice for removal of the neo-cassette (tm1c conversion), and then backcrossed to C57BL/6N mice for Flp removal. Mice were monitored weekly for signs of osteosarcoma. Moribund status was defined as the point when tumors had reached 10% body weight or induced paralysis in the mouse. The University of California Irvine Institutional Animal Care and Use Committee approved all animal procedures. Survival curves were generated using GraphPad Prism. Mantel-Cox test was used for statistical analyzes of the curves.

Osteosarcoma cell lines 143B, SJSA-1, SaOS-2 and U-2 OS, as well as MSCs and HEK293T cells were acquired from the American Type Culture Collection (ATCC). Cells were cultured in a humidified atmosphere at 37° C and 5% CO2. 143B were cultured in MEM (Gibco), with 10% BCS, penicillin/streptomycin, and 0.015 mg/ml BrdU. SJSA-1 were cultured in RPMI (Gibco), with 10% BCS and penicillin/streptomycin. SaOS-2 were cultured in McCoy's 5A (Gibco),

with 15% BCS and penicillin/streptomycin. U-2 OS were cultured in McCoy's 5A (Gibco), with 10% BCS and penicillin/streptomycin. MSCs were cultured in Alpha-MEM (Gibco), with 10% FBS and penicillin/streptomycin. HEK293T cells were culture in high-glucose DMEM (Gibco), with 10% BCS, penicillin/streptomycin and sodium pyruvate. Cells were passaged every 3 to 4 days or when they reached 70–80% confluency. At the time of passage, cells were split to 20% confluence.

Real-time RT-PCR

Total RNA was isolated from cells or tumor tissues by homogenizing samples with TRIzol Reagent. RNA was isolated through chloroform extraction. 1 μg of total RNA was used for cDNA synthesis with the SuperScript™III First-strand synthesis system (Invitrogen) according to manufacturer's protocol at a reaction volume of 20 μl. Quantitative PCR amplification was performed using 1 μl of reverse-transcribed product in Power SYBR Green PCR Master Mix (4367659, Life Technologies). Primers were designed using IDT Real-Time PCR tool (Integrated DNA Technologies). Reaction was carried out using 7500 Real-Time PCR system (Applied Biosciences). Data were normalized to those obtained with endogenous control 18S and GAPDH mRNA and analyzed using ΔΔCt method. Primer sequence for PCR amplification are as follows: HELLS (Forward 5′-ACAGGCTGATGTGTACTTAACC-3′; Reverse 5′- TCCCCATGAAAAGCCTACTTC-3′), CDK4 (Forward 5′-ACACTGAGAGCGCAATCTTTG-3′; Reverse 5′-GAGAAATGGGAAGGAGAAGGAG-3′), CDK6 (Forward 5′-AAAGTGTTCCCTGCTACCATC-3′; Reverse 5′-CAG CATCAGGAACCATCTCTAG-3′), GAPDH (Forward: 5′-AGCAAGAGCACAAGAGGAAG-3′; Reverse: 5′-TCTACATGGCAACTGTGAGG-3′), 18S (Forward 5′-GTAACCCGTTGAACCCCATT-3′; Reverse 5′-CCATCCAATCGGTAGTAGCG-3′).

Western blotting

Cell pellets or tumor tissues were homogenized by pipetting or pellet pestle in RIPA buffer (50 mM Tris-HCl, pH = 8, 150 mM NaCl, 1% NP-40, 0.5% Sodium deoxycholate, 0.1% SDS, 1 mM EDTA) supplemented with protease inhibitor (cOmplete™, Mini, EDTA-free Protease Inhibitor Cocktail, Roche). Samples were allowed to lyse for 30 min on ice before centrifugation at 14000 RPM at 4° C for 30 min. Protein concentration was measured using BCA protein assay (Pierce™ BCA Protein Assay Kit). 40 µg of total protein were resolved in 4–15% SDS-PAGE gel (Mini-PROTEAN TGX Gels (4–15%), Bio-rad), and transferred onto PVDF membrane (Immobilon-P Membrane, PVDF, EMD Millipore) using semi-dry transfer apparatus (Bio-rad). Ponceau S stain was used to validate successful transfer. Non-specific binding was prevented by incubating the membrane in 3% non-fat dry milk in TBS-0.25% Tween (TBS-T) for 1 hour at room temperature, shaking. Primary antibodies were diluted in 0.5% non-fat dry milk in TBS-T as follows: 1:1000 anti-HELLS (sc-28202, Santa Cruz Biotechnology), 1: 5000 anti-actin (A1978, Sigma), 1:1000 anti-Rb (9313T, Cell Signaling). Membranes were incubated in primary antibody overnight, shaking, at 4° C. Membranes were then rinsed 3 times with TBS-T on shaker and incubated with secondary antibody for 40min at room temperature, shaking. Secondary antibodies were diluted in 0.5% non-fat dry milk in TBS-T as follows: 1:1000 peroxidase labeled anti-mouse IgG (PI-2000, Vector Laboratories), 1:1000 peroxidase labeled anti-rabbit IgG (PI-1000, Vector Laboratories). Membranes were again rinsed 3 times with TBS-T on shaker. Chemiluminescence was detected using SuperSignal™ West Pico Chemiluminescent Substrate (34077, Thermo Scientific). Relative band intensity was analyzed using ImageJ software.

Chromatin immunoprecipitation (ChIP assay)

ChIP assays were essentially performed as previously described [123, 134]. ChIP DNA was analyzed by qPCR with SYBR Green (Bio-Rad) in ABI-7500 (Applied Biosystems) using the following primers: Forward: 5′-CCTGAGAGAGGTCCAGGTAAA-3′; Reverse 5′-CTGTCATCTCGCGATACCTAAC-3′. The antibodies used were anti-E2F1 (3742; Cell Signaling) and rabbit IgG (sc-2027, Santa Cruz Biotechnologies).

Palbociclib treatment

Osteosarcoma cells were seeded at a density of 500000 cells/well of 6-well plate and allowed to adhere overnight. Two concentrations of Palbociclib, 0.5 μM and 1 μM, were used to treat cells for 24 h prior to collection. DMSO was used as drug vehicle control.

Lentivirus production and transduction

Lentiviral particles were produced by co-transfecting the envelope plasmid pCMV-VSV-G (Addgene), packaging plasmid pCMV-dR8.2 dvpr (Addgene), and GIPZ shRNA vectors (GE Dharmacon): HELLS shRNA (V2LHS_155497), or GIPZ lentiviral empty vector shRNA control into HEK293T cells using calcium phosphate transfection method. Supernatants containing lentiviral particles were harvested at 24- and 48-hours post-transfection. Cell debris were cleared by centrifugation at 1600 × g for 10 min at 4° C. Supernatants were then filtered through 0.45μm PES filter (25–223, Genesee Scientific), and concentrated by ultracentrifugation at 23000 RPM for 2 hours at 4° C. Lentiviral particles were resuspended in ice-cold PBS and stored at −80° C. Transduction of target cells were achieved by exposing

cells to viral particles in serum-free condition for 6 hours. Puromycin selection was carried out at a concentration of 2 μg/ml.

Cell viability assay

All cells were seeded into 96-well black assay plates (Costar) at a density of 3,000 cells per well. Cell viability was determined at 24, 72, and 96 hours after seeding using CellTiter-Glo (Promega) according to manufacturer's instructions. Luminescence readings were normalized to the 24 h post-seeding reading. Survival curves were generated using GraphPad Prism.

Colony formation assay

Lentiviral transduced cells were seeded at a low-density (20 cells/cm^2) as single cells onto 6-well cell culture plates in the appropriate cell culture medium. Fresh medium was supplemented every 4 days. Cells were incubated at 37° C with 5% CO2 until cells in control dishes have formed sufficiently large colonies (~50 cells). Cells were washed once in PBS before fixing and staining in a mixture consisting of 6% glutaraldehyde and 0.5% crystal violet for 30 min. Stains were washed out with tap water and the plates left to dry at room temperature. Colonies were counted from triplicate experiments.

Scratch-wound healing assay

Scratch-wound assay was performed as previously described [123] Cells (1×10^6/well) were plated on 6-well plates. The day after, once cells were grown to a confluence of about 80%, the monolayer was scratched using a 10 μl sterile pipette tip. Images were captured

immediately and 8 h after the wound. The exact location of the image was marked to identify the same gap. The distances between the boundaries of the wound at 0 and 8 h at 10 different locations were measured in pixels using Zen software (Zeiss).

CHAPTER 4

UHRF1 overexpression drives the poor prognosis associated with functional inactivation of the RB-E2F pathway in osteosarcoma

Summary

The primary cause of mortality in OS stems from its highly metastatic nature, with 15-20% of OS patients diagnosed after the cancer has already metastasized (pulmonary metastasis being the most common), which translates to 5-year survival rate of <40% [2]. Genetic alterations at the *RB1* gene have been long associated with poor clinical outcome in OS. We investigate in this study, a downstream effector of RB-mediated malignancy. Ubiquitin-like with PHD and Ring Finger domains 1 (UHRF1) has been identified as a critical downstream target of the RB/E2F signaling pathway that is overexpressed in various cancers. Here, we show that UHRF1 upregulation is critical in rendering OS cells more aggressive. We confirmed that *UHRF1* is transcriptionally regulated by the RB/E2F pathway and found that the *UHRF1* gene is upregulated and its protein overexpressed in osteosarcoma. Based on gain- and loss-of-function assays, we report that UHRF1 promotes cell proliferation, migration, invasion, and metastasis. Genetic engineered mouse models also substantiated that *Uhrf1* loss dramatically reverses the effects of *Rb1* loss. Using RNA-seq, we've identified the involvement of Urokinase-type plasminogen activator (uPA) in UHRF1-mediated cell mobility. Our work presents a new mechanistic insight into RB loss-associated poor prognosis, revealing UHRF1 as a critical driver of tumor promotion and tumor progression in OS. This study provides substantial support for UHRF1 targeting as a novel therapeutic option to improve current treatment for OS and other cancers with RB/E2F pathway inactivation.

Introduction

A previous study in retinoblastoma identified Ubiquitin-like, containing PHD and RING finger domains 1 (UHRF1) as a key target gene downstream of the RB/E2F signaling pathway that is abnormally upregulated following the loss of RB, and contributes to tumorigenesis [84]. In normal cells, the expression of UHRF1 peaks during G1-S transition as it is required for S-phase entry [135]. While its expression in normal cells oscillates during cell cycle, UHRF1 is constitutively expressed throughout all phases in cancer cells and was recognized as a putative oncogene [136]. However, beyond its association with cell cycle progression, UHRF1 is a multi-domain protein that exerts various functions that include, but are not limited to, reading and writing of epigenetic codes, thus having the potential to significantly impact epigenome upon deregulation. It is most known for its role in maintaining DNA methylation throughout replication by recruiting DNA methyltransferase 1 (DNMT1) to hemi-methylated DNA at the replication fork. In recent years, many reports have emerged having observed the overexpression of UHRF1 in different types of human cancers including lung, breast, prostate, bladder, colorectal cancer, and retinoblastoma [84, 94-96, 137]. Given that loss-of-function mutation in the *RB1* gene is associated with increased risk of developing metastatic OS and resistance to chemotherapy compared to patients with intact *RB1 [61, 65, 66]*, we hypothesized that loss of RB in OS contributes to tumor progression and increased malignancy through deregulation of its downstream target UHRF1.

In this study, we've successfully characterized UHRF1 as a key regulator that promotes proliferation, migration, and invasion of OS cells. *In vitro*, CRISPR-cas9 mediated knockout of

UHRF1 decreased clonogenicity, lengthens doubling time, as well as impairing migratory capacity of OS cells. With RNA-seq and gene ontology analysis, we've uncovered potential mechanism of UHRF1-mediated cell migration through the identification of urokinase-type plasminogen activator (uPA). uPA is a serine protease encoded by the *PLAU* gene that has long been associated with tumor malignancy. Upon conversion of plasminogen into plasmin, uPA triggers a proteolytic cascade that led to the degradation of extracellular matrix, an event necessary for angiogenesis and metastasis. Levels of uPA is therefore an established prognostic marker in several cancers such as breast, lung, bladder cancer, as well as soft tissue sarcomas, with its activity often associated with metastatic behavior [138-141]. We showed that UHRF1 level reflects in the transcriptional activity of *PLAU*, which translate to a positive correlation of UHRF1 and uPA level in OS cells and tumors. Moreover, UHRF1 induced cell migration can be reversed by treatment with amiloride [142], an uPA inhibitor.

To study the role of UHRF1 in a developmental OS model, we further the use of an OS mouse model previously described by the Walkley group, where preosteoblastic knockout of *Tp53* and *Rb1* are facilitated by osterix driven Cre-recombinase (*Osx-Cre*) [21]. Upon introduction of preosteoblast-specific loss of *Uhrf1* in OS mouse model, we found that loss of Uhrf1 lengthens OS mice life span by delaying age of tumor detection, suggesting a role of *Uhrf1* in aiding OS tumorigenesis. We also observed significantly decreased incidence of pulmonary metastasis. The substantial degree of *Uhrf1* loss reverting the malignancy brought about by RB loss presents *Uhrf1* as a novel therapeutic target that holds the potential to eliminate the main cause of mortality of OS.

Results

UHRF1 is overexpressed in human and mouse OS

Our previous work identified *UHRF1* as a target that is overexpressed in cancer when *RB1* is inactivated and plays a significant role in the epigenetic changes that drive tumor progression in retinoblastoma [84]. Upon examination of The Cancer Genome Atlas (TCGA) database, we found that *UHRF1* is significantly overexpressed in sarcomas, with a median expression of 8.63 (log2) in sarcoma tumors compared to 4.47 in normal tissue (>17-fold, Figure 4.1A). *In situ* hybridization of a human OS tissue array identified the presence of *UHRF1* mRNA in the 25 primary OS tumors located in femur, tibia, and rib examined (Figure 4.1B). A larger proportion of samples expressing high *UHRF1* mRNA levels were classified as stage II than stage I OS (Figure 4.1C), suggesting that UHRF1 expression increases in more advanced tumors. However, the limited number of stage III and stage IV samples available restricted our analysis. This led us to examine UHRF1 mRNA and protein levels in 4 different human OS cell lines: 143B, SJSA-1, SaOS-2 (RB-null cell line), and U-2 OS, along with 5 patient-derived orthotopic xenografts (PDX1-5). QPCR analysis of human OS cell lines and patient derived xenografts (PDX1-5) showed a significant upregulation of *UHRF1* mRNA level in all samples except PDX2 when compared to human mesenchymal stem cells (MSCs), independent of whether they express RB protein or not (Figure 4.1D-E , 4.2A). At the protein level, UHRF1 is highly overexpressed across all analyzed OS subjects compared to control (Figure 4.1F-G). Furthermore, overexpression of UHRF1 protein is also observed in genetic engineered mouse models of OS in comparison to mouse MSCs (mMSCs) (Figure 4.1H).

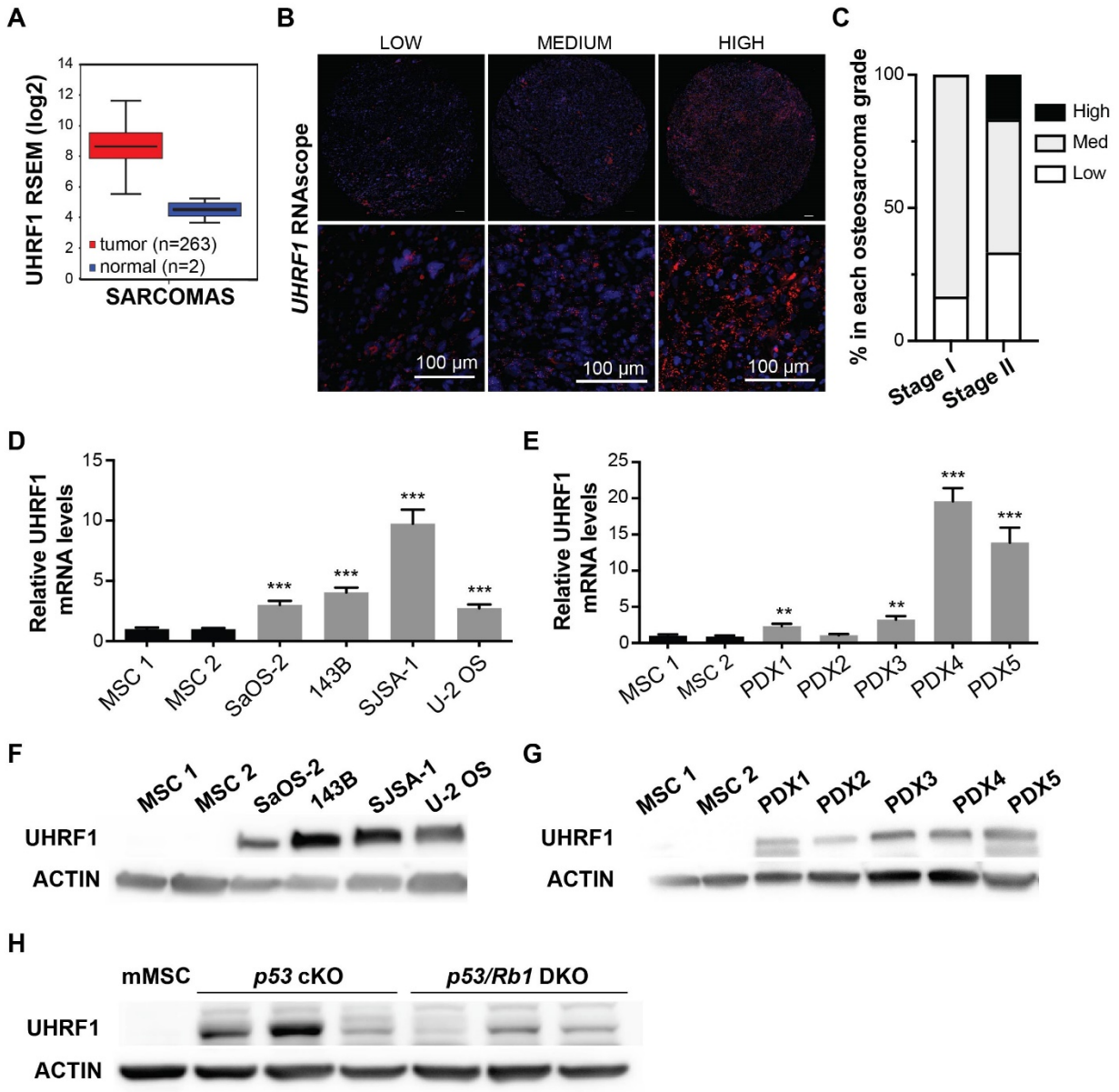

Figure 4.1. UHRF1 is upregulated and overexpressed in human and mouse OS.

(A) The Cancer Genome Atlas data of RNA-Seq by expectation-maximization (RSEM) values from 263 human sarcoma tumor samples (red) compared to normal tissue (n=2; blue). (B) Representative fluorescent images in 2X (top) and 20X (bottom) magnification of *in situ* hybridizations using RNAscope scored as low, medium or high based on signal intensity for *UHRF1* mRNA. (C) Quantification of the percentage of low, medium and high signal score acquired from RNAscope in stage I and II OS. (D-E) RT-qPCR analysis of *UHRF1* mRNA in (D) human OS cell lines (143B, SJSA-1, SaOS-2 and U-2 OS) and (E) patient-derived xenografts (PDX1-5), normalized to mesenchymal stem cells (MSC). (F-H) Western blot detection of UHRF1 in (F) human OS cell lines, (G) PDXs, and (H) tumors from genetically engineered OS mice (*p53* cKO and *p53/Rb1* DKO), β-actin was used as loading control. ** $p < 0.0021$, *** $p < 0.002$ by two-tailed *t* test.

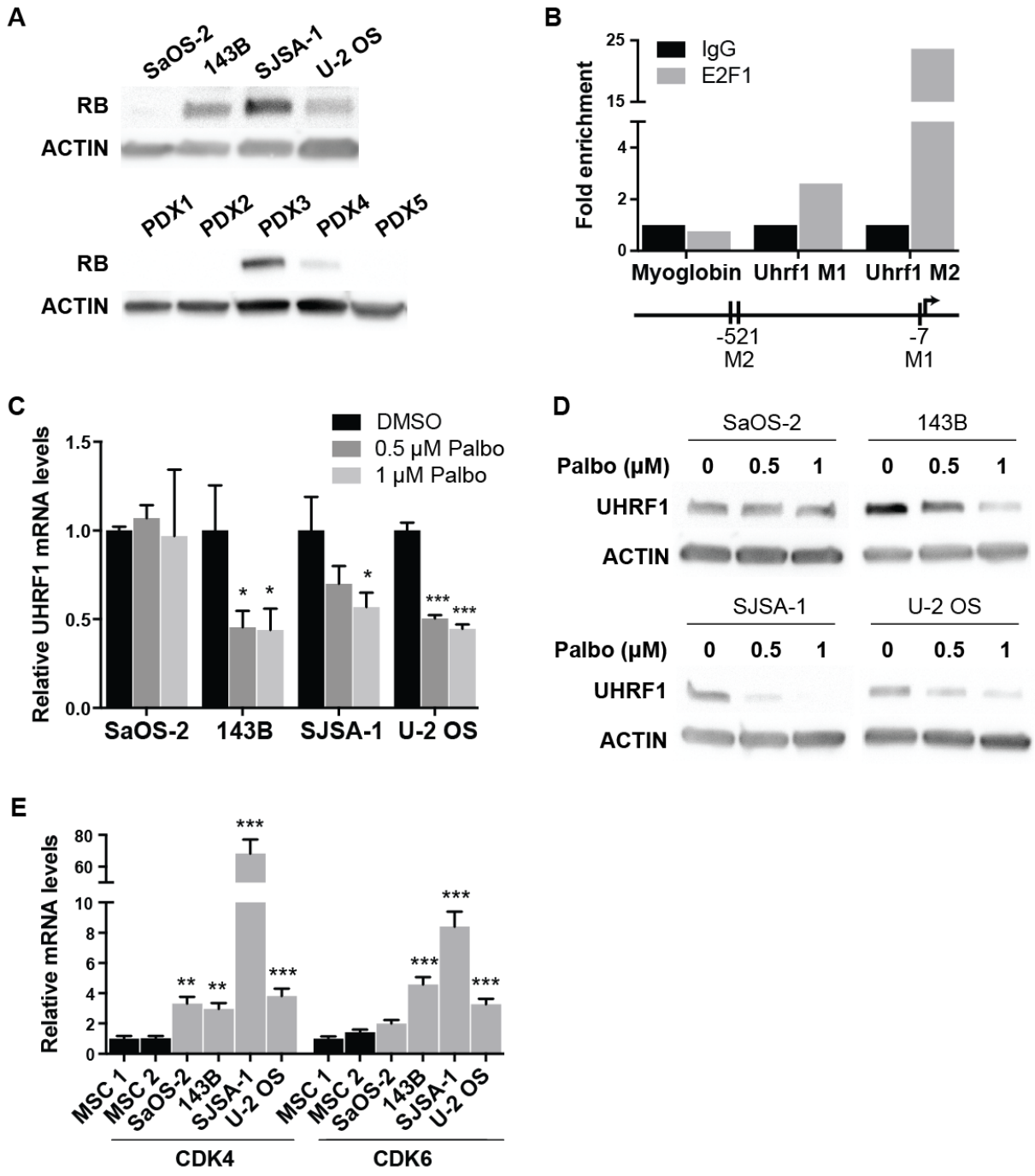

Figure 4.2. *UHRF1* is a direct target of the RB/E2F signaling pathway in the osteogenic lineage.

(A) Western blot detection of RB in human OS cell lines and PDXs. (B) Chromatin immunoprecipitation (ChIP) assay reveals enrichment of E2F1 within two putative binding motifs within *UHRF1* promoter. (C) QPCR analysis of *UHRF1* mRNA expression and (D) Western blot detection of UHRF1 level in OS cells treated with Palbociclib, normalized to DMSO control. (E) QPCR analysis of *CDK4* and *CDK6* mRNA expression, normalized to MSCs. Each data point is mean ± s.d. of triplicate samples. *$p < 0.0332$, ** $p < 0.0021$, ***$p < 0.0002$ by two-tailed t test.

UHRF1 is a direct target of the RB/E2F signaling pathway in the osteogenic lineage

A few studies have reported UHRF1 as a direct E2F1 transcriptional target [143, 144]. Following our observation that UHRF1 is overexpressed in all OS samples analyzed, we aimed to confirm whether UHRF1 is a direct E2F1 target in the osteogenic lineage. We performed chromatin immunoprecipitation (ChIP) analysis in MSCs and found E2F1 enrichment at both putative E2F1 consensus binding motifs located within the UHRF1 promoter (Figure 4.2B). To further investigate whether UHRF1 expression is transcriptionally regulated by the canonical RB/E2F pathway, we treated human OS cell lines with CDK4/6 inhibitor, palbociclib, to inhibit RB hyperphosphorylation. QPCR analysis revealed decreases in *UHRF1* mRNA levels upon palbociclib treatment, with the exception of the RB-null cell line, SaOS-2, which served as a negative control (Figure 4.2C). Palbociclib treatment also decreased UHRF1 protein levels in a dose-dependent manner in RB-positive OS cells, as revealed by Western Blot analysis (Figure 4.2D). In line with these results, we observed an upregulation of *CDK4* and/or *CDK6* transcripts in RB-wildtype OS cell lines (Figure 4.2E). Together, these data confirmed transcriptional regulation of *UHRF1* by the RB/E2F pathway through direct transcriptional activation by E2F1.

UHRF1 promotes human OS cell proliferation in vitro and in vivo

Emerging reports have linked UHRF1 overexpression in cancers with its ability to promote proliferation or migration/invasion, or both [84, 105, 145-149]. To study the role of UHRF1 overexpression in OS, we first generated UHRF1-knockdown OS cell lines using shRNA; however, we discovered that UHRF1 knockdown cannot be sustained for more than two weeks, challenging the reproducibility of our results over time (data not shown). To overcome this challenge, we generated lentiviral CRISPR vectors encoding a gRNA sequence

complimentary to UHRF1 to facilitate UHRF1 gene knockout (KO) in OS cell lines, as well as non-targeting vector control (VC). Western blot analysis revealed successful UHRF1 KO in all four OS cell lines tested (Figure 4.3A). To assess whether UHRF1 is required for OS cell proliferation, we first performed growth curve analysis, where UHRF1 KO cells displayed longer doubling times compared to vector control OS cells (VC, Figure 4.3B). The decrease in proliferation potential was further evidenced through clonogenic assays (Figure 4.3C). UHRF1 loss decreased the OS cells' ability to give rise to colonies at a single cell level, as seen by a significant reduction in both the number and the size of colonies in UHRF1 KO compared to VC cells; except for SaOS-2, where we observed a decrease in number and size but the magnitude of the change did not reach statistical significance (Figure 4.3D). To directly assay for cell proliferation, we pulsed the VC and UHRF1 KO OS cells with EdU, a nucleoside analog of thymidine, for 1 hr. We found that UHRF1 KO in OS cells decreased EdU incorporation, as seen in significantly lowered percentage of EdU-positive cells when compared to VC, suggesting a slower rate of active DNA synthesis; with the exception of U-2 OS, albeit a trend of decreased incorporation was still observed (Figure 4.3F). UHRF1 depletion has been reported to sensitize retinoblastoma cells to chemotherapeutic drugs [150]. Loss of UHRF1 has also been shown to enhance chemosensitivity to cisplatin in breast cancer cells [151]. We evaluated whether UHRF1 loss in OS cells would alter their sensitivity to standard-of-care drugs, doxorubicin, cisplatin and methotrexate. As observed from the dose-response curves generated using the Cell TiterGlo viability assay, we found that both single agent treatment and combination treatment with these drugs resulted in a moderate reduction of drug sensitivity in UHRF1 KO cells compared to VC, as evidenced by mild increases in EC50 (Figure 4.4). These observations are consistent with the decreased proliferation rate seen in

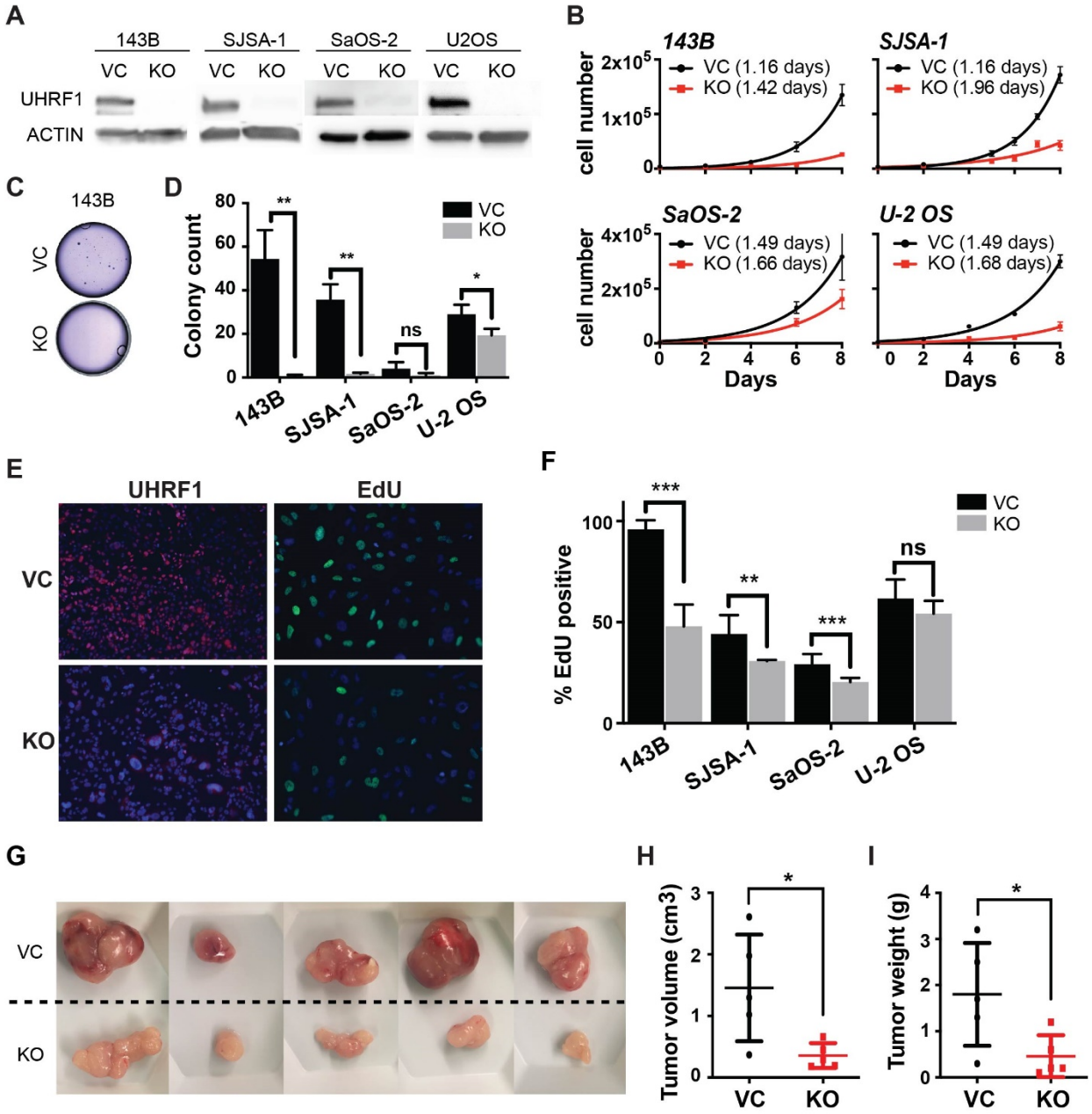

Figure 4.3. UHRF1 promotes human OS cell proliferation *in vitro* and *in vivo.*

(A) Western blot verification of CRISPR/Cas9-mediated UHRF1 knockout of human OS cell lines (KO) in comparison to vector only control (VC). (B) Growth curves of UHRF1 knockout cells (KO) compared to control (VC), population doubling time indicated in parentheses (n=3). (C) Representative images and (D) quantification of colony counts from clonogenic assay (n=3). (E) Representative fluorescent images and (F) quantification of EdU signal from immunocytochemistry probing UHRF1 and EdU in VC and UHRF1 KO human OS cell lines (n=5). (G) Tumors collected from subcutaneous injection of VC (n=5) and UHRF1 KO (n=5) SJSA-1 and quantification of (H) tumor volume and (I) weight. Each data point is mean ± s.d.. *p < 0.0332, ** p < 0.0021, ***p < 0.0002 by two-tailed t test.

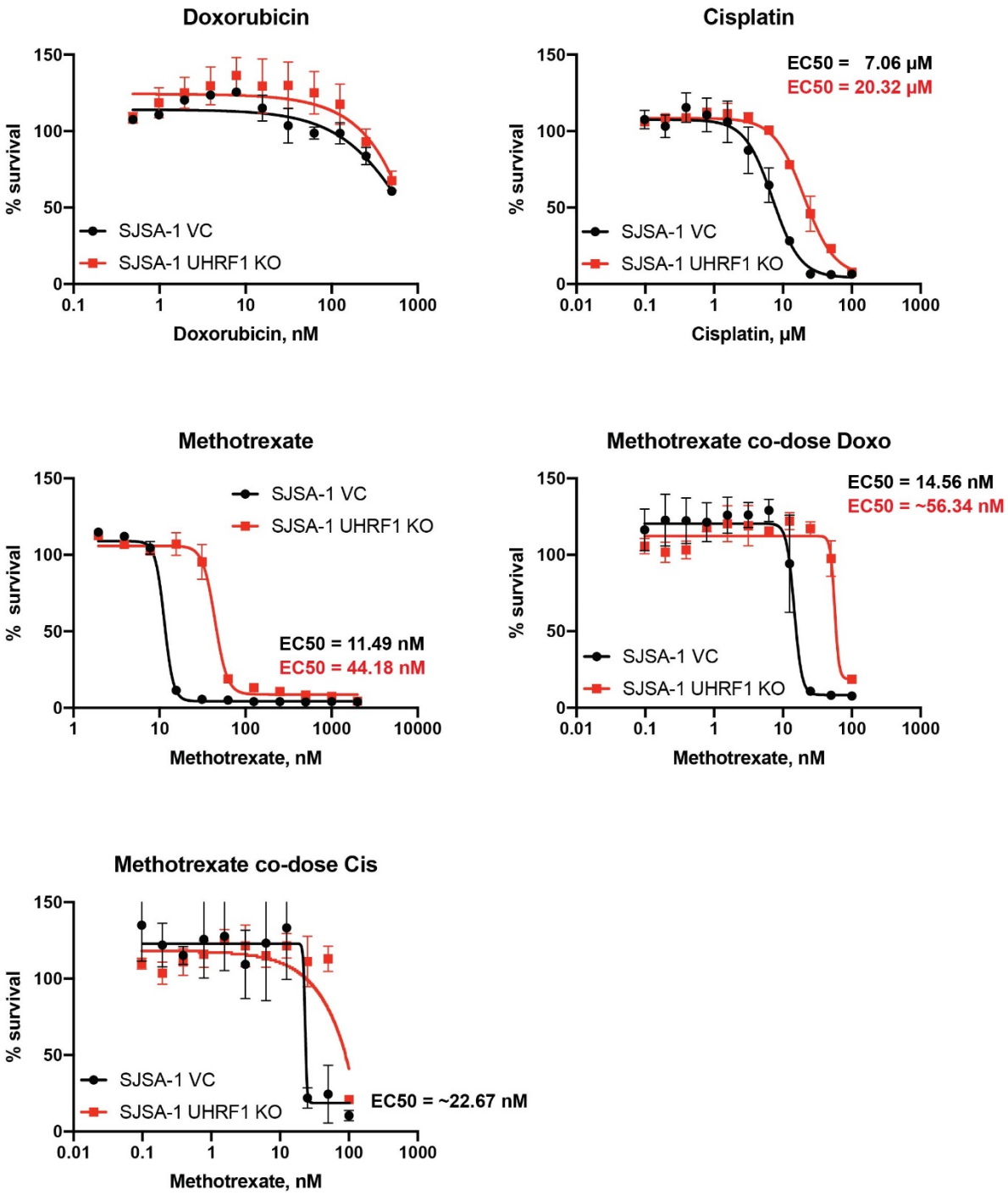

Figure 4.4. UHRF1 loss mildly desensitizes OS cells to chemotherapeutics targeting highly proliferative cells.

Dose-response curves of OS cell cultures were generated by CellTiter-Glo. Vector control (VC, black) or CRISPR-mediated UHRF1 knockout (UHRF1 KO, red) SJSA-1 cells were treated with doxorubicin, cisplatin, and methotrexate as single agents or undergo combinatorial treatment of methotrexate co-dosed with doxorubicin or cisplatin. Each data point is mean ± s.d. of triplicate samples.

KO cells and the mechanism of action of these drugs, which are more efficacious in reducing viability of cells with higher proliferation rates.

To assess proliferative capacity *in vivo*, UHRF1 KO and VC OS cells were injected subcutaneously into either flank regions, respectively, of immune-deficient mice. UHRF1 KO cells gave rise to tumors with significantly lighter burden when compared to VC. Tumors formed from UHRF1 KO cells reached an average weight of 0.70 ± 0.69 g and average size of 0.49 ± 0.37 cm^3 as compared to an average weight of 1.62 ± 1.09 g (p= 0.02, n=10) and average volume of 1.233 ± 0.75 cm^3 (p=0.01, n=10) from tumors formed by VC cells (data not shown). To test the therapeutic potential of targeting UHRF1 in established tumors, we utilized a doxycycline-inducible system to drive the expression of the CRISPR gRNA against UHRF1. Inducible UHRF1 KO and VC OS cells were subcutaneously injected and tumors were allowed to establish for one week, followed by the induction of CRISPR/Cas-9 gRNAs using orally delivered doxycycline. Tumors formed from UHRF1 KO cells were significantly smaller, with an average tumor volume of 0.356 ± 0.201 cm^3 in UHRF1 KO tumors compared to 1.455 ± 0.865 cm^3 in VC tumors (p=0.02; n=5; Figure 4.3G, H). The average tumor weight was also reduced, with UHRF1 KO tumors averaging 0.46 ± 0.45 g compared to 1.80 ± 1.11 g in VC tumors (p=0.01, n=5; Figure 4.3I). UHRF1 KO tumors also presented phenotypic features of less aggressive tumors, as seen by lessened vasculature and ulceration compared to tumors formed from VC cells (Figure 4.3G and data not shown). Taken together, both *in vitro* and *in vivo* data suggest that UHRF1 is critical for OS cell proliferation.

UHRF1 loss alters global DNA methylation without significant changes in chromatin accessibility in OS

UHRF1 is required for maintenance of DNA methylation during DNA replication through the recruitment of DNMT1 [152]. However, UHRF1 ubiquitin ligase activity also targets DNMT1 for degradation, with some studies reporting that UHRF1 overexpression results in decreased DNA methylation [153, 154]. To determine the effects of UHRF1 loss on DNA methylation, chromatin structure, and transcription, we analyzed global DNA methylation, chromatin accessibility, and transcriptome. We probed genomic DNA isolated from UHRF1 KO and VC cell lines with an antibody against 5-methyl cytosine (5meC) to assess global DNA methylation. We found significant hypomethylation in UHRF1 KO OS cell lines compared to VC (Figure 4.5A).

We also analyzed changes in the chromatin landscape upon loss of UHRF1 by performing ATAC-seq in 143B, SJSA-1, and SaOS-2 UHRF1 KO compared to VC (Figure 4.5B). Despite the role of UHRF1 in heterochromatin maintenance, we identified only 16 chromatin regions with significant changes in chromatin accessibility across these 3 biological replicates (Table 4.1). Within these changes, the majority were consistent with the role of UHRF1 chromatin repression, with approximately 69% (11/16) resulting in opening of chromatin upon UHRF1 loss.

In line with modest changes in chromatin accessibility, gene expression analysis using RNA-seq revealed that the gene expression profile from UHRF1 KO cell lines were virtually indistinguishable from VC cells, as portrayed by the PCA plot (Figure 4.5C). We identified a

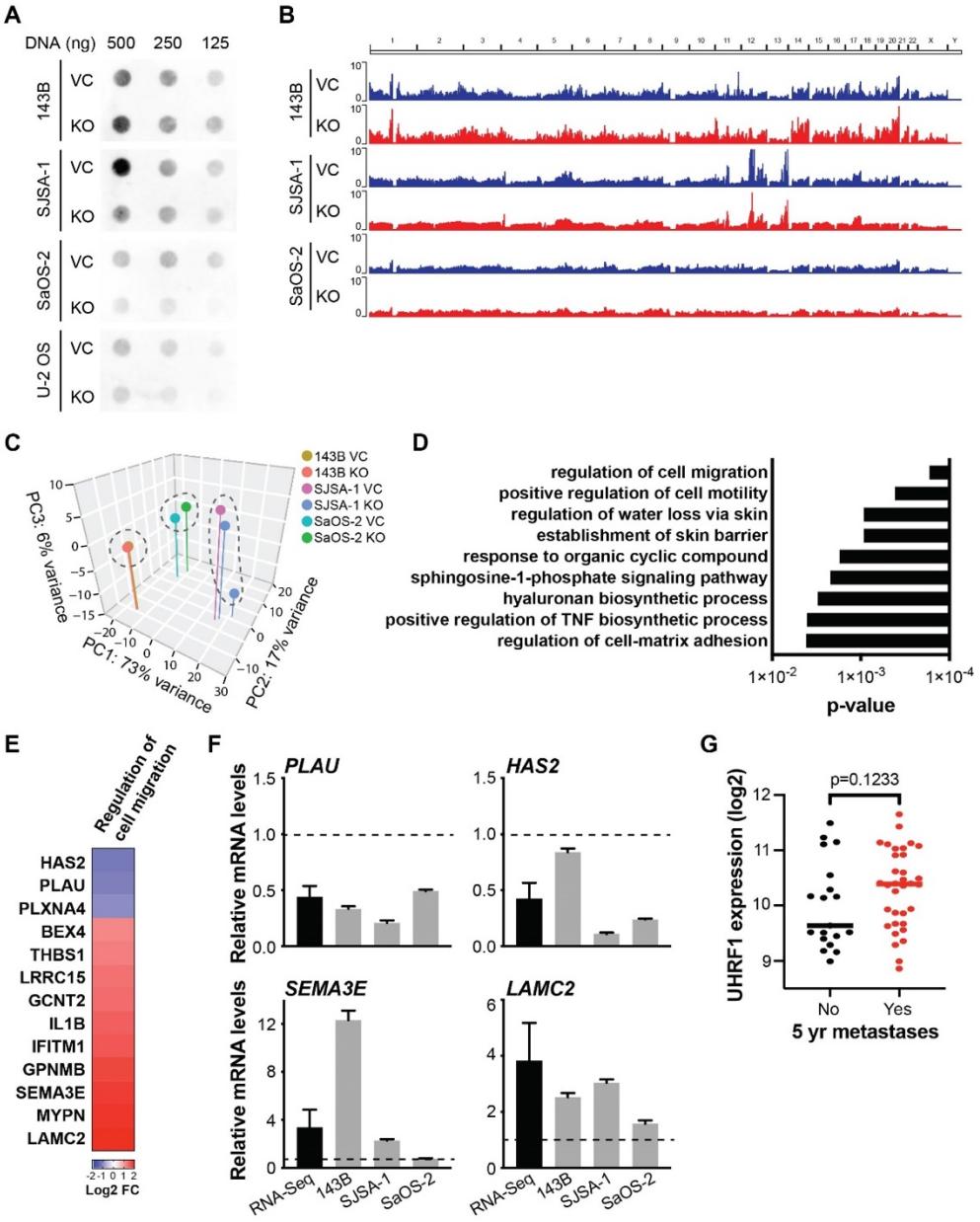

Figure 4.5. UHRF1 loss alters global DNA methylation without significant changes in chromatin accessibility in OS.

(A) Dot blot detection of 5-methyl cytosine signal in control (VC) and UHRF1 KO (KO) OS cells, comparing global methylation levels. (B) Chromatin landscape generated from ATAC-seq showing peaks of chromatin accessibility across the genome of VC and KO OS cells. (C) Principle component analysis (PCA) plot generated from RNA-seq displaying gene expression profile in VC and KO OS cells. (D) Gene ontology (GO) analysis for biological process of differentially expressed genes (DEGs) identified through RNA-seq. (E) Heat map of top 13 genes involved in regulation of cell migration, decreased (blue) or increased (red) in expression level upon UHRF1 loss. (F) QPCR analysis confirming expression changes of migration related genes in individual cell lines upon UHRF1 loss, fold change of mRNA level normalized to vector control (gray), compared with average fold change from RNA-seq analysis (black). (G) RNA-seq analysis of high-grade OS biopsies comparing UHRF1 expression in patients who did or did not develop metastasis within 5 years from diagnoses.

Table 4.1. ATAC-seq results p<0.05

	seqnames	start	end	Conc_VO	Conc_UHRF	Fold	p.value
7763	chr5	38147946	38148446	3.36	6.07	-2.71	0.000352
3317	chr15	33406160	33406660	4.57	6.72	-2.14	0.0129
7767	chr5	38756061	38756561	4.92	6.76	-1.85	0.0249
4377	chr17	68223297	68223797	4.56	6.3	-1.74	0.015
8608	chr6	44084322	44084822	4.31	5.99	-1.67	0.0285
5989	chr20	23125981	23126481	4.16	5.77	-1.62	0.0167
5965	chr20	17519102	17519602	3.91	5.45	-1.54	0.0138
5084	chr2	23637633	23638133	5.18	6.5	-1.31	0.0293
5213	chr2	49056145	49056645	4.48	5.78	-1.3	0.0492
4829	chr19	30369822	30370322	5.99	7.24	-1.25	0.034
6767	chr3	46688121	46688621	4.46	5.66	-1.2	0.0402
2655	chr13	36705232	36705732	6.35	5.38	0.97	0.0439
9982	chr9	4741018	4741518	7.73	6.66	1.07	0.0374
1176	chr10	63422386	63422886	6.64	5.38	1.26	0.0303
9071	chr7	25990604	25991104	6.38	4.93	1.45	0.0352
5460	chr2	125593939	125594439	6.54	4.93	1.61	0.0328

total of 272 differentially expressed genes (DEGs), with 191 upregulated genes and 81 downregulated genes in UHRF1 KO compared to VC cells. Gene ontology (GO) analysis for biological processes of these 272 DEGs showed an enrichment of genes involved in regulation of cell migration and cellular adherence, as seen by the classification of the top 10 most significant GO terms (Figure 4.5D). We confirmed the changes in gene expression observed among top 13 genes involved in regulation of cell migration (Figure 4.5E) through qPCR (Figure 4.5F and data not shown).

Given the interesting possibility of a role of UHRF1 in OS migration, we also analyzed *UHRF1* expression from an RNA-Seq dataset of pretreatment biopsies from 53 high-grade OS patients who did or did not develop metastasis within 5 years [155]. We found that while all biopsies analyzed expressed high levels of *UHRF1*, biopsies from patients that developed metastasis within 5 years from the time of biopsy expressed ~70% more *UHRF1* mRNA (log2 mean = 10.39) compared to patients who did not develop metastasis (log2 mean = 9.64; p = 0.1233; Figure 4.5G). Together, these data suggested that UHRF1 overexpression may not only contribute to proliferation, but also potentially to cell migration, invasion, and metastasis in OS.

UHRF1 promotes human OS cell migration and invasion in vitro and in vivo

The high metastatic potential of OS is the main cause of mortality in patients. Given that our RNA-seq data indicated a possible involvement of UHRF1 in OS metastasis, we sought to evaluate the role of UHRF1 in promoting cell migration, invasion, and metastasis. Scratch-wound assay was carried out to assess the migratory potential of UHRF1 KO OS cell lines

(Figure 4.6A). We observed a significant decrease in the distance migrated in UHRF1 KO compared to VC OS cells for all cell lines studied, with an average of 56.8 ± 2.3% reduction in migration across the three cell lines (Figure 4.6B). In addition to the decrease in migratory potential, Transwell invasion assay revealed a significant reduction in the number of UHRF1 KO OS cells capable of mobilizing across Matrigel-coated inserts in all OS cell lines (Figures 4.6C-D). Plasminogen activator, Urokinase (*PLAU*) was identified through GO analysis to be potentially involved in UHRF1-mediated cell migration. Significant decrease in the level of *PLAU* transcript was observed in UHRF1 KO OS cells (Figure 4.5F), as well as the tumors they form subcutaneously in immune-deficient mice, with an average 0.45 fold decrease when compared to tumors formed from VC cells ($p=0.02$, Figure 4.7A). Treatment with amiloride, an inhibitor for *PLAU* encoded protein urokinase-type plasminogen activator (uPA), decreased migratory potential and invasiveness of OS cells (Figure 4.7B, C). Finally, to test whether the reduced migratory and invasive capacities *in vitro* translate into less metastatic potential *in vivo*, we injected SJSA-1 UHRF1 KO and VC cells into the tail vein of immune-deficient mice and assessed the rate of lung colonization 3-weeks post injection. We found that the lungs of mice injected with UHRF1 KO cells had a reduced number of metastatic nodules and a significantly reduced tumor nodule size when compared to the lungs of mice injected with VC cells (Figures 4.6E-G).

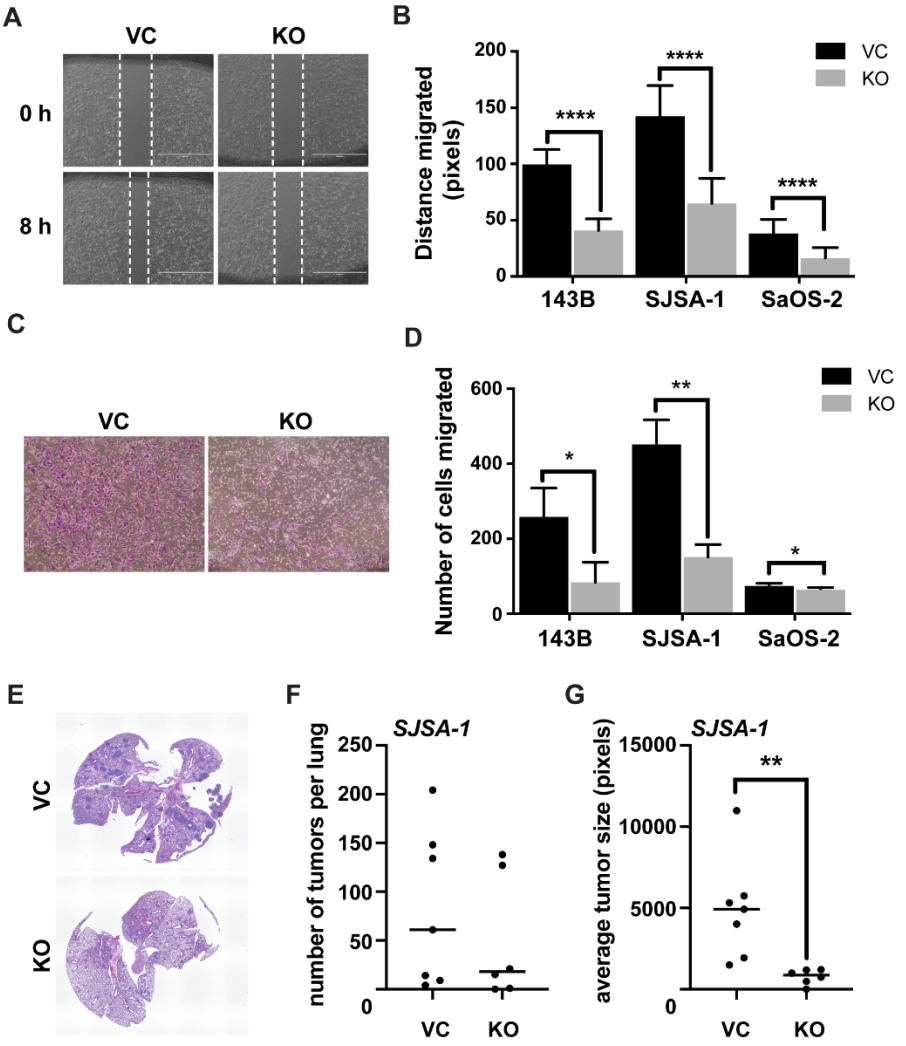

Figure 4.6. UHRF1 promotes human OS cell migration and invasion *in vitro* and *in vivo*

(A) Representative image of scratch-wound assay in OS culture comparing wound closure of VC and UHRF1 KO cells over 8hr span. White dashed lines represent wound edge. Same view was captured for both time points. (B) Quantification of distance migrated in pixels. Average was taken from 10 points along the wound area. (C) Representative images of crystal violet stain comparing levels of invasion between VC and UHRF1 KO OS cells. (D) Quantification of number of cells invaded across Transwell membrane. (E) Representative H&E stains of lung sections collected from mice injected intravenously with VC or UHRF1 KO SJSA-1 cells. Pulmonary nodules were quantified by (F) number and by (G) size. *p < 0.0332, ** p < 0.0021, ***p < 0.0002, ****p<0.0001 by two-tailed t test.

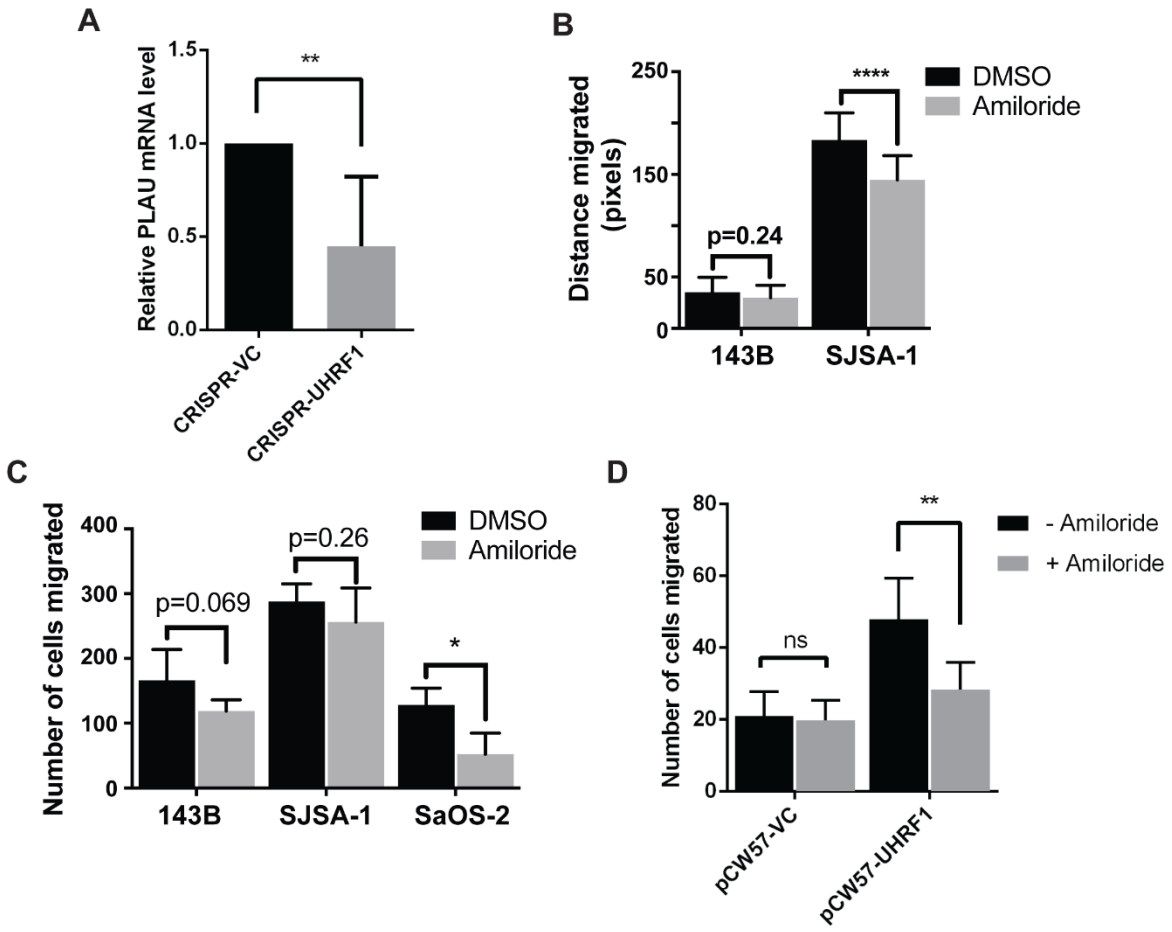

Figure 4.7 uPA mediates UHRF1-induced cell migration and invasion.

(A) QPCR analysis of *PLAU* mRNA level in tumors formed from subcutaneously injected OS cells. (B) Quantification of distance migrated in OS cells upon amiloride treatment in scratch wound assay and (C) number of cells invaded in Transwell invasion assay. (D) Quantification of distance migrated in MSCs upon amiloride treatment in Transwell invasion assay. *p < 0.0332, ** p < 0.0021, ***p < 0.0002, ****p<0.0001 by two-tailed t test.

UHRF1 overexpression promotes human MSC cell migration and invasion in vitro

In order to determine whether UHRF1 overexpression is sufficient to drive cell migration, we performed gain-of-function studies using normal MSCs. For this, we generated a doxycycline-inducible lentiviral vector system to drive UHRF1 overexpression (pCW57-UHRF1; Figure 4.8A) and used the empty backbone vector as control (pCW57-VC). Western blot analysis was performed to validate successful induction of UHRF1 overexpression upon doxycycline treatment in transduced MSCs (Figure 4.8B). We observed that the rate of cell proliferation upon induction of UHRF1 overexpression in MSCs was indistinguishable from doxycycline-induced VC (data not shown). Nonetheless, we found that UHRF1 overexpression in MSCs significantly increased migratory potential as evidenced by the significant increase in the distance migrated upon doxycycline induction in pCW57-UHRF1 cells compared to pCW57-VC using scratch-wound assay (Figures 4.8C-D). Furthermore, induction of UHRF1 overexpression also led to a significant increase in the number of cells invaded across Matrigel-coated Transwell membranes (Figures 4.8E-F). Taken together, we established a positive correlation between UHRF1 expression levels and migration/invasion potential in the osteogenic lineage. Treatment with amiloride inhibited invasion upon overexpression of UHRF1 in MSCs (Figure 4.7D), functionally validating the involvement of uPA in UHRF1-mediated cell migration/invasion.

UHRF1 is a critical driver of the increased malignancy observed in Rb1-null OS

An OS developmental model previously described utilizes transgenic mice with *Osx-cre* to facilitate preosteoblast-specific loss of *Tp53*, which results in tumor formation with complete penetrance and gene expression profiles, histology, and metastatic potential comparable to

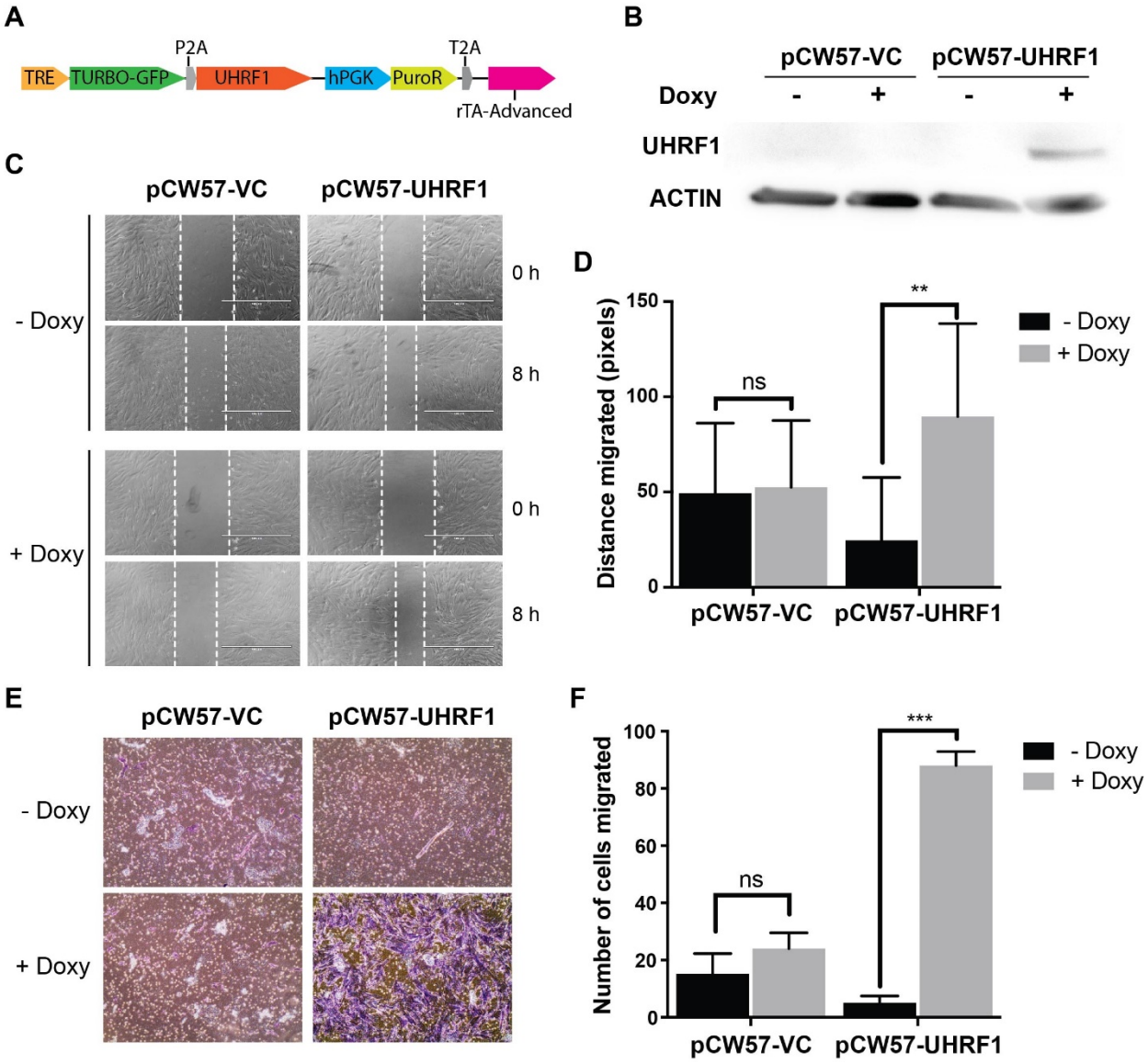

Figure 4.8. UHRF1 overexpression promotes human MSC cell migration and invasion *in vitro.*

(A) Plasmid map of doxycycline inducible UHRF1 overexpression. Tet Response Element (TRE) is activated by doxycycline binding to the reverse tetracycline-controlled transactivator (rTA), allowing transcription of GFP and pCW57 promoter driven UHRF1. (B) Western blot detection of UHRF1 in MSCs transduced with vector control (pCW57-VC) or UHRF1 overexpression (pCW57-UHRF1) plasmid, treated with DMSO or doxycycline. (C) Scratch-wound assay in MSC culture comparing wound closure of control (pCW57-VC) and UHRF1 overexpressed (pCW57-UHRF1) cells over 8hr span. White dashed lines represent wound edge. Same view was captured for both time points. (D) Quantification of distance migrated in pixels. Average was taken from 10 points along the wound. (E) Representative images of crystal violet stain comparing levels of invasion between VC and UHRF1 overexpressed MSCs. (F) Quantification of number of cells invaded across Transwell membrane. Ns=not significant, ** $p < 0.0021$, ***$p < 0.0002$ by two-tailed t test.

that of human OS [21, 29]. Preosteoblast-specific loss of *Rb1* in addition to *Tp53* potentiates OS in mice, strongly mimicking the behavior of the disease in human. In order to study the role of UHRF1 in OS development *in vivo*, we first assessed whether loss of *Uhrf1* in osteogenic progenitors affected normal bone development. Since *Uhrf1* knockout mice result in mid-gestational lethality [156], we generated mice with preosteoblast-specific knockout of *Uhrf1* (*Osx-cre Uhrf1*$^{lox/lox}$). Preosteoblastic loss of *Uhrf1* did not result in aberrant bone development in either young (5 wks.) or old (55 wks.) mice, as determined by bone density analysis in prime locations of OS occurrence including femur, tibia, and humerus (Figures 4.9A, B).

We subsequently generated a series of genetically engineered mice to facilitate preosteoblast-specific knockout of *Uhrf1* in two different OS genetic background mice, *Tp53* single conditional-knockout (cKO; *Osx-cre Tp53*$^{lox/lox}$) and *Tp53*/*Rb1* double conditional-knockout (DKO; *Osx-cre Tp53*$^{lox/lox}$ *Rb1*$^{lox/lox}$), resulting in *Tp53*/*Uhrf1* DKO (*Osx-cre Tp53*$^{lox/lox}$ *Uhrf1*$^{lox/lox}$) and *Tp53*/*Rb1*/*Uhrf1* triple knockout (TKO; *Osx-cre Tp53*$^{lox/lox}$ *Rb1*$^{lox/lox}$ *Uhrf1*$^{lox/lox}$). OS mice often times develop tumors with calcified interior and highly proliferative exterior, which can be captured by microCT and FDG-PET scans, respectively (Figure 4.9C). The resulting *Tp53*/*Uhrf1* DKO and *Tp53*/*Rb1*/Uhrf1 TKO mice were compared to their corresponding littermate controls (*Tp53* cKO and *Tp53/Rb1* DKO, respectively) for the assessment of the role of UHRF1 in promoting OS development and metastasis. *In situ* hybridization performed on the OS mouse tumors confirmed high levels of *Uhrf1* transcripts in *Tp53* cKO and *Tp53*/*Rb1* DKO and a significant reduction of *Uhrf1* in *Tp53*/*Uhrf1* DKO and *Tp53*/*Rb1*/*Uhrf1* TKO (Figure 4.9D). All genotypes analyzed lead to the

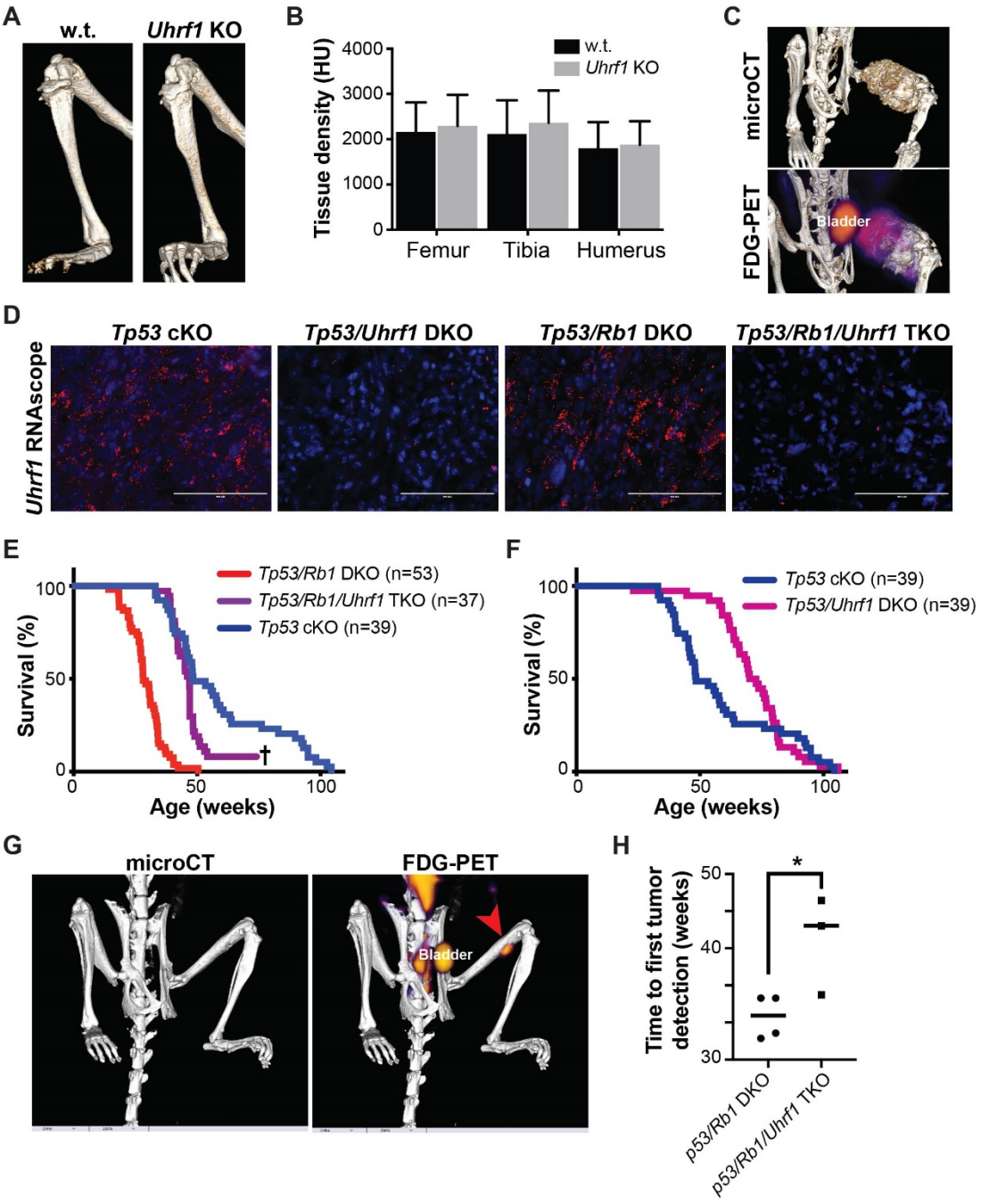

Figure 4.9. UHRF1 is a critical driver of the increased malignancy observed in *Rb1* null OS.

(A) Micro-CT scan of hind limb from wildtype (w.t.) and preosteoblastic *Uhrf1* knockout (*Uhrf1* KO) mice (B) Bone density analysis of prime OS locations in Hounsfield units. (C) Representative micro-CT (top) and micro-PET (bottom) scans on OS arises in mouse femur. (D) Representative fluorescent images of in-situ hybridizations using RNAscope on tumors from genetically engineered OS mice. (E, F) Kaplan-Meier curves comparing survival curve of (E) *Tp53*/*Rb1*/*Uhrf1* TKO (purple) to OS background mice, *Tp53* cKO (blue) and *Tp53*/*Rb1* DKO (red), (F) *Tp53*/*Uhrf1* DKO (pink) to *Tp53* cKO (blue). (G) Representative micro-CT (left) and FDG-PET (right) scans for detecting early tumor development. (H) Age of mice at earliest tumor detection via micro-CT and FDG-PET scans.

development of OS in mice, but with different survival rates and disease presentation. In line with previous reports, in our OS background mouse strains, *Tp53*/*Rb1* DKO mice presented a significantly shorter median survival of 28.1 weeks (n=53) than the 48.4 weeks seen in *Tp53* cKO mice (n=39, p<0.0001; Figure 4.9E). UHRF1 loss in *Tp53/Rb1/Uhrf1* TKO mice resulted in a significant increase in survival compared to *Tp53/Rb1* DKO mice (p<0.0001), with a median survival of 46.9 weeks (n=37). Remarkably, the increase in median survival of *Tp53/Rb1/Uhrf1* TKO (46.9 weeks) is comparable to that of *Tp53* cKO (48.4 weeks, p=0.0577), suggesting that elevated UHRF1 protein levels are critical for the poor prognosis associated with RB loss. However, past the early time points, the *Tp53/Rb1/Uhrf1* TKO and *Tp53* cKO survival curves become distinct from each other (p=0.0126), suggesting that early UHRF1 overexpression is not the unique factor contributing to RB-loss outcomes. Since three *Tp53/Rb1/Uhrf1* TKO mice had not acquired tumors well beyond the average of the rest of their study group (> 69 weeks; Figure 4.9E), we performed FDG-PET/microCT scans on them followed by autopsy. FDG-PET/microCT scans revealed no detectable tumors (Figure 4.10), which was further confirmed through autopsy.

Since we observed elevated UHRF1 protein levels in human OS with RB/E2F pathway inactivation beyond *RB1* loss-of-function mutations and detected increased *Uhrf1* mRNA and protein levels in *Tp53* cKO mouse tumors (Figures 4.1 and 4.9D), we also analyzed the survival time of *Tp53/Uhrf1* DKO compared to *Tp53* cKO mice. We observed a significant increase in the median survival of *Tp53/Uhrf1* DKO mice (71.4 weeks; n=39), compared to *Tp53* cKO (n=39; p=0.0007), but not in overall survival (p=0.1189). Interestingly, we found

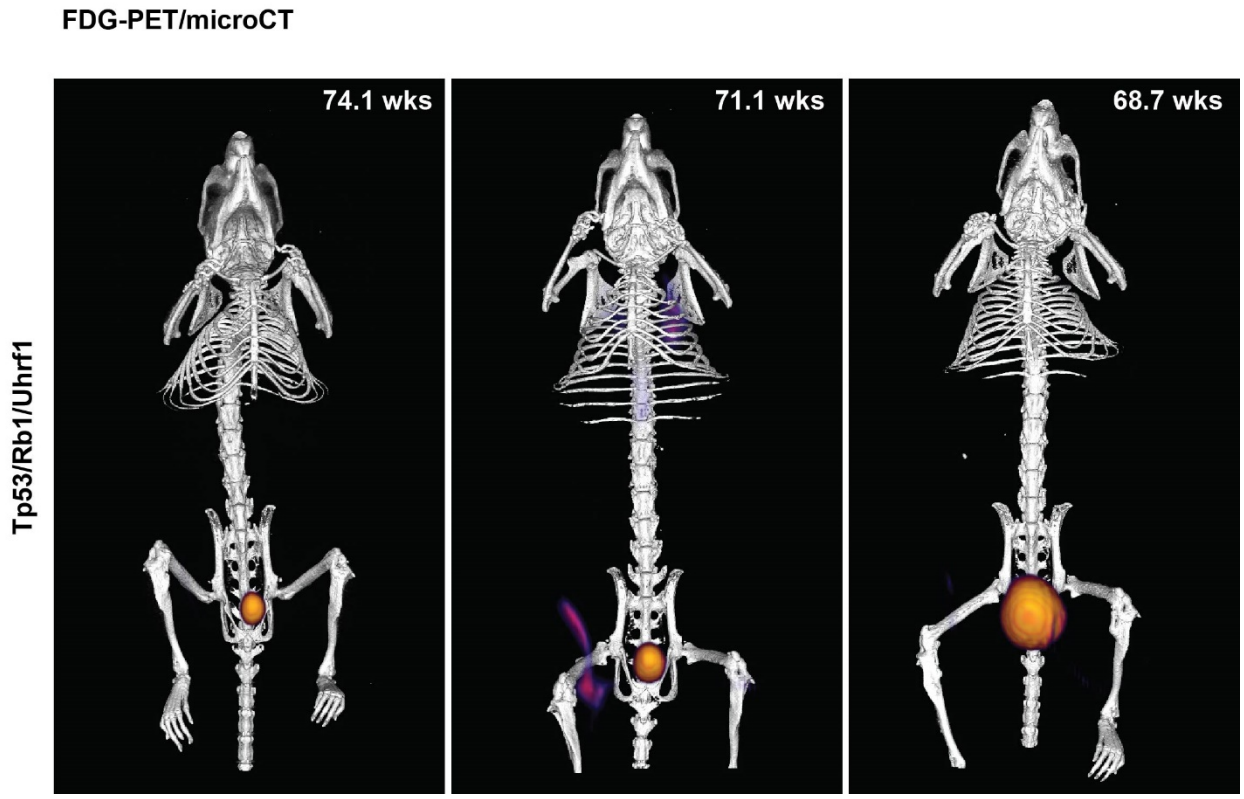

Figure 4.10. Loss of Uhrf1 in OS mice significantly delayed tumor formation

FDG-PET/microCT scans of the three *Tp53/Rb1/Uhrf1* TKO mice that remained tumor-free well beyond the average of the rest of their study group (> 69 weeks). No detectable tumors were observed, this is further validated by autopsy.

that all *Tp53* cKO mice analyzed with earlier morbidity (< 60 weeks) presented tumors with signs of RB/E2F pathway inactivation, including increased *Uhrf1* mRNA levels; while only a third of tumors analyzed from mice that reached moribund status later in life displayed *Uhrf1* overexpression (data not shown). In addition to the dramatic improvement in survival in *Tp53/Rb1/Uhrf1* TKO mice, these mice also presented a significant reduction in pulmonary metastatic potential with only 10% presenting lung metastases compared to 40% of *Tp53/Rb1* DKO mice, in addition to lighter burden of metastatic nodules (data not shown). Furthermore, pathology analysis of histological sections for tumors from the four OS mouse models analyzed linked *Uhrf1* loss with lower mitotic index and decreased anaplasia (Figure 4.11, Table 4.2).

Following the observation of the three *Tp53/Rb1/Uhrf1* TKO mice without detectable tumors, we sought to determine if loss of *Uhrf1* contributes to delayed tumor promotion or decreased rate of tumor progression. To address this question, we performed periodic FDG-PET/microCT scans on *Tp53/Rb1* DKO and *Tp53/Rb1/Uhrf1* TKO mice to determine the earliest age at which tumors could be detected. In *Tp53/Rb1* DKO mice, tumors were detected after 30.8 ± 2.9 weeks (n=4). In *Tp53/Rb1/Uhrf1* TKO mice tumors were detected significantly later at 41.1 ± 6.6 weeks (p=0.0362; Figure 4.9G, H). In contrast, all test subjects reached humane end of study within 3 weeks of first tumor detection. These data suggest that *Uhrf1* plays a pivotal role in OS tumor promotion following loss of *Rb1*.

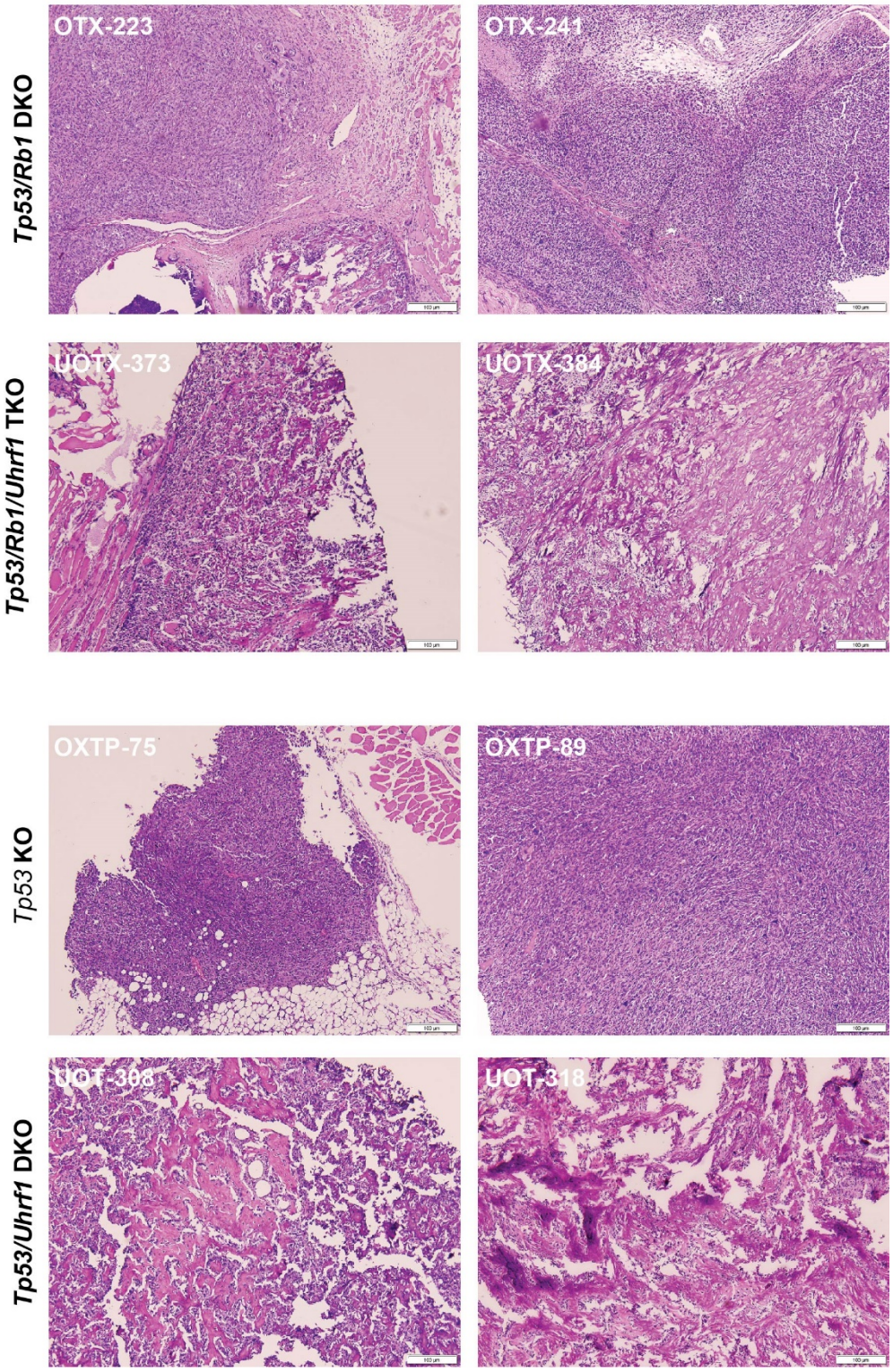

Figure 4.11. H&E stains of tumor sections acquired from all four strains of genetically engineered mouse model.

Table 4.2. Pathology analysis of mouse osteosarcoma strains

Genotype	Tumor ID	Malignant osteoid formation	Tumor nuclear size	Anaplasia/Significant pleomorphism	Mitotic activity	Necrosis
p53 cKO	OXTP75	No	Medium to large sized with epithelioid features	Focal	3/10 HPF	Yes, small focus
	OXTP89	No	Medium to large sized	Yes	3/10 HPF	No
	OXTP73	Yes, abundant	Medium to large sized	No	1/10 HPF	No
p53/Rb1 DKO	OTP223	Yes, rare	Medium to large sized with epithelioid features	Yes	4/10 HPF	No
	OTP196	Yes, abundant	Medium sized, frequent MNT cells	No	1-2/10 HPF	No
	OTP241	No	Small to medium sized	Yes	10/10 HPF	Yes
p53/Uhrf1 DKO	UOTX414	Yes, abundant	Small sized	No	0/10 HPF	No
	UOTX373	Yes, abundant	small to Medium sized, rare MNT cells	No	0/10 HPF	No
	UOTX384	Yes, abundant	small to Medium sized, rare MNT cells	No	1/10 HPF	No
p53/Rb1/Uhrf1 TKO	UOT259	Yes, abundant	Medium sized, frequent MNT cells	No	1/10 HPF	No
	UOT318	Yes, abundant	Medium sized, occasional MNT cells	No	1/10 HPF	No
	UOT308	Yes, abundant	Medium sized, occasional MNT cells	No	1/10 HPF	No

Discussion

Metastasis remains the most important fatal complication of OS. The lack of significant breakthroughs beyond the scope of standard chemotherapeutics targeting highly proliferative underscores a pressing clinical need for new therapeutic strategies for OS. For decades, genetic alterations at the *RB1* gene have been associated with increased mortality, metastasis and poor response to chemotherapy in osteosarcoma [60-66]. However, the precise mechanism through which this occurs remains to be elucidated. In this study, we identified UHRF1 as a gene upregulated and its protein levels markedly elevated in OS, and its expression correlates with increased malignancy and metastatic disease. The RB/E2F pathway directly regulates *UHRF1* expression. Moreover, UHRF1 facilitates OS cell proliferative, invasive and metastatic capacity. Overall, we found that the decreased survival associated with loss-of-function mutations at the *RB1* gene is critically mediated through the overexpression of UHRF1.

Studies from retinoblastoma, a cancer initiated by biallelic inactivation of the *RB1* gene, defined a central role of RB in epigenetic control and a key role of RB/E2F-regulated chromatin remodelers in tumorigenesis [77, 84, 157]. Among these chromatin remodelers, UHRF1 was identified as a potential critical regulator of tumor initiation and progression following RB-pathway deregulation and is overexpressed in several cancers [84, 94-96, 137]. We confirmed *UHRF1* upregulation in human OS cell lines, PDXs, and primary OS tissue. Further, UHRF1 protein overexpression is recapitulated in both *p53* cKO and *Tp53*/*Rb1* DKO OS mouse model, validating the suitability of this mouse model for the study of OS. Direct regulation of UHRF1 by the RB/E2F signaling pathway was described previously, though in

limited context [143, 144]. We established that *UHRF1* expression is transcriptionally regulated by the RB/E2F signaling pathway in the osteogenic lineage. ChIP analysis revealed enrichment of E2F1 at putative binding motifs within the promoter region of *UHRF1*. However, as discussed in chapter 2, E2F1 knockdown was insufficient in reducing UHRF1 expression. Rather, significant reduction of UHRF1 level was achieved only through combinatorial knockdown of E2F1 and E2F3, suggesting compensatory mechanisms between activator E2Fs in regulating the transcription of downstream targets. As the RB/E2F signaling pathway is often inactivated in cancer through mechanisms other than *RB1* loss-of-function mutations, most common being RB hyperphosphorylation through CDK4/6 activation, or p16 inactivation [158-160], it is not surprising that UHRF1 upregulation and overexpression in OS is not restricted to *RB1*-null cases, but rather a generalized event among all samples. UHRF1 overexpression in RB-wildtype in OS cell lines can be explained by upregulation of *CDK4* and/or *CDK6*, which leads to RB hyperphosphorylation, preventing the repression of E2F binding activities. Increased CDK4/6 activity being the predominant mechanism of pathway inactivation in OS is further confirmed by the down-regulation of *UHRF1* and dose-dependent decrease of UHRF1 upon treatment with palbociclib, a known CDK4/6 inhibitor [129].

UHRF1 expression is positively correlated with cell proliferation and cell mobility in both normal and malignant cells *in vitro [84, 145, 146, 148, 149]* . Although it is clear that UHRF1 expression is linked to cellular phenotypes that strongly associate with tumor malignancy, the link between UHRF1, OS tumor progression, and its role in the poor prognosis associated with *RB1* loss has not been established. Our results show that UHRF1 KO decreases

clonogenicity and prolongs doubling time. Subcutaneous injection of UHRF1 KO OS cells resulted in lighter tumor burden, further suggesting that UHRF1 expression level is crucial for tumor growth. Independent of the effects on proliferation, UHRF1 KO dramatically reduced migration, invasion and metastatic capacity of OS cells.

Genetically engineered mouse models show the critical role of UHRF1 in osteosarcomagenesis, with *Uhrf1* KO resulting in a dramatic increase in overall survival and decrease in metastases, particularly in RB-null OS. We previously reported that loss of *E2f1* or *E2f3* in *Tp53*/*Rb1* DKO OS mice only provided partial improvements in OS survival [158]. As E2F1 and E2F3 are most likely redundant for transcriptional activation of UHRF1 as previously discussed, UHRF1 is presented as a better suited target. Indeed, median survival of *Tp53*/*Rb1*/*Uhrf1* TKO closely resembled that of *Tp53* cKO mice, indicating that UHRF1 is a major component that mediates RB loss-associated deregulation, and that UHRF1 KO substantially reverses the increase malignancy observed upon RB loss. Interestingly, our results also showed that the increased survival in *Tp53*/*Rb1*/*Uhrf1* TKO mice is likely a result of delayed tumor promotion rather than decelerated proliferation. Further studies on tumors arising from these developmental OS models may provide insight on compensatory mechanisms of *Uhrf1* loss which may be relevant for predicting mechanisms of resistance to future UHRF1-targeted therapeutics.

The drastic decrease in incidence of spontaneous metastases in *Tp53*/*Rb1*/*Uhrf1* TKO mice, along with the increase in migration and invasion upon UHRF1 gain-of-function in an otherwise non-migratory normal cell, MSCs, suggests that UHRF1 expression is both

necessary and sufficient to initiate cellular mechanisms that promote OS metastasis. Transcriptome analysis identified putative downstream targets of UHRF1 that may be responsible for mediating this process. Among these targets, uPA is a promising mediator of UHRF1-induced cell migration. The role of plasmin in degradation of extracellular matrix and angiogenesis could explain the decrease cell mobility and angiogenesis in observed OS cells line and the tumors formed from them. UHRF1 KO led to the decrease of *PLAU* level in OS cells and tumor, inconsistent with the major functions of UHRF1 involving chromatin repression and ubiquitination-mediated degradation, suggesting the involvement of other factors between the UHRF1-uPA axis. Nonetheless, the observation that increased migratory potential in MSCs induced by UHRF1 overexpression can be reversed with treatment of uPA inhibitor, amiloride, gave functional evidence associating uPA activity with UHRF1-mediated cell migration.

To summarize, our study provided multifaceted evidences both *in vitro* and *in vivo* supporting UHRF1 targeting as a novel therapeutic strategy in treating OS. The involvement of UHRF1 in OS cell proliferation and its critical role in tumor promotion strongly outweighs the mild desensitization of OS to standard care therapeutics. We showed that UHRF1 targeting holds great potential in overcoming the highly metastatic characteristic of OS, the main reason why survival rate has remained stagnant in past decades. We stand to be the first to model the effect of UHRF1 throughout development and showed minimal on-target toxicity, as opposed to various chemotherapeutic agents known to affect bone homeostasis [161]. Moreover, the degree to which UHRF1 loss reverted the increased malignancy upon

RB loss suggests that the benefit of UHRF1 targeting could go beyond the scope of OS by improving treatment paradigms of other cancers harboring RB/E2F pathway inactivation.

Materials and methods

In situ hybridization

Osteosarcoma tissue microarrays, containing 40 cases of osteosarcoma, duplicate cores per case, were purchased from US Biomax, Inc. Formalin-fixed, paraffin-embedded (FFPE) slides were incubated at 60°C for 1hr for deparaffinization, followed by two washes of xylene and two washes of 100% ethanol for dehydration, 5min each at RT, before air-drying. RNAscope® technology was utilized for *in situ* hybridization. Assay was performed following manufacturer's protocol. Human and mouse UHRF1-specific probes were customized by Bio-Techne. RNAscope® Positive Control Probe- Hs-PPIB/Mm-PP1B and RNAscope® Negative Control Probe- DapB were used. OpalTM 570 fluorophore was used at a 1:1000 dilution. Slides were mounted with ProLong Gold Antifade Mountant.

Xenografts, mouse models and cell lines

The five orthotopic xenografts used in this study: SJOS001105 (PDX1), SJOS001112 (PDX2), SJOS001107 (PDX3), SJSO010930 (PDX4), and SJOS001121 (PDX5) were obtained from the Childhood Solid Tumor Network [133]. Athymic nude (NU/J) mice were obtained from The Jackson Laboratories. The *p53*^{lox} and *Rb1*^{lox} conditional-knockout mice were obtained from the Mouse Models of Human Cancer Consortium at the National Cancer Institute; the *Osx-cre* mice were obtained from The Jackson Laboratory. The *Uhrf1*-conditional knockout mouse was generated from mice obtained from the European Mouse Mutant Archive, backcrossed to flipasse (Flp) mice for removal of the neo-cassette (tm1c conversion), and then backcrossed to C57BL/6N mice for Flp removal. Mice were monitored weekly for signs of OS. Moribund status was defined as the point when tumors had reached 10% body weight or

induced paralysis in the mouse. The University of California Irvine Institutional Animal Care and Use Committee approved all animal procedures. OS cell lines 143B, SJSA-1, SaOS-2 and U-2 OS, as well as MSCs and HEK293T cells were acquired from ATCC. 143B were cultured in MEM (Gibco), with 10% BCS, penicillin/streptomycin, and 0.015mg/ml BrdU. SJSA-1 were cultured in RPMI (Gibco), with 10% BCS and penicillin/streptomycin. SaOS-2 were cultured in McCoy's 5A (Gibco), with 10% BCS and penicillin/streptomycin. U-2 OS were cultured in McCoy's 5A (Gibco), with 15% BCS and penicillin/streptomycin. MSCs were cultured in Alpha-MEM (Gibco), with 10% FBS and penicillin/streptomycin, HEK293T cells were culture in high-glucose DMEM (Gibco), with 10% BCS, penicillin/streptomycin and sodium pyruvate. Cells were passaged every 3 to 4 days or when they reached 70-80% confluence. At the time of passage, cells were split to 20% confluence.

Lentivirus production and transduction

Lentiviral particles were produced by co-transfecting the envelope plasmid pCMV-VSV-G (Addgene), packaging plasmid pCMV-dR8.2 dvpr (Addgene), and lentiCRISPRv2 (Addgene) or plentiCRISPRv2 with UHRF gRNA (gRNA sequence: TCAATGAGTACGTCGATGCT; GenScript) into HEK293T cells using calcium phosphate transfection method. Supernatants containing lentiviral particles were harvested at 24 hours and 48 hours post-transfection. Cell debris were cleared by centrifugation at 1600 × g for 10 min at 4°C. Supernatants were then filtered through 0.45 μm PES filter (25-223, Genesee Scientific), and concentrated by ultracentrifugation at 23000 RPM for 2 hours at 4°C. Lentiviral particles were resuspended in ice-cold PBS and stored at -80°C. Transduction of target cells were achieved by exposing

cells to viral particles in serum –free condition for 6 hours. Puromycin selection was carried out at a concentration of 2 μg/ml.

Real-time RT-PCR

Total RNA was isolated from cells or tumor tissues by homogenizing samples with TRIzol Reagent. RNA was isolated through chloroform extraction. 1 μg of total RNA was used for cDNA synthesis with the SuperScript™III First-strand synthesis system (Invitrogen) according to manufacturer's protocol at a reaction volume of 20 μl. Quantitative PCR amplification was performed using 1 μl of reverse-transcribed product in Power SYBR Green PCR Master Mix (4367659, Life Technologies). Primers were designed using IDT Real-Time PCR tool (Integrated DNA Technologies). Reaction was carried out using 7500 Real-Time PCR system (Applied Biosciences). Data were normalized to those obtained with endogenous control 18S mRNA and analyzed using ΔΔCt method. Primer sequence for PCR amplification are as follows: UHRF1 (sense: 5'-GCTGTTGATGTTTCTGGTGTC-3'; antisense: 5'-TGCTGTCAGGAAGATGCTTG-3'), PLAU (sense: 5'-GAGCAGAGACACTAACGACTTC-3'; antisense: 5'-CTCACACTTACACTCACAGCC-3'), SEMA3E (sense: 5'-CTGGCTCGAGACCCTTACTG-3' ; antisense: 5'- CAAAGCATCCCCAACAAACT-3'), HAS2 (sense: 5'-TCCATGTTTTGACGTTTGCAG-3'; antisense: 5'-AGCAGTGATATGTCTCCTTTGG-3'), LAMC2 (sense: 5'-CACCATACTCCTTGCTTCCTG-3'; antisense: 5'-GTGCAGTTTGTCTTTCCATCC-3'), 18S (sense: 5'-GTAACCCGTTGAACCCCATT-3'; antisense: 5'-CCATCCAATCGGTAGTAGCG-3').

Western blotting

Cell pellets or tumor tissues were homogenized by pipetting or pellet pestle in RIPA buffer (50 mM Tris-HCl, pH=8, 150 mM NaCl, 1% NP-40, 0.5 % Sodium deoxycholate, 0.1% SDS, 1 mM EDTA) supplemented with protease inhibitor (cOmplete™, Mini, EDTA-free Protease Inhibitor Cocktail, Roche). Samples were allowed to lyse for 30 min on ice before centrifugation at 14000 RPM at 4° for 30 min. Protein concentration was measured using BCA protein assay (Pierce™ BCA Protein Assay Kit). 40µg of total protein were resolved in 4-15% SDS-PAGE gel (Mini-PROTEAN TGX Gels (4-15%), Bio-rad), and transferred onto PVDF membrane (Immobilon-P Membrane, PVDF, EMD Millipore) using semi-dry transfer apparatus (Bio-rad). Ponceau S stain was used to validate successful transfer. Non-specific binding was prevented by incubating the membrane in 3% non-fat dry milk in TBS-0.25% Tween (TBS-T) for 1 hour at room temperature, shaking. Primary antibodies were diluted in 0.5% non-fat dry milk in TBS-T as follows: 1:1000 anti-Uhrf1 (sc-373750, Santa Cruz Biotechnology), 1:1000 anti-Rb (9313T, Cell Signaling). Membranes were incubated in primary antibody overnight, shaking, at 4°C. Membranes were then rinsed 3 times with TBS-T on shaker and incubated with secondary antibody for 40min at room temperature, shaking. Secondary antibodies were diluted in 0.5% non-fat dry milk in TBS-T as follows: 1:1000 peroxidase labeled anti-mouse IgG (PI-2000, Vector Laboratories), 1:1000 peroxidase labeled anti-rabbit IgG (PI-1000, Vector Laboratories). Membranes were again rinsed 3 times with TBS-T on shaker. Chemiluminescence were detected using SuperSignal™ West Pico Chemiluminescent Substrate (34077, Thermo Scientific). Relative band intensities were analyzed using ImageJ software.

Clonogenic assay

4% agarose stock was prepared by mixing agarose with water and kept warm in 55°C heat bath. Appropriate cell culture medium was used for subsequent dilution of the agarose stock. 6-well plates were coated with 1ml of 0.75% agarose prior to seeding. Single cell suspension was mixed with agarose to achieve a final agarose concentration of 0.36%, the mixture was then layered on top of the 0.75% agarose coating (Seeding density 200 cells/cm^2). Cells were incubated at 37°C with 5% CO_2 until cells in control wells have formed sufficiently large colonies (>50 cells). Colonies were fixed with 10% methanol for 15 min and stained with 5% Giemsa for 30 min for visualization.

Subcutaneous injection

Human OS cell lines were dissociated in 0.25% trypsin-EDTA, washed with PBS prior to counting. $2 \cdot 10^6$ cells were resuspended in 100 µl of PBS and injected subcutaneously into the flank region of mice. Tumors were collected 3 weeks post injection. For cells that require doxycycline induction for the expression CRISPR/Cas9, 2 mg/ml doxycycline hyclate supplemented water was administered *ad libitum*. 10 mg/ml of sucrose was added to doxycycline supplemented water to increase consumption.

RNA Sequencing

Total RNA was isolated using the RNA Micro Kit (Qiagen). Subsequently, 500 ng of total RNA was used to create the RNA-seq library following the manufacturer's protocol from purification, mRNA fragmentation through the adenylation of end-repaired cDNA fragments and cleanup (TruSeq Stranded mRNA, Illumina). The collected sample was cleaned with

AMPure XP beads (Beckman Coulter) and eluted in 20 µl of 10 mM Tris buffer, pH 8, 0.1% Tween 20. A paired-end 100-bp sequencing run was performed on HiSeq 4000 yielding 348M PE reads with a final library concentration of 2 nM as determined by qPCR (KAPA Biosystem).

Sequencing reads were aligned to the mouse or human reference genome (GRCm38 or GRCh38, ENSEMBL v.92) using STAR (v2.5.2a) [162]. Each read pair was allowed a maximum number of mismatches of 10. Each read was allowed a maximum number of multiple alignments of 3. Gene counts for each sample were produced using HTSeq (v0.6.1p1) [163]. Read count normalization and differential expression analysis were performed using DESeq2 (v1.22.2) in R (v3.5.2) [164]. Genes with low reads (sum across samples < 10) were removed. Differentially expressed genes (DEG) were calculated by comparing UHRF1 knockouts to matching controls, genes with base mean ≥ 10, Log2FoldChange ≥ 1 or ≤ -1, and adjusted p value (Benjamini-Hockberg) ≤ 0.05 were called differentially expressed genes. 3D PCA plot was generated using the R package plot3D (v1.1.1).

Scratch-wound assay

Cells were seeded the day before the scratch at a density of $1.1\times10^5/cm^2$ and grown to 100% confluency in 6-well cell culture plates. Two hours before the scratch, cells were treated with 5 µg/ml of mitomycin C (S8146, Sigma). At time 0, a 1000 µl tip was used to create a wound across the cell monolayer. The cells were then placed back to the incubator for 8 hours at 37°C with 5% CO_2. Images of the wound at the exact same field were taken at 0 and 8 h and analyzed using the ZEISS ZEN microscope software. A total of 20 measurements in pixels

were made based on the image taken. The pixels migrated was calculated as the difference between the average width of the scratches before and after the incubation period. P-values were calculated using two-tailed t-test.

Transwell invasion assay

PET track-etched membrane with 8μm pore (353097, Corning) were inserted into 24-well cell culture plate. Membranes were coated with Matrigel at a density of 25 μg/insert. 2×10^4 cells were seeded onto the membrane in 100 μl of appropriate cell culture medium and placed into the incubator for 2 hours at 37°C with 5% CO_2 to allow cell attachment. After the cells have attached to the membrane, 100 μl of medium were added to the inner chamber. If doxycycline is required, 2 μg/ml doxycycline was prepared in 100 μl medium in order to reach a final concentration of 1μg/ml. 600 μl of appropriate cell culture medium supplemented with 100 ng/ml fibroblast growth factor (FGF) were pipetted into the outer chamber. Cells were then placed back into the incubator for no more than 16 hours at 37°C with 5% CO_2. Cell culture medium was aspirated, and cotton swabs were used to scrape off non-migratory cells on the top side of the insert. The remaining cells at the bottom side of the insert were then fixed and stained with a solution consists of 6% glutaraldehyde and 0.5% crystal violet for 2 hours. Stains were washed out with tap water and the inserts left to dry at room temperature. Images of 5 different fields within each insert were taken for analysis by cell count.

Tail vein injection

Human OS cells lines were dissociated in 0.25% trypsin-EDTA, washed with PBS prior to counting. For the experimental metastasis model, 2×10^6 cells were resuspended in 200 µl of PBS and injected intravenously through the tail vein. Mice lungs were collected 3 weeks after injection, fixed in 4% formaldehyde for histological analysis.

FDG-PET/microCT scan

Mice were fasted overnight. Mice were injected with 0.1-0.5 mCi of ^{18}F-FDG in sterile saline (~ 0.05 to 0.2 ml) intraperitoneally (i.p.) and allow to uptake the ^{18}F-FDG for 60 min prior to imaging. Animals were anesthetized and laid in supine position on the scanner holder with continued anesthesia. Scanning data was acquired in full list mode and sorted into a single frame, 3 dimensional sinogram, which was rebinned using a Fourier rebinning algorithm. The images were reconstructed using 2-dimensional filter back projection using a Hanning Filter with a Nyquist cut off at 0.5 and corrected for attenuation using the Co-57 attenuation scan data. Analysis of PET was conducted using PMOD 3.0 and IRW software. The PET data was co-registered to the CT template for drawing regions-of-interest (ROI). The ROI data was converted to standard uptake value (SUV) of ^{18}F-FDG.

CHAPTER 5

CONCLUDING REMARKS AND FUTURE DIRECTIONS

The study detailed in this dissertation proposed a novel mechanism of action for the tumor suppressor protein RB. **Chapter 2** concluded that the implication of the RB/E2F signaling pathway has on the clinical outlook of OS is heavily dependent on the association of RB with E2F1 and E2F3, rather than with other E2F members. Downstream targets of the RB-E2F1 and RB-E2F3 axis are more likely to be the effectors that promotes tumor progression. As the RB/E2F signaling pathway is perturbed in most cancers, our discovery narrows down the search for potential therapeutic targets for RB-related neoplasms. We followed this result with the investigation of two direct targets of the RB-E2F1 axis, HELLS and UHRF1. **Chapters 3** and **4** discusses their role in promoting osteosarcoma tumorigenesis/progression. We showed that HELLS overexpression is dispensable for OS tumorigenesis, the fact that HELLS expression is implicated in various other human neoplasms to be either the driver of tumorigenesis or is involved in promoting tumor progression suggests that the role of HELLS may vary in a context-dependent manner. On the other hand, our data provided strong evidence-based support towards the hypothesis that loss of *RB1* contributes to OS via elevated UHRF1 expression and activity. We established the significant degree of reversal in OS tumor phenotype upon UHRF1 loss in the context of RB-dependent UHRF1 overexpression. UHRF1 overexpression plays a part in all three major benchmarks of a developing neoplasm: Tumorigenesis, progression, and metastasis; as we demonstrated that UHRF1 activity in OS promotes osteosarcomagenesis, increases OS cell proliferation, and contributes to pulmonary metastasis. Following the establishment of the role of UHRF1 in OS metastasis, we further hypothesized that UHRF1 facilitates increase in cell mobility through uPA. Although further testing is needed, the

plasmin activity induced by elevated uPA level could begin to explain the increased mobility, degradation of extracellular matrix and angiogenesis associated with UHRF1 expression.

While there are no detectable differences in terms of UHRF1 expression between RB-null and RB-wildtype OS cases, UHRF1 may serve as a conduit for poor prognosis following RB loss. The RB/E2F complex is known not only for its role in direct transcriptional repression, but also as epigenetic modifiers through the recruitment of chromatin remodelers [73-77]. Two UHRF1 domains, PHD and RING, contain LXCXE RB-binding motifs [107]. Our preliminary data showed a preferential binding of UHRF1 to hyperphosphorylated RB. Combined with our finding that hyperphosphorylated RB being the predominant form in RB-wildtype cells due to increased CDK4/6 activity (data not shown), this hints a potential protein-protein interaction between RB and UHRF1 that only exists in RB-wildtype but not RB-null OS. The possible loss of this layer of epigenetic regulation could account for the drastic difference in clinical prognosis, supporting the view that loss-of-function due to genetic ablation of the RB1 gene is not completely synonymous to functional inactivation of RB by phosphorylation (Figure 5.1).

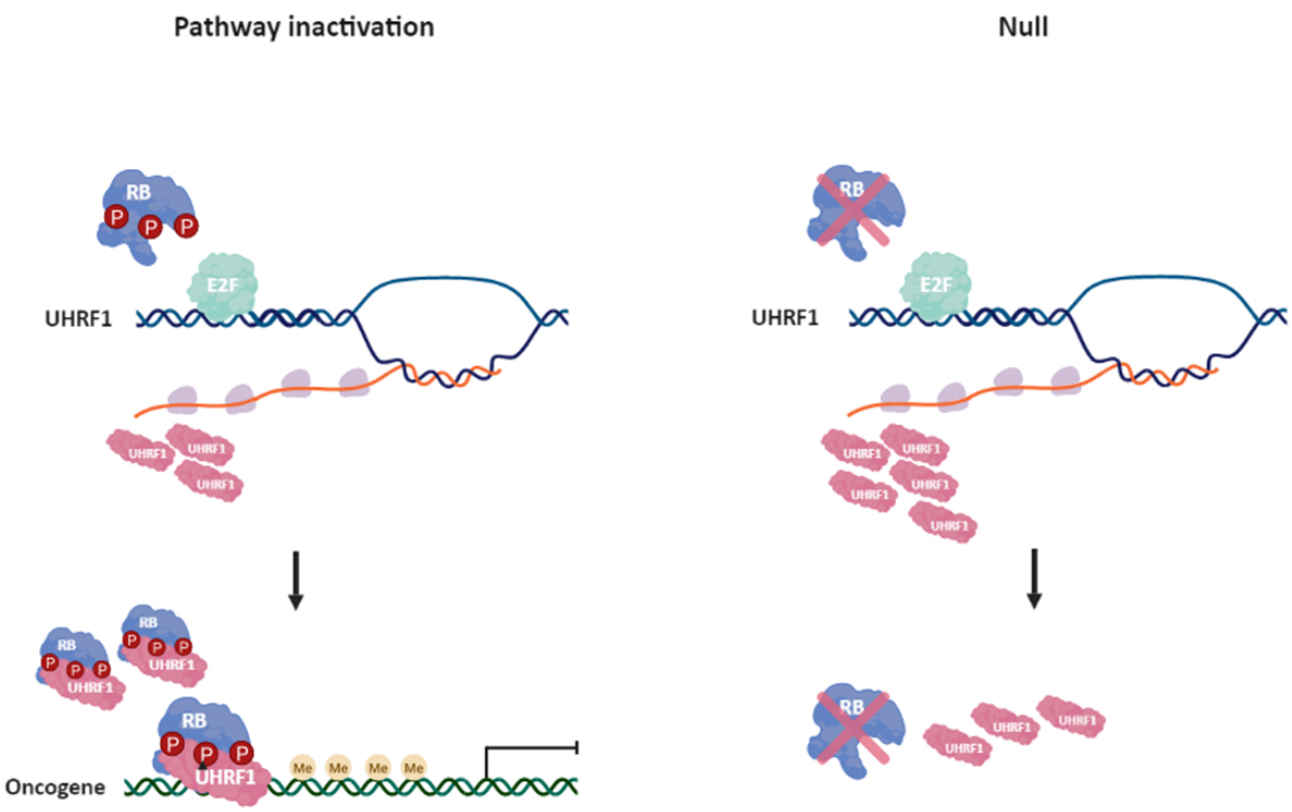

Figure 5.1. Proposed schematic of UHRF1-mediated poor prognosis.

In RB-wildtype OS, where the RB/E2F pathway is functionally inactivated, although transcriptional control of RB targets are diminished, RB are still able to exert epigenetic regulation upon its association with UHRF1. Both levels of regulations are absent in RB-null OS, which presents a worsened clinical outlook.

A model has been proposed for DNA methylation inheritance in replicating cells consisting of a complex formed by DNMT1, UHRF1, PCNA, G9a, RB and PARP1 proteins [165], describing the role of UHRF1 in coordinating DNA methylation and histone modifications for the maintenance of heterochromatin and proper gene expression in nascent cells. While UHRF1 is often characterized by its crucial role in DNA methylation [136, 152, 166, 167]. The homeostasis between its epigenetic functions and its ligase activity remains to be studied, this results in conflicting reports regarding the outcome associated with increased expression of UHRF1 in cancer. While some evidences points toward increased recruitment of DNMT1 upon increase of UHRF1 activity, resulting in the facilitation of epigenetic silencing of tumor suppressor genes through DNA hypermethylation [95, 136]; others support that UHRF1 mediates DNMT1 ubiquitination and degradation, which lead to global DNA hypomethylation that results in oncogene activation [153, 154, 168, 169]. This indicates that multiple functional domains of UHRF1 are involved in different cancer promoting phenotypes.

Following the study described in this dissertation, we seek to (1) pinpoint specific functional domain(s) of UHRF1 implicated in UHRF1-mediated increase of migratory potential, (2) investigate further the interaction between RB and UHRF1 at the protein level. This serves to not only provide deeper mechanistic insight extending beyond the RB-UHRF1 network, but to narrow down areas of interest for the potential development of small molecule inhibitor for UHRF1 targeting. To evaluate whether the loss of RB-UHRF1 interaction differentiates RB-wildtype and RB-null OS, we propose to generate mutations that interferes RB-UHRF1 interaction. Two consensus RB-binding motifs (LXCXE), are located at positions

L331 to E335 and L725 to E729 of UHRF1 [107]. To this end, the following mutations at the conserved cysteine residue (C to G and C to R) within LXCXE motifs: (1) C333G, (2) C333R, (3) C727G and (4) C727R, will be generated. Such site-directed mutagenesis can be achieved in other domains of UHRF1. The following point-mutations/truncation located within the RING domain ablates E3-ligase activity of UHRF1: (1) C724A, (2) H741A, (3) C724A, (4) H741A, (5) Δ724-762. Point-mutations Y188A and Y191A prevents interaction with histone H3 at the TTD domain. Point-mutations D334A, E335A, and W238A prevents interaction with histone H3 at the PHD domain [101, 170]. Point-mutations D469G, Y478A, and R491A blocks the interaction between SRA domain and hemi-methylated DNA. We propose to introduce UHRF1 mutants into MSCs followed by the evaluation of the degree in UHRF1-mediated increase of migratory/invasive potential in comparison to wildtype UHRF1. Thus, identifying functional domain(s) responsible for UHRF1-mediated migration, invasion and metastasis.

Taken together, this dissertation brought to attention the potential therapeutic value and efficacy of UHRF1 targeting. We've provided strong evidences supporting UHRF1 targeting as a novel therapeutic strategy, as well as substantial preliminary knowledge sufficient for a more comprehensive mapping of the regulatory network in the near future. Understanding the mechanism of UHRF1-mediated malignant phenotypes upon RB/E2F inactivation not only serves to provide improvement in treatment options of OS, but various human neoplasms in which RB/E2F pathway inactivation is implicated.

REFERENCES

1. Cormier, J.N. and R.E. Pollock, *Soft tissue sarcomas.* CA Cancer J Clin, 2004. **54**(2): p. 94-109.
2. Ottaviani, G. and N. Jaffe, *The epidemiology of osteosarcoma.* Cancer Treat Res, 2009. **152**: p. 3-13.
3. Cotterill, S.J., et al., *Stature of young people with malignant bone tumors.* Pediatric Blood & Cancer, 2004. **42**(1): p. 59-63.
4. Huang, Y.M., et al., *The metastasectomy and timing of pulmonary metastases on the outcome of osteosarcoma patients.* Clin Med Oncol, 2009. **3**: p. 99-105.
5. Damron, T.A., W.G. Ward, and A. Stewart, *Osteosarcoma, chondrosarcoma, and Ewing's sarcoma: National Cancer Data Base Report.* Clin Orthop Relat Res, 2007. **459**: p. 40-7.
6. Kaste, S.C., et al., *Metastases detected at the time of diagnosis of primary pediatric extremity osteosarcoma at diagnosis: imaging features.* Cancer, 1999. **86**(8): p. 1602-8.
7. Mirabello, L., R.J. Troisi, and S.A. Savage, *Osteosarcoma incidence and survival rates from 1973 to 2004: data from the Surveillance, Epidemiology, and End Results Program.* Cancer, 2009. **115**(7): p. 1531-43.
8. Chen, X., et al., *Recurrent somatic structural variations contribute to tumorigenesis in pediatric osteosarcoma.* Cell Rep, 2014. **7**(1): p. 104-12.
9. Kovac, M., et al., *Exome sequencing of osteosarcoma reveals mutation signatures reminiscent of BRCA deficiency.* Nat Commun, 2015. **6**: p. 8940.
10. Perry, J.A., et al., *Complementary genomic approaches highlight the PI3K/mTOR pathway as a common vulnerability in osteosarcoma.* Proc Natl Acad Sci U S A, 2014. **111**(51): p. E5564-73.
11. Martin, J.W., J.A. Squire, and M. Zielenska, *The genetics of osteosarcoma.* Sarcoma, 2012. **2012**: p. 627254.
12. Visvader, J.E., *Cells of origin in cancer.* Nature, 2011. **469**(7330): p. 314-22.
13. Mutsaers, A.J. and C.R. Walkley, *Cells of origin in osteosarcoma: mesenchymal stem cells or osteoblast committed cells?* Bone, 2014. **62**: p. 56-63.
14. Jacks, T., et al., *Tumor spectrum analysis in p53-mutant mice.* Curr Biol, 1994. **4**(1): p. 1-7.
15. Belchis, D.A., et al., *Loss of heterozygosity and microsatellite instability at the retinoblastoma locus in osteosarcomas.* Diagn Mol Pathol, 1996. **5**(3): p. 214-9.
16. Heinsohn, S., et al., *Determination of the prognostic value of loss of heterozygosity at the retinoblastoma gene in osteosarcoma.* Int J Oncol, 2007. **30**(5): p. 1205-14.
17. Patino-Garcia, A., et al., *Genetic and epigenetic alterations of the cell cycle regulators and tumor suppressor genes in pediatric osteosarcomas.* J Pediatr Hematol Oncol, 2003. **25**(5): p. 362-7.
18. Rubio, R., et al., *Deficiency in p53 but not retinoblastoma induces the transformation of mesenchymal stem cells in vitro and initiates leiomyosarcoma in vivo.* Cancer Res, 2010. **70**(10): p. 4185-94.
19. Rubio, R., et al., *The differentiation stage of p53-Rb-deficient bone marrow mesenchymal stem cells imposes the phenotype of in vivo sarcoma development.* Oncogene, 2013. **32**(41): p. 4970-80.
20. Lin, P.P., et al., *Targeted mutation of p53 and Rb in mesenchymal cells of the limb bud produces sarcomas in mice.* Carcinogenesis, 2009. **30**(10): p. 1789-95.
21. Walkley, C.R., et al., *Conditional mouse osteosarcoma, dependent on p53 loss and potentiated by loss of Rb, mimics the human disease.* Genes Dev, 2008. **22**(12): p. 1662-76.
22. Quist, T., et al., *The impact of osteoblastic differentiation on osteosarcomagenesis in the mouse.* Oncogene, 2015. **34**(32): p. 4278-84.
23. Torreggiani, E., et al., *Preosteocytes/osteocytes have the potential to dedifferentiate becoming a source of osteoblasts.* PLoS One, 2013. **8**(9): p. e75204.
24. Sottnik, J.L., et al., *Osteocytes serve as a progenitor cell of osteosarcoma.* J Cell Biochem, 2014. **115**(8): p. 1420-9.
25. Uluckan, O., et al., *Preclinical mouse models of osteosarcoma.* Bonekey Rep, 2015. **4**: p. 670.
26. Grigoriadis, A.E., et al., *Osteoblasts are target cells for transformation in c-fos transgenic mice.* J Cell Biol, 1993. **122**(3): p. 685-701.
27. Baker, S.J., et al., *Chromosome-17 Deletions and P53 Gene-Mutations in Colorectal Carcinomas.* Science, 1989. **244**(4901): p. 217-221.
28. Vogelstein, B., D. Lane, and A.J. Levine, *Surfing the p53 network.* Nature, 2000. **408**(6810): p. 307-310.
29. Berman, S.D., et al., *Metastatic osteosarcoma induced by inactivation of Rb and p53 in the osteoblast lineage.* Proc Natl Acad Sci U S A, 2008. **105**(33): p. 11851-6.

30. Momand, J., et al., *The mdm-2 oncogene product forms a complex with the p53 protein and inhibits p53-mediated transactivation.* Cell, 1992. **69**(7): p. 1237-45.
31. Gu, J., et al., *Mutual dependence of MDM2 and MDMX in their functional inactivation of p53.* J Biol Chem, 2002. **277**(22): p. 19251-4.
32. Barak, Y., et al., *mdm2 expression is induced by wild type p53 activity.* EMBO J, 1993. **12**(2): p. 461-8.
33. Wu, X., et al., *The p53-mdm-2 autoregulatory feedback loop.* Genes Dev, 1993. **7**(7A): p. 1126-32.
34. Lengner, C.J., et al., *Osteoblast differentiation and skeletal development are regulated by Mdm2-p53 signaling.* J Cell Biol, 2006. **172**(6): p. 909-21.
35. Li, M.Y., et al., *Mono-versus polyubiquitination: Differential control of p53 fate by Mdm2.* Science, 2003. **302**(5652): p. 1972-1975.
36. Ladanyi, M., et al., *MDM2 gene amplification in metastatic osteosarcoma.* Cancer Res, 1993. **53**(1): p. 16-8.
37. Yoshida, A., et al., *MDM2 and CDK4 immunohistochemical coexpression in high-grade osteosarcoma: correlation with a dedifferentiated subtype.* Am J Surg Pathol, 2012. **36**(3): p. 423-31.
38. Lenos, K., et al., *Alternate splicing of the p53 inhibitor HDMX offers a superior prognostic biomarker than p53 mutation in human cancer.* Cancer Res, 2012. **72**(16): p. 4074-84.
39. Matijasevic, Z., et al., *The Zn-finger domain of MdmX suppresses cancer progression by promoting genome stability in p53-mutant cells.* Oncogenesis, 2016. **5**(10): p. e262.
40. Hirose, M., et al., *MDM4 expression as an indicator of TP53 reactivation by combined targeting of MDM2 and MDM4 in cancer cells without TP53 mutation.* Oncoscience, 2014. **1**(12): p. 830-43.
41. Pan, Y. and J. Chen, *MDM2 promotes ubiquitination and degradation of MDMX.* Mol Cell Biol, 2003. **23**(15): p. 5113-21.
42. Zhang, Y.P., Y. Xiong, and W.G. Yarbrough, *ARF promotes MDM2 degradation and stabilizes p53: ARF-INK4a locus deletion impairs both the Rb and p53 tumor suppression pathways.* Cell, 1998. **92**(6): p. 725-734.
43. Oh, J.H., et al., *Aberrant methylation of p14ARF gene correlates with poor survival in osteosarcoma.* Clin Orthop Relat Res, 2006. **442**: p. 216-22.
44. el-Deiry, W.S., et al., *WAF1, a potential mediator of p53 tumor suppression.* Cell, 1993. **75**(4): p. 817-25.
45. Harper, J.W., et al., *The p21 Cdk-interacting protein Cip1 is a potent inhibitor of G1 cyclin-dependent kinases.* Cell, 1993. **75**(4): p. 805-16.
46. Waldman, T., K.W. Kinzler, and B. Vogelstein, *p21 is necessary for the p53-mediated G1 arrest in human cancer cells.* Cancer Res, 1995. **55**(22): p. 5187-90.
47. Chen, Z., et al., *CRL4B(DCAF11) E3 ligase targets p21 for degradation to control cell cycle progression in human osteosarcoma cells.* Sci Rep, 2017. **7**(1): p. 1175.
48. Ding, Y., et al., *p21 overexpression sensitizes osteosarcoma U2OS cells to cisplatin via evoking caspase-3 and Bax/Bcl-2 cascade.* Tumour Biol, 2014. **35**(4): p. 3119-23.
49. Zhan, Q.M., F. Carrier, and A.J. Fornace, *Induction of Cellular P53 Activity by DNA-Damaging Agents and Growth Arrest (Vol 13, Pg 4249, 1993).* Molecular and Cellular Biology, 1993. **13**(9): p. 5928-5928.
50. Zhan, Q.M., et al., *Association with Cdc2 and inhibition of Cdc2/cyclin B1 kinase activity by the p53-regulated protein Gadd45.* Oncogene, 1999. **18**(18): p. 2892-2900.
51. Wang, X.W., et al., *GADD45 induction of a G(2)/M cell cycle checkpoint.* Proceedings of the National Academy of Sciences of the United States of America, 1999. **96**(7): p. 3706-3711.
52. Al-Romaih, K., et al., *Modulation by decitabine of gene expression and growth of osteosarcoma U2OS cells in vitro and in xenografts: identification of apoptotic genes as targets for demethylation.* Cancer Cell Int, 2007. **7**: p. 14.
53. Al-Romaih, K., et al., *Modulation by decitabine of gene expression and growth of osteosarcoma U2OS cells in vitro and in xenografts: Identification of apoptotic genes as targets for demethylation.* Cancer Cell International, 2007. **7**.
54. Liu, H., et al., *New roles for the RB tumor suppressor protein.* Curr Opin Genet Dev, 2004. **14**(1): p. 55-64.
55. Burkhart, D.L. and J. Sage, *Cellular mechanisms of tumour suppression by the retinoblastoma gene.* Nat Rev Cancer, 2008. **8**(9): p. 671-82.
56. Belchis, D.A., et al., *Loss of heterozygosity and microsatellite instability at the retinoblastoma locus in osteosarcomas.* Diagnostic Molecular Pathology, 1996. **5**(3): p. 214-219.
57. Patino-Garcia, A., et al., *Genetic and epigenetic alterations of the cell cycle regulators and tumor suppressor genes in pediatric osteosarcomas.* Journal of Pediatric Hematology Oncology, 2003. **25**(5): p. 362-367.

58. Heinsohn, S., et al., *Determination of the prognostic value of loss of heterozygosity at the retinoblastoma gene in osteosarcoma.* International Journal of Oncology, 2007. **30**(5): p. 1205-1214.
59. Chen, X., et al., *Recurrent Somatic Structural Variations Contribute to Tumorigenesis in Pediatric Osteosarcoma.* Cell Reports, 2014. **7**(1): p. 104-112.
60. Feugeas, O., et al., *Loss of heterozygosity of the RB gene is a poor prognostic factor in patients with osteosarcoma.* J Clin Oncol, 1996. **14**(2): p. 467-72.
61. Benassi, M.S., et al., *Altered G1 phase regulation in osteosarcoma.* Int J Cancer, 1997. **74**(5): p. 518-22.
62. Goto, A., et al., *Association of loss of heterozygosity at the p53 locus with chemoresistance in osteosarcomas.* Jpn J Cancer Res, 1998. **89**(5): p. 539-47.
63. Wadayama, B., et al., *Mutation spectrum of the retinoblastoma gene in osteosarcomas.* Cancer Res, 1994. **54**(11): p. 3042-8.
64. Ren, W. and G. Gu, *Prognostic implications of RB1 tumour suppressor gene alterations in the clinical outcome of human osteosarcoma: a meta-analysis.* Eur J Cancer Care (Engl), 2017. **26**(1).
65. Benassi, M.S., et al., *Alteration of pRb/p16/cdk4 regulation in human osteosarcoma.* Int J Cancer, 1999. **84**(5): p. 489-93.
66. Maitra, A., et al., *Loss of p16(INK4a) expression correlates with decreased survival in pediatric osteosarcomas.* Int J Cancer, 2001. **95**(1): p. 34-8.
67. Macaluso, M., et al., *Modulation of cell cycle components by epigenetic and genetic events.* Semin Oncol, 2005. **32**(5): p. 452-7.
68. Dowdy, S.F., et al., *Physical interaction of the retinoblastoma protein with human D cyclins.* Cell, 1993. **73**(3): p. 499-511.
69. Harbour, J.W. and D.C. Dean, *Chromatin remodeling and Rb activity.* Curr Opin Cell Biol, 2000. **12**(6): p. 685-9.
70. Morris, E.J. and N.J. Dyson, *Retinoblastoma protein partners.* Adv Cancer Res, 2001. **82**: p. 1-54.
71. Talluri, S. and F.A. Dick, *Regulation of transcription and chromatin structure by pRB: here, there and everywhere.* Cell Cycle, 2012. **11**(17): p. 3189-98.
72. Viatour, P. and J. Sage, *Newly identified aspects of tumor suppression by RB.* Dis Model Mech, 2011. **4**(5): p. 581-5.
73. Benetti, R., et al., *A mammalian microRNA cluster controls DNA methylation and telomere recombination via Rbl2-dependent regulation of DNA methyltransferases.* Nat Struct Mol Biol, 2008. **15**(9): p. 998.
74. Chi, P., C.D. Allis, and G.G. Wang, *Covalent histone modifications--miswritten, misinterpreted and mis-erased in human cancers.* Nat Rev Cancer, 2010. **10**(7): p. 457-69.
75. Lu, J., et al., *A genome-wide RNA interference screen identifies putative chromatin regulators essential for E2F repression.* Proc Natl Acad Sci U S A, 2007. **104**(22): p. 9381-6.
76. Wen, H., et al., *Epigenetic regulation of gene expression by Drosophila Myb and E2F2-RBF via the Myb-MuvB/dREAM complex.* Genes Dev, 2008. **22**(5): p. 601-14.
77. Zhang, J., et al., *A novel retinoblastoma therapy from genomic and epigenetic analyses.* Nature, 2012. **481**(7381): p. 329-34.
78. Geiman, T.M. and K. Muegge, *Lsh, an SNF2/helicase family member, is required for proliferation of mature T lymphocytes.* Proc Natl Acad Sci U S A, 2000. **97**(9): p. 4772-7.
79. Dennis, K., et al., *Lsh, a member of the SNF2 family, is required for genome-wide methylation.* Genes Dev, 2001. **15**(22): p. 2940-4.
80. Sun, L.Q., et al., *Growth retardation and premature aging phenotypes in mice with disruption of the SNF2-like gene, PASG.* Genes Dev, 2004. **18**(9): p. 1035-46.
81. Tao, Y., et al., *Lsh, chromatin remodeling family member, modulates genome-wide cytosine methylation patterns at nonrepeat sequences.* Proc Natl Acad Sci U S A, 2011. **108**(14): p. 5626-31.
82. Zhu, H., et al., *Lsh is involved in de novo methylation of DNA.* The EMBO journal, 2006. **25**(2): p. 335-45.
83. Burrage, J., et al., *The SNF2 family ATPase LSH promotes phosphorylation of H2AX and efficient repair of DNA double-strand breaks in mammalian cells.* Journal of Cell Science, 2012. **125**(22): p. 5524-5534.
84. Benavente, C.A., et al., *Chromatin remodelers HELLS and UHRF1 mediate the epigenetic deregulation of genes that drive retinoblastoma tumor progression.* Oncotarget, 2014. **5**(20): p. 9594-608.
85. Niu, J., et al., *Transcriptional activation of the senescence regulator Lsh by E2F1.* Mech Ageing Dev, 2011. **132**(4): p. 180-6.
86. von Eyss, B., et al., *The SNF2-like helicase HELLS mediates E2F3-dependent transcription and cellular transformation.* The EMBO journal, 2012. **31**(4): p. 972-85.

87. Tao, Y., et al., *Treatment of breast cancer cells with DNA demethylating agents leads to a release of Pol II stalling at genes with DNA-hypermethylated regions upstream of TSS.* Nucleic Acids Res, 2011. **39**(22): p. 9508-20.
88. Chen, D., et al., *TOP2A, HELLS, ATAD2, and TET3 Are Novel Prognostic Markers in Renal Cell Carcinoma.* Urology, 2017. **102**: p. 265 e1-265 e7.
89. He, X., et al., *Chromatin Remodeling Factor LSH Drives Cancer Progression by Suppressing the Activity of Fumarate Hydratase.* Cancer Res, 2016. **76**(19): p. 5743-5755.
90. Ryu, B., et al., *Comprehensive expression profiling of tumor cell lines identifies molecular signatures of melanoma progression.* PLoS One, 2007. **2**(7): p. e594.
91. von Eyss, B., et al., *The SNF2-like helicase HELLS mediates E2F3-dependent transcription and cellular transformation.* EMBO J, 2012. **31**(4): p. 972-85.
92. Xiao, D., et al., *Chromatin Remodeling Factor LSH is Upregulated by the LRP6-GSK3beta-E2F1 Axis Linking Reversely with Survival in Gliomas.* Theranostics, 2017. **7**(1): p. 132-143.
93. Mousli, M., et al., *ICBP90 belongs to a new family of proteins with an expression that is deregulated in cancer cells.* British journal of cancer, 2003. **89**(1): p. 120-7.
94. Unoki, M., et al., *UHRF1 is a novel molecular marker for diagnosis and the prognosis of bladder cancer.* Br J Cancer, 2009. **101**(1): p. 98-105.
95. Daskalos, A., et al., *UHRF1-mediated tumor suppressor gene inactivation in nonsmall cell lung cancer.* Cancer, 2011. **117**(5): p. 1027-37.
96. Kofunato, Y., et al., *UHRF1 expression is upregulated and associated with cellular proliferation in colorectal cancer.* Oncol Rep, 2012. **28**(6): p. 1997-2002.
97. Arita, K., et al., *Recognition of hemi-methylated DNA by the SRA protein UHRF1 by a base-flipping mechanism.* Nature (London), 2008. **455**(7214): p. 818.
98. Hashimoto, H., et al., *The SRA domain of UHRF1 flips 5-methylcytosine out of the DNA helix.* Nature (London), 2008. **455**(7214): p. 826.
99. Unoki, M., T. Nishidate, and Y. Nakamura, *ICBP90, an E2F-1 target, recruits HDAC1 and binds to methyl-CpG through its SRA domain.* Oncogene, 2004. **23**(46): p. 7601-7610.
100. Karagianni, P., et al., *ICBP90, a novel methyl K9 H3 binding protein linking protein ubiquitination with heterochromatin formation.* Mol Cell Biol, 2008. **28**(2): p. 705-17.
101. Rothbart, S.B., et al., *Multivalent histone engagement by the linked tandem Tudor and PHD domains of UHRF1 is required for the epigenetic inheritance of DNA methylation.* Genes Dev, 2013. **27**(11): p. 1288-98.
102. Rajakumara, E., et al., *PHD Finger Recognition of Unmodified Histone H3R2 Links UHRF1 to Regulation of Euchromatic Gene Expression.* Molecular Cell, 2011. **43**(2): p. 275-284.
103. Nishiyama, A., et al., *Uhrf1-dependent H3K23 ubiquitylation couples maintenance DNA methylation and replication.* Nature, 2013. **502**(7470): p. 249-53.
104. Harrison, J.S., et al., *Hemi-methylated DNA regulates DNA methylation inheritance through allosteric activation of H3 ubiquitylation by UHRF1.* Elife, 2016. **5**.
105. Guan, D., et al., *The epigenetic regulator UHRF1 promotes ubiquitination-mediated degradation of the tumor-suppressor protein promyelocytic leukemia protein.* Oncogene, 2013. **32**(33): p. 3819-28.
106. Heir, R., et al., *The UBL domain of PLIC-1 regulates aggresome formation.* EMBO Rep, 2006. **7**(12): p. 1252-8.
107. Jeanblanc, M., et al., *The retinoblastoma gene and its product are targeted by ICBP90: a key mechanism in the G1/S transition during the cell cycle.* Oncogene, 2005. **24**(49): p. 7337-45.
108. Hopfner, R., et al., *ICBP90, a novel human CCAAT binding protein, involved in the regulation of topoisomerase IIalpha expression.* Cancer Research, 2000. **60**(1): p. 121-128.
109. Trotzier, M.-A., et al., *Phosphorylation of ICBP90 by protein kinase A enhances topoisomerase IIalpha expression.* Biochemical and Biophysical Research Communications, 2004. **319**(2): p. 590-595.
110. Groeger, A.M., et al., *Independent prognostic role of p16 expression in lung cancer.* Journal of Thoracic and Cardiovascular Surgery, 1999. **118**(3): p. 529-535.
111. Miki, Y., et al., *A strong candidate for the breast and ovarian cancer susceptibility gene BRCA1.* Science (Washington D C), 1994. **266**(5182): p. 66-71.
112. Wang, F., et al., *UHRF1 Promotes Cell Growth and Metastasis Through Repression of p16(ink4a) in Colorectal Cancer.* Annals of Surgical Oncology, 2012. **19**(8): p. 2753-2762.
113. Boukhari, A., et al., *CD47 Activation-induced UHRF1 Over-expression Is Associated with Silencing of Tumor Suppressor Gene p16(INK4A) in Glioblastoma Cells.* Anticancer Research, 2015. **35**(1): p. 149-157.

114. Jin, W., et al., *UHRF1 is associated with epigenetic silencing of BRCA1 in sporadic breast cancer.* Breast Cancer Research and Treatment, 2010. **123**(2): p. 359-373.
115. Jeanblanc, M., et al., *The retinoblastoma gene and its product are targeted by ICBP90: a key mechanism in the G1/S transition during the cell cycle.* Oncogene, 2005. **24**(49): p. 7337-7345.
116. Geller, D.S. and R. Gorlick, *Osteosarcoma: a review of diagnosis, management, and treatment strategies.* Clin Adv Hematol Oncol, 2010. **8**(10): p. 705-18.
117. Luetke, A., et al., *Osteosarcoma treatment - where do we stand? A state of the art review.* Cancer Treat Rev, 2014. **40**(4): p. 523-32.
118. DeGregori, J. and D.G. Johnson, *Distinct and Overlapping Roles for E2F Family Members in Transcription, Proliferation and Apoptosis.* Curr Mol Med, 2006. **6**(7): p. 739-48.
119. Sangwan, M., et al., *Established and new mouse models reveal E2f1 and Cdk2 dependency of retinoblastoma, and expose effective strategies to block tumor initiation.* Oncogene, 2012. **31**(48): p. 5019-28.
120. Parisi, T., et al., *Selective requirements for E2f3 in the development and tumorigenicity of Rb-deficient chimeric tissues.* Mol Cell Biol, 2007. **27**(6): p. 2283-93.
121. Yamasaki, L., et al., *Loss of E2F-1 reduces tumorigenesis and extends the lifespan of Rb1(+/-)mice.* Nat Genet, 1998. **18**(4): p. 360-4.
122. Ziebold, U., et al., *E2F3 loss has opposing effects on different pRB-deficient tumors, resulting in suppression of pituitary tumors but metastasis of medullary thyroid carcinomas.* Mol Cell Biol, 2003. **23**(18): p. 6542-52.
123. Zocchi, L., et al., *The cyclin-dependent kinase inhibitor flavopiridol (alvocidib) inhibits metastasis of human osteosarcoma cells.* Oncotarget, 2018. **9**(34): p. 23505-23518.
124. Burrage, J., et al., *The SNF2 family ATPase LSH promotes phosphorylation of H2AX and efficient repair of DNA double-strand breaks in mammalian cells.* J Cell Sci, 2012. **125**(Pt 22): p. 5524-34.
125. Zhu, H., et al., *Lsh is involved in de novo methylation of DNA.* EMBO J, 2006. **25**(2): p. 335-45.
126. Daily, K., et al., *MotifMap: integrative genome-wide maps of regulatory motif sites for model species.* BMC Bioinformatics, 2011. **12**: p. 495.
127. Wei, G., et al., *CDK4 gene amplification in osteosarcoma: reciprocal relationship with INK4A gene alterations and mapping of 12q13 amplicons.* Int J Cancer, 1999. **80**(2): p. 199-204.
128. Al-Assar, O., et al., *Transformed diffuse large B-cell lymphomas with gains of the discontinuous 12q12-14 amplicon display concurrent deregulation of CDK2, CDK4 and GADD153 genes.* Br J Haematol, 2006. **133**(6): p. 612-21.
129. Fry, D.W., et al., *Specific inhibition of cyclin-dependent kinase 4/6 by PD 0332991 and associated antitumor activity in human tumor xenografts.* Mol Cancer Ther, 2004. **3**(11): p. 1427-38.
130. Shew, J.Y., et al., *C-terminal truncation of the retinoblastoma gene product leads to functional inactivation.* Proc Natl Acad Sci U S A, 1990. **87**(1): p. 6-10.
131. Gump, J., D. Stokoe, and F. McCormick, *Phosphorylation of p16INK4A correlates with Cdk4 association.* J Biol Chem, 2003. **278**(9): p. 6619-22.
132. Han, Y., et al., *Lsh/HELLS regulates self-renewal/proliferation of neural stem/progenitor cells.* Sci Rep, 2017. **7**(1): p. 1136.
133. Stewart, E., et al., *The Childhood Solid Tumor Network: A new resource for the developmental biology and oncology research communities.* Dev Biol, 2016. **411**(2): p. 287-293.
134. Benavente, C.A., et al., *Cross-species genomic and epigenomic landscape of retinoblastoma.* Oncotarget, 2013. **4**(6): p. 844-859.
135. Tien, A.L., et al., *UHRF1 depletion causes a G2/M arrest, activation of DNA damage response and apoptosis.* Biochem J, 2011. **435**(1): p. 175-85.
136. Alhosin, M., et al., *Down-regulation of UHRF1, associated with re-expression of tumor suppressor genes, is a common feature of natural compounds exhibiting anti-cancer properties.* J Exp Clin Cancer Res, 2011. **30**: p. 41.
137. Mousli, M., et al., *ICBP90 belongs to a new family of proteins with an expression that is deregulated in cancer cells.* Br J Cancer, 2003. **89**(1): p. 120-7.
138. Duffy, M.J., et al., *Urokinase-plasminogen activator, a new and independent prognostic marker in breast cancer.* Cancer Res, 1990. **50**(21): p. 6827-9.
139. Oka, T., et al., *Immunohistochemical evidence of urokinase-type plasminogen activator in primary and metastatic tumors of pulmonary adenocarcinoma.* Cancer Res, 1991. **51**(13): p. 3522-5.

140. Hasui, Y., et al., *The content of urokinase-type plasminogen activator antigen as a prognostic factor in urinary bladder cancer.* Int J Cancer, 1992. **50**(6): p. 871-3.
141. Choong, P.F., et al., *Urokinase-plasminogen-activator levels and prognosis in 69 soft-tissue sarcomas.* Int J Cancer, 1996. **69**(4): p. 268-72.
142. Vassalli, J.D. and D. Belin, *Amiloride selectively inhibits the urokinase-type plasminogen activator.* FEBS Lett, 1987. **214**(1): p. 187-91.
143. Magri, L., et al., *E2F1 coregulates cell cycle genes and chromatin components during the transition of oligodendrocyte progenitors from proliferation to differentiation.* J Neurosci, 2014. **34**(4): p. 1481-93.
144. Unoki, M., T. Nishidate, and Y. Nakamura, *ICBP90, an E2F-1 target, recruits HDAC1 and binds to methyl-CpG through its SRA domain.* Oncogene, 2004. **23**(46): p. 7601-10.
145. Cui, L., et al., *Up-regulation of UHRF1 by oncogenic Ras promoted the growth, migration, and metastasis of pancreatic cancer cells.* Mol Cell Biochem, 2015. **400**(1-2): p. 223-32.
146. Li, X.L., et al., *Exogenous expression of UHRF1 promotes proliferation and metastasis of breast cancer cells.* Oncol Rep, 2012. **28**(1): p. 375-83.
147. Zhang, Y., et al., *Upregulated UHRF1 promotes bladder cancer cell invasion by epigenetic silencing of KiSS1.* PLoS One, 2014. **9**(10): p. e104252.
148. Zhang, Z.Y., et al., *Clinicopathological analysis of UHRF1 expression in medulloblastoma tissues and its regulation on tumor cell proliferation.* Med Oncol, 2016. **33**(9): p. 99.
149. Zhu, M., et al., *Regulation of UHRF1 by microRNA-9 modulates colorectal cancer cell proliferation and apoptosis.* Cancer Sci, 2015. **106**(7): p. 833-9.
150. He, H., C. Lee, and J.K. Kim, *UHRF1 depletion sensitizes retinoblastoma cells to chemotherapeutic drugs via downregulation of XRCC4.* Cell Death Dis, 2018. **9**(2): p. 164.
151. Fang, L., et al., *Gene therapy with RNAi targeting UHRF1 driven by tumor-specific promoter inhibits tumor growth and enhances the sensitivity of chemotherapeutic drug in breast cancer in vitro and in vivo.* Cancer Chemother Pharmacol, 2012. **69**(4): p. 1079-87.
152. Bostick, M., et al., *UHRF1 plays a role in maintaining DNA methylation in mammalian cells.* Science, 2007. **317**(5845): p. 1760-4.
153. Du, Z., et al., *DNMT1 stability is regulated by proteins coordinating deubiquitination and acetylation-driven ubiquitination.* Sci Signal, 2010. **3**(146): p. ra80.
154. Mudbhary, R., et al., *UHRF1 overexpression drives DNA hypomethylation and hepatocellular carcinoma.* Cancer Cell, 2014. **25**(2): p. 196-209.
155. Buddingh, E.P., et al., *Tumor-infiltrating macrophages are associated with metastasis suppression in high-grade osteosarcoma: a rationale for treatment with macrophage activating agents.* Clin Cancer Res, 2011. **17**(8): p. 2110-9.
156. Muto, M., et al., *Targeted disruption of Np95 gene renders murine embryonic stem cells hypersensitive to DNA damaging agents and DNA replication blocks.* J Biol Chem, 2002. **277**(37): p. 34549-55.
157. Benavente, C.A. and M.A. Dyer, *Genetics and epigenetics of human retinoblastoma.* Annu Rev Pathol, 2015. **10**: p. 547-62.
158. Wu, S.C. and C.A. Benavente, *Chromatin remodeling protein HELLS is upregulated by inactivation of the RB-E2F pathway and is nonessential for osteosarcoma tumorigenesis.* Oncotarget, 2018. **9**(66): p. 32580-32592.
159. Rane, S.G., et al., *Germ line transmission of the Cdk4(R24C) mutation facilitates tumorigenesis and escape from cellular senescence.* Mol Cell Biol, 2002. **22**(2): p. 644-56.
160. Nuovo, G.J., et al., *In situ detection of the hypermethylation-induced inactivation of the p16 gene as an early event in oncogenesis.* Proc Natl Acad Sci U S A, 1999. **96**(22): p. 12754-9.
161. Madan, B., et al., *Bone loss from Wnt inhibition mitigated by concurrent alendronate therapy.* Bone Res, 2018. **6**: p. 17.
162. Dobin, A., et al., *STAR: ultrafast universal RNA-seq aligner.* Bioinformatics, 2013. **29**(1): p. 15-21.
163. Anders, S., P.T. Pyl, and W. Huber, *HTSeq--a Python framework to work with high-throughput sequencing data.* Bioinformatics, 2015. **31**(2): p. 166-9.
164. Love, M.I., W. Huber, and S. Anders, *Moderated estimation of fold change and dispersion for RNA-seq data with DESeq2.* Genome Biol, 2014. **15**(12): p. 550.
165. Hervouet, E., F.M. Vallette, and P.F. Cartron, *Dnmt1/Transcription factor interactions: an alternative mechanism of DNA methylation inheritance.* Genes Cancer, 2010. **1**(5): p. 434-43.
166. Sharif, J., et al., *The SRA protein Np95 mediates epigenetic inheritance by recruiting Dnmt1 to methylated DNA.* Nature, 2007. **450**(7171): p. 908-12.

167. Papait, R., et al., *Np95 is implicated in pericentromeric heterochromatin replication and in major satellite silencing.* Mol Biol Cell, 2007. **18**(3): p. 1098-106.
168. Nakamura, K., et al., *UHRF1 regulates global DNA hypomethylation and is associated with poor prognosis in esophageal squamous cell carcinoma.* Oncotarget, 2016. **7**(36): p. 57821-57831.
169. Qin, W., H. Leonhardt, and F. Spada, *Usp7 and Uhrf1 control ubiquitination and stability of the maintenance DNA methyltransferase Dnmt1.* J Cell Biochem, 2011. **112**(2): p. 439-44.
170. Liu, X., et al., *UHRF1 targets DNMT1 for DNA methylation through cooperative binding of hemi-methylated DNA and methylated H3K9.* Nat Commun, 2013. **4**: p. 1563.